Angiogenesis: From tumor initiation to therapeutic resistance

Inauguraldissertation

zur
Erlangung der Würde eines Doktors der Philosophie
vorgelegt der
Philosophisch-Naturwissenschaftlichen Fakultät
der Universität Basel

von

Laura Estelle Pisarsky

aus Sarrebourg, Frankreich

Basel, 2016

Genehmigt von der Philosophisch-Naturwissenschaftlichen Fakultät
auf Antrag von

Prof. Dr. Gerhard Christofori
Prof. Dr. Markus Affolter

Basel, den 19. April 2016

Prof. Dr. Jörg Schibler

Summary

Cancer is a leading cause of morbidity and mortality worldwide. In 2012 approximately 14 million new cases were diagnosed and 8.2 million cancer-related deaths were recorded. A better understanding of the strategies employed by cancer cells to grow and disseminate through the body is still required. Precise characterization of the signaling pathways involved in these processes will allow us to propose new diagnostic and prognostic markers but also to improve therapeutic strategies.

Angiogenesis, the formation of new blood vessels from a pre-existing vasculature, has been proposed as a suitable target in order to curtail cancer. In particular, it has been proposed that preventing the supply of nutrients and oxygen supply to the tumor would starve it to death. However, the clinical outcome of anti-angiogenic therapy has been sobering; despite initial therapeutic effects, patients relapse with cancers that have developed resistance to the therapy. Tumors treated with bevacizumab, a monoclonal antibody targeting the master regulator of angiogenesis, Vascular Endothelial Growth Factor-A (VEGF-A), have been found to activate alternative pro-angiogenic signaling pathways in order to revascularize and resume growth. Therefore, it becomes critical to decipher the molecular mechanisms implicated in tumor angiogenesis in general but also the mechanisms underlying the development of resistance to anti-angiogenic therapies.

In my Ph.D. thesis, I first aimed to decipher the mechanisms of resistance to anti-angiogenic therapy. In order to overcome revascularization through activation of alternative pro-angiogenic signaling pathways, several pan-tyrosine kinase inhibitors have been developed. They demonstrated increased efficacy compared with bevacizumab. Here, we assessed the efficacy of nintedanib, a multikinase inhibitor targeting VEGFRs, FGFRs and PDGFRs in a mouse model of breast cancer. While tumors primarily responded to nintedanib treatment and demonstrated decreased tumor mass after short-term treatment, prolonged nintedanib treatment was associated with tumor regrowth. However, angiogenesis was still repressed in tumors escaping therapy and no revascularization was observed. Microarray analysis of FAC-sorted tumor cells revealed a metabolic shift towards anaerobic glycolysis. Moreover, tumors established metabolic symbiosis as suggested by the alternation between

highly hypoxic, glycolytic and normoxic areas. Indeed, the inhibition of glycolysis or the disruption of metabolic symbiosis by genetically ablating MCT4 expression, a protein involved in metabolic symbiosis, efficiently overcame resistance to anti-angiogenic therapy.

In order to reach blood vessels and to metastasize, epithelial cancer cells have to gain motile properties. The first step of the metastatic cascade consists of an epithelial-mesenchymal transtition (EMT). Epithelial cells undergoing this program lose apico-basal polarity and their epithelial markers and cell-cell and cell-matrix contacts, yet express mesenchymal markers and gain migratory capacity. Moreover, cells undergoing an EMT acquire cancer stem cell (CSC) traits. Mesenchymal cells are, for example, able to initiate tumor formation in a more efficient way compared to epithelial cells. While this feature is expected to rely on increased self-renewal capacity in mesenchymal cells, our laboratory identified VEGF-A as a causal agent in tumor initiation. By secreting VEGF-A, mesenchymal cells induce a precocious angiogenic switch, therefore sustaining tumor growth.

In a second project, I aimed to identify the upstream regulator of VEGF-A in cells undergoing an EMT. Here, by performing a low throughput siRNA screen for transcription factors possessing a binding site on the *VEGF-A* gene promoter, I could identify JunB as the main regulator of VEGF-A expression in mesenchymal cells. JunB inhibition in diverse mesenchymal cell lines led to decreased VEGF-A expression, suggesting a key role for JunB in EMT-induced angiogenesis and thus tumor growth.

In summary, my Ph.D. work provided new insights into tumor angiogenesis as:

- I identified a new mechanism of resistance to anti-angiogenic therapy, in which tumor cells resumed growth despite lack of blood vessels by switching their metabolism towards glycolysis. This work highlighted the use of glycolysis inhibitors to overcome anti-angiogenic resistance;

- I highlighted a new role for JunB as a regulator of EMT-induced angiogenesis and tumor growth.

In memory of Florian

Table of Contents

1. General introduction

1.1. Cancer involves complex gene regulatory networks and heterotypic interactions

1.1.1. What is cancer?

Cancer is a collection of deadly diseases initiated by cells that grow out of control and become invasive (Virchow 1859). The first description of cancer, the Edwin Smith Papyrus, dates back from 1500 BC (Sudhakar 2009). Cancer can virtually affect all tissues. Therefore, more than 200 types of cancers have been described and are now referenced by the National Cancer Institute. Cancer is a leading cause of morbidity and mortality worldwide. In 2012 approximately 14 million new cases were diagnosed and 8.2 million cancer-related deaths were recorded by the World Health Agency. Genetic predisposition and environmental factors, such as ultra violets, tobacco or infectious agents were shown to be responsible for cancer development (Weinberg 2014).

Tumors were long considered to be simple masses of homogeneous proliferative neoplastic cells. However, cancerous cells are surrounded by several non-cancerous cell types and, as organs, tumors reveal high degree of organization (Figure 1) (Egeblad, Nakasone et al. 2010). In fact, cancer development does not only depend on intracellular cancer cell signaling but rather on a collaborative effort between tumor cells and the surrounding microenvironment. Through their secretion of hormones and growth factors, stromal cells support the growth of tumor cells and, as postulated by the stromal progression model, the phenotypic characteristics of the microenvironment evolve during tumor progression to support tumor cell growth in the most efficient manner (Sleeman, Christofori et al. 2012). As another proof of the importance of the microenvironment in cancer progression, the tumor/stroma ratio has recently been defined as a novel prognostic marker in triple-negative breast cancer. Thus, patients presenting with stroma-rich tumors have 2.92 times higher risk of relapse compared with patients with stroma-poor tumors (de Kruijf, van Nes et al. 2011).

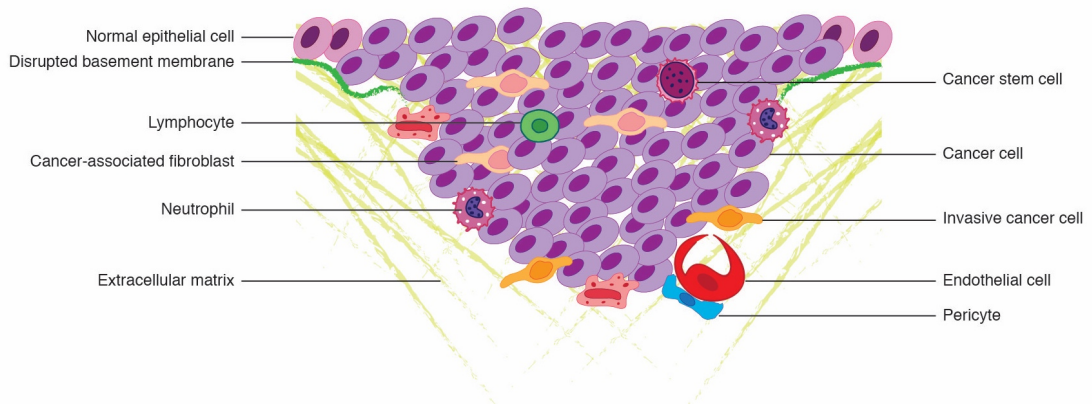

Figure 1: Tumors reveal a heterotypic composition.
Far from being simple masses of homogeneous proliferative cancer cells, tumors are composed of several cell types. Endothelial cells, stabilized by pericytes, are responsible for the appropriate blood supply of the tumor. Immune cells (macrophages, lymphocytes, neutrophils) and fibroblasts secrete growth factors and cytokines that induce tumor cell proliferation and migration. Tumor cells themselves present a high degree of heterogeneity (cancer stem cells, invasive cancer cells). Proteins forming the extracellular matrix also support tumor progression. Only tumors that have disrupted the basement membrane and invaded the stroma are referred as cancer.

The role of the different types of stromal cells in tumor progression is very complex. However, some examples of their tumor-promoting activities are described below.

Cancer cells and cancer stem cells: These cells represent the essence of cancer. Indeed, they carry the genetic alterations responsible of the disease. Based on their morphology, their metabolism or their degree of differentiation, cancer cells present a high level of heterogeneity. Cancer stem cells (CSC) are the cells of origin for the tumor (Dean, Fojo et al. 2005). They are characterized by their increased ability to initiate tumor formation compared with other types of cancer cells. Originally identified in leukemia, CSCs have also been described in solid cancers (Bonnet and Dick 1997, Al-Hajj, Wicha et al. 2003). Their low-division rate make them particularly resistant to conventional cancer therapy and they are, therefore, particularly prone to cause relapse (Dean, Fojo et al. 2005).

Endothelial cells and pericytes: Endothelial cells form blood vessels that, once stabilized by pericytes, guarantee tumor adequate access to oxygen and nutrients. Endothelial cells also secrete factors that directly affect tumor cell behavior. For example, a study performed in our laboratory suggests that endothelial cell secretome can induce epithelial-mesenchymal transition (EMT) in human breast cancer cell lines (Ferraro, unpublished data). Ghajar and collaborators also demonstrated the ability of endothelial cells to promote metastatic tumor cell proliferation or to maintain them in a dormant state (Ghajar, Peinado et al. 2013). The implication of endothelial cells in

tumor progression will be developed in more details in the third chapter, dedicated to tumor angiogenesis.

Immune cells: Immune cells infiltrates are a major component of most if not all tumors (Pages, Galon et al. 2010). They have a dichotomous role in cancer, and are therefore able to facilitate or antagonize tumor progression. One could imagine that cancer cells essentially express self-antigens. However, due to the mutations they carry, they are also antigenic (Gajewski, Schreiber et al. 2013). Cytotoxic T lymphocytes and natural killer cells are certainly characterized by tumor-antagonizing activities. However, increasing evidence associates macrophages, mast cells, neutrophils but also B and T cells to tumor progression. By secreting high levels of growth factors, chemokines and cytokines, these cells promote tumor angiogenesis, cancer cell proliferation and metastatic spread (Kitamura, Qian et al. 2015). Myeloid cells can repress cytotoxic T lymphocytes' and natural killer cells' tumor-suppressing activities (Coffelt, Lewis et al. 2010, Egeblad, Nakasone et al. 2010, Casazza, Laoui et al. 2013, Bonapace, Coissieux et al. 2014, Kuchnio, Moens et al. 2015).

Cancer-associated fibroblasts: Cancer-associated fibroblasts (CAFs) are the major component of the microenvironment. They secrete large amounts of extracellular matrix (ECM) and are, therefore, responsible for the formation of the desmoplastic stroma characteristic of advanced carcinomas (Kalluri and Zeisberg 2006). Furthermore, they have been shown to promote breast cancer progression via the secretion of matrix metalloproteinases (MMPs) (Sternlicht, Lochter et al. 1999).

Extracellular matrix: ECM cannot be only considered as a stable structure supporting tumor cells. It is rather a dynamic niche, constantly remodeled during tumor progression (Lu, Weaver et al. 2012, Venning, Wullkopf et al. 2015). Increased ECM stiffness has been shown to correlate with tumor progression in breast cancer (Levental, Yu et al. 2009). Moreover, ECM degradation by matrix MMPs has been shown to induce angiogenesis through the release of sequestered growth factors (Bergers, Brekken et al. 2000). Recently, ECM has been suggested as a highway for facilitating tumor cell migration (Oudin, Jonas et al. 2016).

1.1.2. Cancer, a multistep process

In most cases, cancer is a silent killer that develops over years or even decades (Hahn and Weinberg 2002). Cancer development consists of a multistep process that relies on serial acquisition of mutations in proto-oncogenes or tumor suppressor genes. Several attempts to identify the oncogene responsible of cancer failed, as no single oncogene is sufficient to transform normal human cells (Sager, Tanaka et al. 1983). Indeed, the identification of new molecular targets for therapeutic intervention greatly depended on the recent development of gene expression profiling and the wide variety of omics (transcriptomics, proteomics, metabolomics e.g.). Far from identifying a limited number of pathways implicated in tumor development, this array of techniques revealed the inherent heterogeneity of signals supporting neoplastic transformation. However, some hub genes were shown to be sufficient to transform normal cells into malignant ones and support tumor progression. The key concepts in which they participate are known as the "hallmarks of cancer".

1.1.3. The hallmarks of cancer

In two seminal reviews, Hanahan and Weinberg have described the common characteristics of cancers (Hanahan and Weinberg 2000, Hanahan and Weinberg 2011).

Sustained proliferative factors: Normal tissue architecture and homeostasis rely on a precise control of the cell growth-and-division cycle by a diversity of growth factors. Cancer cells are able to produce their own growth factors and directly respond to these autocrine and/or intracrine stimulations. In order to palliate the lack of growth factors, tumors cells can also overexpress the associated receptors. Alternatively, tumors cells can attract stromal cells that will in turn support tumor cell proliferation by secreting these growth factors. Another possibility for tumor cells to become independent of growth factors expression is to constitutively activate downstream signaling pathways. This ploy is recurrent in human melanomas, where mitogen-activated protein kinase (MAPK) signaling is constitutively activated as the result of B-Raf mutations (Davies and Samuels 2010). Additionally, MAPK signaling is activated in pancreas, lung and colon cancer or in leukemia following K-Ras or N-Ras

mutations, respectively. In a similar manner, mutated isoforms of the phosphoinositide 3-kinase (PI3K) lead to constitutive activation of the PI3K signaling pathway. Loss of negative feedback loop, as observed with loss-of-function mutation of PTEN - a negative regulator of PI3K - leads to hyperactivation of the targeted signaling pathway (Yuan and Cantley 2008, Jiang and Liu 2009).

Evasion to growth suppressors: In order to guarantee tissue homeostasis, proliferation is inhibited by cell-cell contacts. Cancer cells lose contact inhibition mechanisms and, as a result, grow out of control. Moreover, loss of retinoblastoma-associated (RB) gene or TP53, two tumor-suppressor genes controlling cycle proliferation are commonly observed in cancer (Sherr and McCormick 2002).

Resisting cell death: As a safeguard against cancer, TP53 induces apoptosis in response to DNA damages. In tumor cells, loss of TP53 allows abnormal cells to survive.

Replicative immortality: Telomeres protect the extremities of each chromosome. During repeated cell divisions, telomeres shorten and lose the ability to protect chromosomal extremity from end-to-end fusions. These fusions result in genomic instability and cell death. In cancer cells, telomerases extent the telomeric DNA, protecting chromosomal ends. Thus, cancer cells display an unlimited replicative potential.

Genome instability and mutation: Selective growth advantages are acquired through genetic and epigenetic changes. During the course of tumor development, tumors present with increased sensitivity to mutagenic agents and defective DNA-maintenance machinery. Resulting mutations and deletion/amplification of large chromosomal segments lead to a complete loss of genome integrity and a huge growth selection advantage (Kinzler and Vogelstein 1997).

Tumor-promoting inflammation: Inflammation contributes to tumor progression via the release of factors capable of inducing mutations in cancer cells - reactive oxygen species -, but also to sustain angiogenesis, invasion and metastasis (Grivennikov, Greten et al. 2010).

Reprogrammed energy metabolism: Normal cells rely on oxidative phosphorylation when cultured under normoxic conditions but switch to glycolysis under anaerobic conditions. The Warburg effect defines the ability of cancer cells to use glycolysis even in the presence of oxygen (Warburg 1956, Warburg 1956). The Warburg effect

is observed in rapidly dividing cells, such as embryonic tissues and tumors, suggesting that it might facilitate the productions of building blocks required to create new cells (Vander Heiden, Cantley et al. 2009). The emerging concept of metabolic symbiosis suggests that tumor cells can exchange metabolites (Sonveaux, Vegran et al. 2008). This observation, based on cooperation between lactate-producing and lactate-consuming cells in supporting tumor growth, has been made between different tumor cell populations but can also implicate other cell types present in the microenvironment (CAFs, immune cells) (Semenza 2008, Pavlides, Whitaker-Menezes et al. 2009).

Evading immune destruction: Increased propensity of cancer cells to establish tumors in immunodeficient mice supposes the implication of the immune system in tumor eradication (Kim, Emi et al. 2007). However, it is now clear that cancer cells can evade immune system by hindering CTLs or NK cell activity or by recruiting immunosuppressive cells, such as regulatory T cells or myeloid-derived suppressor cells that are able to repress cytotoxic lymphocytes (Ostrand-Rosenberg and Sinha 2009, Shields, Kourtis et al. 2010).

The two last hallmarks of cancer, the induction of angiogenesis and the activation of invasion and metastasis, are central to the present work and will be described in more detail in the following chapters.

1.2. When cancer turns deadly: the invasion-metastasis cascade

1.2.1. The metastatic odyssey

The metastatic cascade defines the migration of cancer cells from the primary tumor to distant organs that they colonize. Metastases account for 90% of cancer-related deaths (Christofori 2006). The kinetic of metastasis and organ-specific colonization vary greatly amongst different tumor types suggesting that the ability of neoplastic cells to infiltrate a distant organ does not necessarily correlates with their competence to colonize this organ (Nguyen, Bos et al. 2009). Isolation of circulating tumor cells in the blood of cancer patients implies that tumors shed thousands of cancer cells everyday (Nagrath, Sequist et al. 2007). However, only a small proportion of these

cells (<0.01%) overtly develops as macrometasases (Chambers, Groom et al. 2002). This observation suggests that a strong selective pressure applies to cells leaving the primary tumor (Vanharanta and Massague 2013). Interestingly, the metastatic cascade is not necessarily a late event occurring in slowly developing tumors. Instead, metastases have been shown to develop concurrently with the primary tumor (Weng, Penzner et al. 2012).

Cancer cells acquire mutations that render them resistant to apoptosis and allow them to grow out of control. As the primary tumor grows, hypoxic areas appear. This harsh tumor environment selects for aggressive clones with high metastatic propensities (Gupta and Massague 2006). Such clones acquire additional genetic and epigenetic alterations and gain proliferative and survival advantage at each subsequent round of clonal selection. The different steps of the invasion-metastasis cascade, as reviewed by Valastyan and Weinberg, are depicted in Figure 2 and briefly described below (Valastyan and Weinberg 2011).

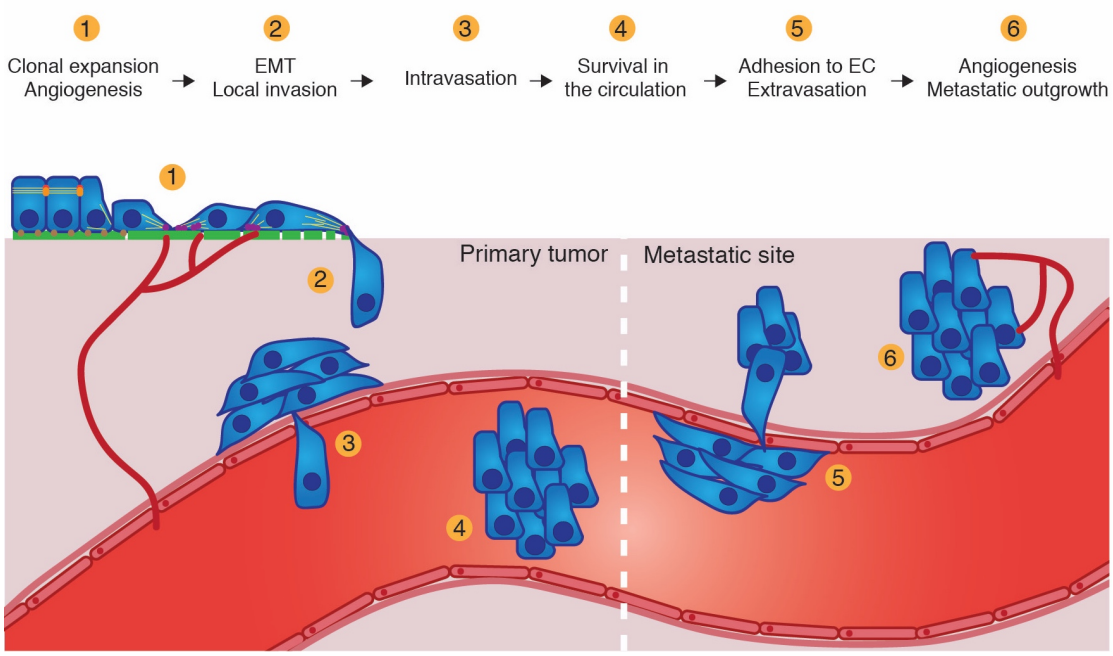

Figure 2: The invasion-metastasis cascade.
After an initial phase of clonal expansion and angiogenesis, cancer cells undergo an epithelial-mesenchymal transition (EMT) and start to invade locally. Tumor cells enter circulation by intravasation. Cells surviving in the blood can attach to the endothelial cells (EC) and extravasate at the metastatic site. Following vascularization, micrometastases resume growth and form clinically detectable metastases. Figure drawn based on (Robbins, Kumar et al. 2010).

Local invasion: Some cancer cells respond to increasing selective pressure by undergoing an epithelial-mesenchymal transition (EMT; a process described in more

details in the following paragraph). In order to invade, these aggressive cells initiate the degradation of the basement membrane. Once the tumor cells have degraded the basement membrane, they encounter the stroma. As described earlier, the tumor microenvironment further fosters tumor growth and invasiveness. For example, the degradation of the ECM by MMPs releases the growth factors that are trapped in the ECM and that will, in turn, nurture cancer cell proliferation and migration (Kessenbrock, Plaks et al. 2010). Tumor progression is also associated with recruitment of blood and lymphatic vessels.

Intravasation: Once they reach the blood vessels, tumor cells can intravasate and enter circulation. For this, they need to cross the pericyte and endothial cell barriers, a step greatly facilitated by the leakiness and weak cell-cell interactions encountered in tumor blood vessels (Carmeliet and Jain 2011).

Survival in the circulation: Anchorage is essential for cell survival. Cells that lose anchorage to extracellular matrix or neighboring cells experience anoikis, a cell-detachment-related apoptosis. Cancer cells have developed mechanisms of resistance to anoikis that allow them to survive in the circulation (Simpson, Anyiwe et al. 2008). Furthermore, once in the bloodstream, cancer cells have to protect themselves from hemodynamic shear stresses and recognition by the innate immune system. Platelets offer them protection against these dangers.

Arrest at a distant organ site and extravasation: Circulating tumor cells have been shown to present affinity for specific organs, a phenomenon called metastatic organotropism (Hoshino, Costa-Silva et al. 2015). Breast cancer cells can, for example, specifically bind to the lung vasculature, allowing them to particularly home to this organ (Paget 1989, Brown and Ruoslahti 2004). Once attached to the endothelium, cancer cells can extravasate and finally reach their metastatic niche.

Metastatic outgrowth: Yet, the effort does not stop there. The rare cells that have survived this journey still have to endure exposure to innate immunity and rigorous conditions encountered at the metastatic site. Indeed, this new microenvironment differs significantly from the primary tumor microenvironment. Therefore, most of the cells will stay in a dormant state until favorable conditions are met for their proliferation (Psaila and Lyden 2009). Moreover, it is thought that cancer cells have to undergo a mesenchymal-epithelial transition (MET) before they can start to

proliferate again. Ultimately, cancer cells can resume growth and form clinically detectable metastases.

1.2.2. Epithelial-mesenchymal transition

1.2.2.1. Molecular mechanisms of EMT

In order to reach the blood vessels and metastasize, epithelial cancer cells have to gain motile properties. Therefore, the initial step of the metastatic cascade consists of undergoing an epithelial-mesenchymal transition (EMT). The EMT process has first been described in embryonic development, but is now known to be reactivated in wound healing and cancer (Hay 1995). Epithelial cells undergoing this program will lose apico-basal polarity, shed their epithelial markers and cell-cell and cell-matrix contacts, express mesenchymal markers and gain migratory capacity (Figure 3).

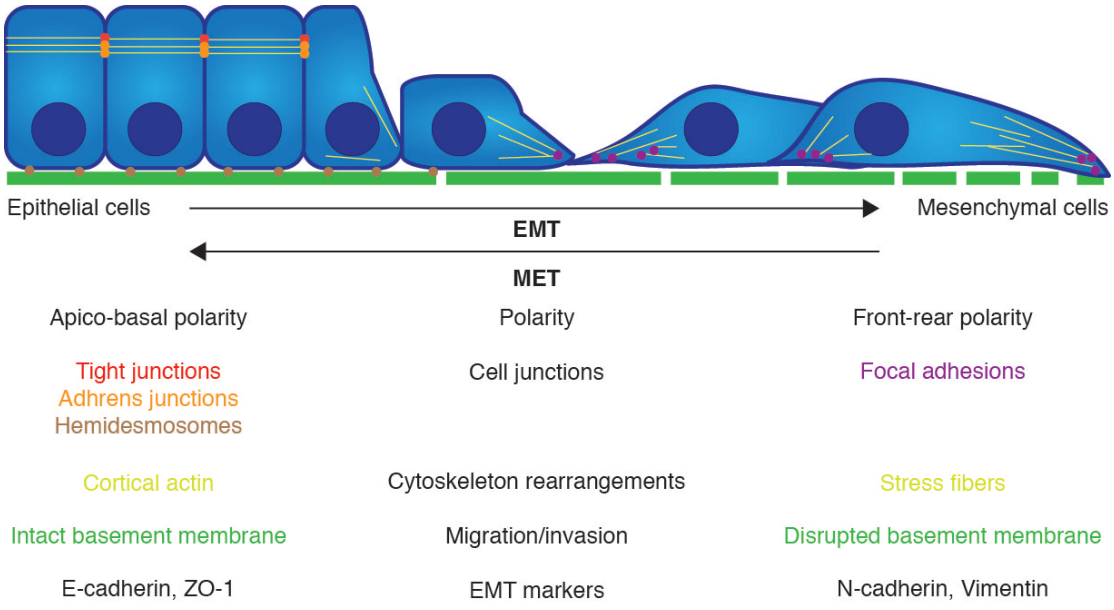

Figure 3: EMT completely remodels cell phenotype.
EMT is a reversible process that consist in the transition from an epithelial phenotype - characterized by apico-basal polarity, cell-cell and cell-ECM junctions, presence of cortical actin and expression of epithelial markers - to a mesenchymal state, defined by front-rear polarity, presence of focal adhesions and stress fiber network. This conversion is associated with a loss of epithelial marker expression (E-cadherin, ZO-1) in favor of mesenchymal marker expression (N-cadherin, vimentin). The colors used in the text refer to the different elements depicted on the scheme.

EMT can be induced by a variety of growth factors such as transforming growth factor (TGF)-β, hepatocyte growth factor (HGF), epidermal growth factor

(EGF), insulin-like growth factor (IGF) and fibroblast growth factor (FGF). They trigger upregulation of transcription repressors (Snail, Slug or Zeb1) that bind to the E-box elements in the E(pithelial)-cadherin promoter, leading the recruitment of histones deacetylases and subsequent repression of E-cadherin expression (Singh and Settleman 2010). Decreased E-cadherin expression invariably leads to dissolution of adherens junctions and loss of apico-basal polarity. E-cadherin loss is associated with increased expression of the neuronal cell adhesion molecule (NCAM) and balanced by overexpression of N(eural)-cadherin, a phenomenon called the cadherin switch (Cavallaro, Schaffhauser et al. 2002, Lehembre, Yilmaz et al. 2008, Wheelock, Shintani et al. 2008). Repression of claudin, occludin, desmoplakin and desmoglobin destabilizes tight junctions and desmosomes (Huang, Guilford et al. 2012). In order to facilitate motility, cells reorganize their cortical actin into stress fibers, allowing them to form sensory extensions such as lamellipodia and filopodia (Yilmaz and Christofori 2009, Yilmaz and Christofori 2010). These actin-rich protrusions participate to ECM degradation though MMP secretion (McNiven 2013).

TGF-β, a master regulator of EMT, induces phosphorylation of TGFβRI/TGFβRII heterotetramers. It leads to the phosphorylation of the downstream effectors Smad2 and 3 and their binding to Smad4. This trimeric Smad complex associates with Zeb1, Zeb2 or Snail and represses E-cadherin expression.

Non-canonical TGF-β signaling involves RHO-like GTPases, PI3K and MAPK signalings (Lamouille, Xu et al. 2014). Phosphorylation of SRC homology 2 domain-containing-transforming A (SHCA) by TGFRβ1 initiates the RAS-RAF-MEK-ERK signaling pathway (Lee, Pardoux et al. 2007). Regarding the p38 MAPK and JNK pathways, their activation results from the stimulation of TAK1 by a TRAF6/TGFβR complex (Sorrentino, Thakur et al. 2008, Yamashita, Fatyol et al. 2008).

Existence of EMT in human cancer and its necessity for tumor metastasis are still debated (Bill and Christofori 2015). E-cadherin is commonly inactivated in cancer by either somatic mutations or epigenetic silencing (van Roy and Berx 2008). However, cancer cells at the metastatic site present with an epithelial phenotype. It has been proposed that cancer cells might revert to an epithelial phenotype in order to colonize distant organs but this hypothesis still remains to be proven using lineage tracing experiments.

1.2.2.2. EMT as a source of cancer stem cells

Tumor-initiating cells have been identified in several cancer types. These cells, able to self-renew by asymmetric division, resemble normal stem cells and have therefore been proposed to be cancer stem cells (CSCs) (Bonnet and Dick 1997, Al-Hajj, Wicha et al. 2003).

EMT is a transient process and tumor cells are thought to undergo mesenchymal-epithelial transition (MET) in order to colonize distant organs. The ability of cancer cells to undergo EMT and MET reflects their high degree of plasticity. Indeed, it has been showed that cells undergoing an EMT acquire CSC traits (Mani, Guo et al. 2008). Mesenchymal cells are able to form mammospheres and they initiate tumor formation in a more efficient way compared with epithelial cells. Reversely, CSCs isolated from mammary carcinomas express an EMT signature.

Reinforcing the link between TGF-β-induced EMT and stemness, the EMT-inducing transcription factor Zeb2 has been implicated in human embryonic stem cell maintenance (Chng, Teo et al. 2010). Moreover, isolated human CSCs express a TGF-β signature and re-express epithelial markers following TGF-β inhibition (Shipitsin, Campbell et al. 2007).

We have recently identified VEGF-A as a causal agent in tumor initiation by EMT-induced CSCs; by secreting VEGF-A, EMT-induced CSCs induce a precocious angiogenic switch that sustains tumor growth (Fantozzi, Gruber et al. 2014).

We have discussed the importance of the metastatic cascade in cancer-related deaths. However, one should not forget that without the recruitment of blood vessels to the primary tumor, none of the steps described earlier (with the exception of local invasion) would take place. Angiogenesis seems to be a rate-limiting step in the transformation of proliferating cells into a deadly disease.

1.3. Mechanisms of normal and pathological angiogenesis

1.3.1. The need for angiogenesis

Blood vessels belong to the circulatory system that first appeared 600 millions years ago to respond to increasing organism size and to overcome the subsequent time-distance constraints of diffusion (Monahan-Earley, Dvorak et al. 2013). Indeed, in order to survive and proliferate, cells need oxygen and nutrients and have to get rid of their metabolic waste. In vertebrates, blood vessels nurture organs by providing them with these elements. Blood has an essential role in maintaining body homeostasis: it transports substances such as nutrients, oxygen or hormones, regulates heat, but also assures a defense role by carrying immune cells and clotting factors. Therefore, blood vessel formation is one of the earliest events occurring during embryonic development.

Angiogenesis, the formation of new blood vessels from a pre-existing vasculature, has been implicated in several physiological processes, such as organ development and healing (Carmeliet 2005). Abnormal blood vessel development can promote cancer, inflammatory diseases, pulmonary hypertension, blinding eye diseases, stroke, myocardial infarction, ulceration, neurogeneration and many more (Carmeliet and Jain 2011).

Moreover, the role of endothelial cells is not limited to organ or tumor perfusion. They also play an active role in organ and tumor growth by secreting a panoply of growth factors and ECM proteins (Butler, Kobayashi et al. 2010). By doing so, they create a vascular niche that supports normal progenitor cell and CSC self-renewal and differentiation (Borovski, De Sousa et al. 2011). Further supporting a role beyond simple tissue perfusion, tissue-specific gene expression signatures of endothelial cells have been reported (Nolan, Ginsberg et al. 2013).

1.3.2. Strategies to recruit blood vessels

In a developing embryo, vessel formation starts with vasculogenesis. This process consists of the differentiation of angioblasts (mesoderm-derived precursors of the endothelial cells) into endothelial cells, which will then coalesce to form a vascular

plexus. With ongoing organ development and in the adult, a second mechanism takes the helm: sprouting angiogenesis.

Sprouting angiogenesis also represents the most common mode of vessel formation in tumors (Figure 4). When oxygen or nutrients become scarce, tumor cells initiate secretion of angiogenesis-promoting molecules, such as VEGF-A. VEGF-A binds to VEGFR2 expressed at the surface of endothelial cells. This binding results in the activation of endothelial cells. In order to regulate the number of sprouts, endothelial cells compete for the tip cell position, a process that rely on the VEGFR-Dll4-Notch signaling pathways (Jakobsson, Franco et al. 2010). The first cell able to express Dll4 and repress Notch activity gets selected as a tip cell. Dll4-mediated Notch activation in the neighboring cells inhibits VEGFR2 expression. As a result, these cells cannot respond to VEGF-A stimulation anymore and become stalk cells. Tip cells polarize and develop filopodia that scan the environment seeking for attractant or repellent signals and initiate sprouting (Gerhardt, Golding et al. 2003). For this, tip cells loosen their cell-cell junctions and secrete proteases that dissolve the basement membrane. While migrating, tip cells pull the sprout, forcing the proliferation of stalk cells and the formation of a lumen. Once tip cells encounter other blood vessels, sprouting stops. The two sprouts establish contacts, form tight junctions via expression of VE-cadherin, and anastomose to allow blood flow (Blum, Belting et al. 2008, Dejana, Orsenigo et al. 2009). Finally, vessels need to be stabilized. To this end, endothelial cells secrete platelet-derived growth factor (PDGF)-β. PDGF-β binds to PDGFRβ on the pericyte membrane and induces their proliferation and recruitment (Abramsson, Lindblom et al. 2003). Tumor vessels are known to be tortuous and leaky. Indeed, pericytes are less abundant in tumors and they are not as tightly attached to the endothelium than in normal organs (Bergers and Song 2005). Tie2, expressed by endothelial cells, and its ligand angiopoietin 1, expressed by pericytes, promote the proper attachment of pericytes on the endothelial wall (Armulik, Abramsson et al. 2005). TGF-β also sustains blood vessel maturation by inducing secretion of ECM by endothelial cells and pericytes (Jain 2003). Once stabilized, endothelial cells return to a quiescent state and blood flow is established (Geudens and Gerhardt 2011).

Other mechanisms of vessel formation exist but their relevance in tumor development is not clear yet. When neo-vessel formation is not possible, tumor cells can co-opt existing blood vessels to obtain sufficient blood supply. Vascular mimicry consists in the trans-differentiation of cancer cells into endothelial-like cells and the subsequent formation of tubular structures able to carry blood in the hypoxic parts of the tumor. Vascular mimicry is a well-established process in melanoma and has been recently identified also in breast cancer (Hendrix, Seftor et al. 2003, Wagenblast, Soto et al. 2015). Vasculogenesis corresponds to the differentiation of bone marrow-derived progenitors into endothelial cells. In a similar manner, CSCs have been shown to differentiate into endothelial cells (Wang, Chadalavada et al. 2010). Finally, during intussusception a single vessel is split into two daughter vessels via the insertion of a tissue pillar into the vessel lumen (Makanya, Hlushchuk et al. 2009).

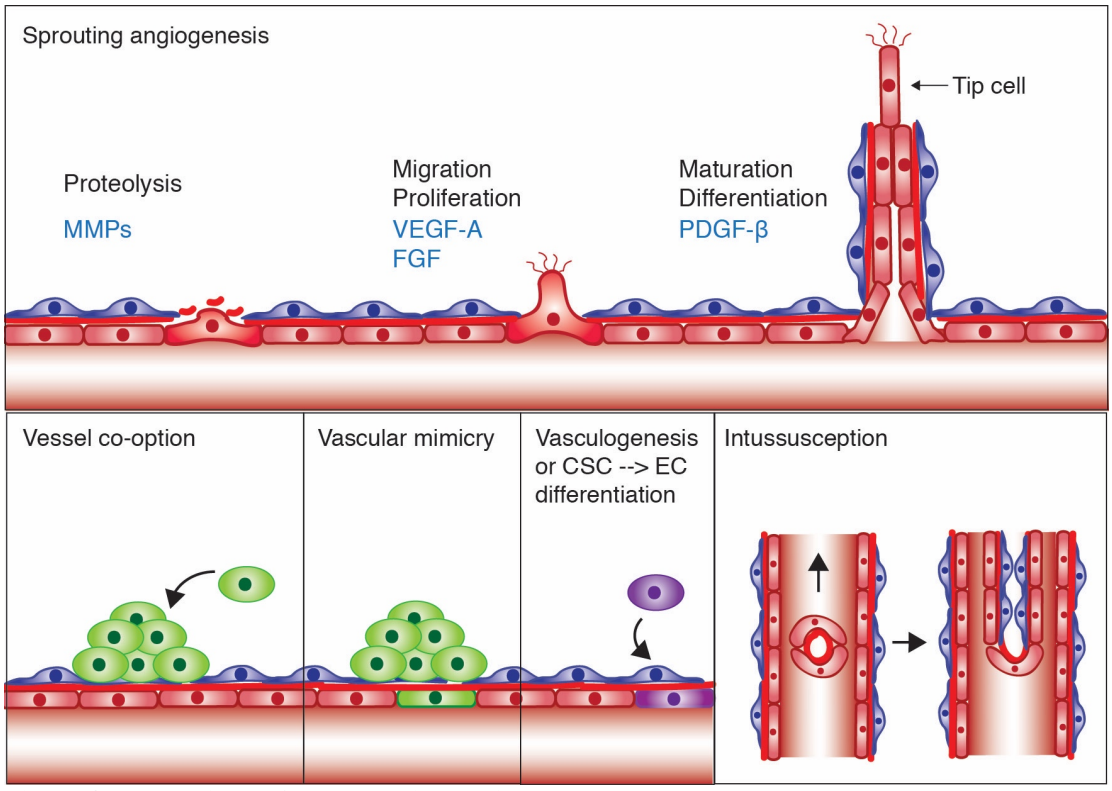

Figure 4: Mechanisms of tumor angiogenesis.
Upper panel: Sprouting angiogenesis is a multi-step process. Once a tip cell has been selected, it secretes MMPs that dissolve the basement membrane. Secretion of pro-angiogenic factors by the tumor microenvironment, such as VEGF-A and FGF, promotes the migration of the tip cell and proliferation of the stalk cells. Finally, blood vessels have to mature, a process mainly fostered by the secretion of PDGF-β.
Lower panel: Besides sprouting angiogenesis, other modes of neovascularization have been described. For example, tumor cells can hijack (co-opt) existing blood vessels to overcome oxygen paucity. Tumor cells can also form their own channels for blood transport, a process known as vascular mimicry. Vasculogenesis consists of the differentiation of bone marrow-derived progenitor cells into endothelial cells. CSCs can, as well, differentiate into endothelial cells. Finally, intussusception is

based on the division of one mother vessel into two new daughter vessels. Figure drawn based on (Carmeliet and Jain 2011) and (Jain and Carmeliet 2012).

1.3.3. VEGF-A plays a crucial role in angiogenesis and tumor progression

1.3.2.1. The VEGF family

VEGF-A, originally known as vascular permeability factor, belongs to the family of homodimeric glycoproteins also including Placental growth factor (PlGF), VEGF-B, VEGF-C, VEGF-D and VEGF-E (Figure 5) (Senger, Galli et al. 1983). The VEGF-A active form consists of a disulfide-linked homodimer (Pages and Pouyssegur 2005). VEGF-A binding to its receptor VEGFR2 activates a plethora of downstream signaling pathways, such as MAPK circuits, PI3K, AKT, phospholipase Cγ (PLCγ) and small GTPases. These pathways support endothelial cell survival, proliferation and migration. VEGF-A can also bind to VEGFR1 (Fong, Rossant et al. 1995), however, VEGFR1 tyrosine kinase activity is rather limited, and VEGFR1 is therefore considered to be a decoy receptor that represses angiogenesis (Krueger, Liu et al. 2011). Moreover, a soluble and catalytically inactive isoform of VEGFR1 freely diffuses and traps VEGF-A. The critical importance of VEGF signaling for embryonic development and for angiogenesis has been demonstrated by mouse genetics approaches. For example, the loss of a single *VEGF-A* allele has led to embryonic lethality at days 11-12, while *VEGFR2*$^{-/-}$ embryos die at days 8.5-9.5. In both cases death is associated with vascular defects (Shalaby, Rossant et al. 1995, Carmeliet, Ferreira et al. 1996, Ferrara, Carver-Moore et al. 1996).

VEGF-B and PlGF also bind to VEGFR1. PlGF has been shown to be dispensable for embryonic angiogenesis. However, its contribution to tumor angiogenesis remains controversial. Indeed, in the Rip1Tag2 (RT2) transgenic mouse model of pancreatic β-cell carcinogenesis PlGF reduces angiogenesis, supporting the observation that PlGF inhibition does not repress angiogenesis in various xenograft models (Schomber, Kopfstein et al. 2007, Bais, Wu et al. 2010). However, PlGF blockade has been associated with vessel normalization and tumor growth inhibition in transgenic models of hepatocellular carcinoma (Carmeliet, Moons et al. 2001, Van de Veire, Stalmans et al. 2010). The contribution of VEGF-B to angiogenesis is essentially limited to cardiac tissues, and VEGF-B expression in the RT2 model does

not affect blood vessel density (Albrecht, Kopfstein et al. 2010, Bry, Kivela et al. 2010).

VEGF-C binding to VEGFR3 is critical for embryonic angiogenesis and lymphangiogenesis, and this signaling pathway is reactivated during tumor angiogenesis and lymphangiogenesis (Tvorogov, Anisimov et al. 2010). In mouse models of cancer, this ligand-receptor couple is implicated in lymphangiogenesis-mediated metastasis (Mandriota, Jussila et al. 2001, Tammela, Zarkada et al. 2008, Tammela and Alitalo 2010). Similar to VEGF-C, VEGF-D also signals through VEGFR3, and the expression of VEGF-D in RT2 mice induces increased tumor lymphangigenesis and lymph node metastasis (Kopfstein, Veikkola et al. 2007).

VEGF-E, the final member of the VEGF gene family, is a viral homolog of the mammalian VEGFs that signals through VEGFR2 (Lyttle, Fraser et al. 1994). It is encoded by orfan viruses (Orf), and infection with Orf viruses results in extensive endothelial cell proliferation associated with severe skin hemorrhages (Kiba, Sagara et al. 2003). When expressed in transgenic model of pancreatic cancer (RT2 mice) VEGF-E leads to the formation of hemangioma-like structures (Fagiani et al., in press).

VEGF receptors often exert their functions with specific co-receptors, neuropilin 1 and 2. Neuropilins are receptors for semaphorins in neurons, yet they can also transduce VEGF signaling either on their own or as co-receptors for VEGFR1, 2 or 3 (Herbert and Stainier 2011).

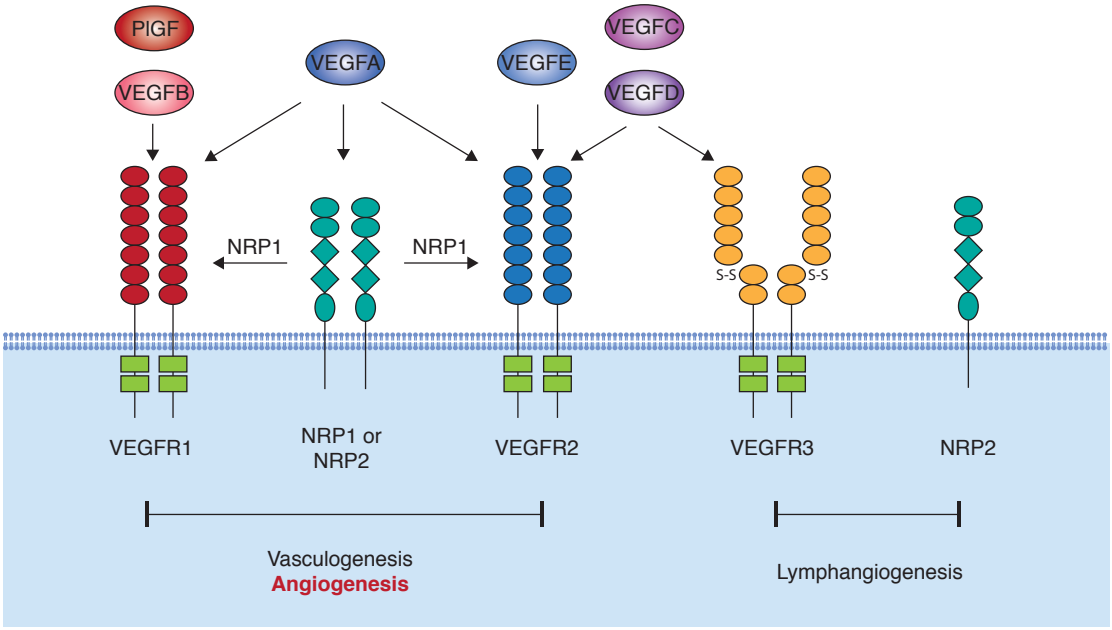

Figure 5: The VEGF family plays a crucial role in angiogenesis.
The members of the VEGF family present diverse expression patterns, receptor specificity and they are involved in varied biological functions. VEGF-A essentially signals through VEGFR2 in endothelial cells but its binding to neuropilin1 (NRP1) and VEGFR1 are involved in CSC renewal and survival. Figure adapted from (Hicklin and Ellis 2005) and (Ellis and Hicklin 2008).

1.3.2.2. VEGF-A, a pleiotropic growth factor

We have previously discussed the role of paracrine VEGF-A secretion during activated angiogenesis, e.g. VEGF-A secreted by tumor cells and targeting endothelial cells. Interestingly, autocrine VEGF-A secretion also occurs and is involved in completely different functions. Indeed, autocrine VEGF-A released by the endothelium maintains endothelial homeostasis (Lee, Chen et al. 2007). But even more intriguing is the autocrine VEGF-A signaling occuring in tumor cells (Goel and Mercurio 2013). Some tumor cells express VEGFRs on their surface and this expression correlates with poor prognosis. Although VEGFR1 is considered to be a decoy receptor in endothelial cells, it seems to be implicated in signal transduction when expressed by tumor cells. Neuropilins, the receptors for neuronal class 3 semaphorins and co-receptors for VEGFRs, are also expressed by tumor cells where they act as receptors for VEGF-A (Soker, Takashima et al. 1998). VEGF-A has been shown to induce survival of neuropilin-expressing breast cancer cells, and VEGF-A-induced neuropilin1 activation regulates the stemness potential of skin cancers (Bachelder, Crago et al. 2001, Beck, Driessens et al. 2011). Both Neuropilin1 and

VEGFR2 inhibition leads to impaired cancer stem cell renewal. Interestingly, VEGF-A and VEGFR1 are upregulated in colon cancer cells undergoing an EMT (Bates, Goldsmith et al. 2003). These data correlate with our own observation that EMT-induced CSCs express high levels of VEGF-A (Fantozzi, Gruber et al. 2014). Moreover, prostate cancer cells have been proposed to undergo an EMT when treated with recombinant VEGF-A (Mak, Leav et al. 2010). Finally, colon cancer cells expressing VEGFR1 present markedly increased migration supporting a role for VEGF-A in this process (Fan, Wey et al. 2005).

1.3.2.3 VEGF-A regulation, a fine-tuned mechanism

In humans, the *VEGF-A* gene comprises 8 exons separated by 7 introns, encompasses 14 kb, and is located on chromosome 6 (Arcondeguy, Lacazette et al. 2013). Different levels of regulation have been reported for VEGF-A: transcriptional regulation, mRNA stability and mRNA translation via IRES sequences (Claffey, Shih et al. 1998, Huez, Creancier et al. 1998, Stein, Itin et al. 1998). The *VEGF-A* gene promoter lacks a TATA box, but carries numerous binding sites for transcription factors, including AP1, AP2 and Sp1. An alternative transcription initiation site, non responsive to hypoxia, has been discovered downstream of the classical start site. VEGF-A transcripts can be alternately spliced into isoforms that present diverse functions and bioavailabilities: VEGF-A121, 145, 165, 189 and 206 (Ladomery, Harper et al. 2007). VEGF-A165 (164 in murine cells) binds to heparin moieties of the extracellular matrix and promotes endothelial cell migration. VEGF-A121 (120 in mice), however, is a diffusible factor implicated in endothelial cell proliferation. These alternatively spliced isoforms also present varying abilities to activate VEGFR2. Angiogenesis therefore relies on a fine-tuned expression of the different VEGF-A isoforms. Although VEGF-A mRNA is very labile under normoxic conditions, AU-rich elements within the 3'-UTR of the VEGF-A mRNA mediate mRNA stability under hypoxic conditions. Moreover, under stress conditions, VEGF-A mRNA can be translated by a cap-independent mechanism. New long non-coding RNAs (lncRNAs) and microRNAs (miRNAs) have also been found to affect VEGF-A regulation (Arcondeguy, Lacazette et al. 2013).

Hypoxia is lethal for most cells. However, poorly oxygenated cancer cells ([pO2] < 7 mmHg) have developed strategies to survive in such environment and can, for example, shift from aerobic to anaerobic metabolism (Venning, Wullkopf et al. 2015). Their adaptability to such environment greatly relies on expression of oxygen sensors and hypoxia-inducible factors (Carmeliet and Jain 2011). VEGF-A, the master regulator of angiogenesis, is tightly regulated by hypoxia. The *VEGF-A* promoter contains a hypoxia response element (HRE) that is bound by HIF1α and HIF2α (Forsythe, Jiang et al. 1996, Blancher, Moore et al. 2000, Pugh and Ratcliffe 2003). Under normoxic conditions, prolyl hydroxylases mediate HIF1α ubiquitylation and degradation. However, when cells encounter hypoxic conditions, HIF1α is stabilized and dimerizes with the constitutively expressed HIF1β (also known as ARNT). This complex translocates to the nucleus where it induces the transcription of several target genes, including VEGF-A. HIF1α- and HIF2α (EPAS)-deficient embryos die prematurely due to abnormal vasculature and both proteins have been associated with tumor growth and vascularization (Ryan, Lo et al. 1998, Peng, Zhang et al. 2000, Harris 2002).

NFκB is another transcription factor induced upon tissue hypoxia. Several studies support its implication in cancer progression and angiogenesis (Schmidt, Textor et al. 2007, Xie, Xia et al. 2010). Inhibition of NFκB has also been associated with decreased VEGF-A mRNA expression in breast cancer cells (Shibata, Nagaya et al. 2002). Consensus sites for NFκB have been detected in the mouse *VEGF-A* promoter but, so far, no equivalent have been identified in the human *VEGF-A* promoter. However, NFκB has also been proposed to regulate VEGF-A expression indirectly, by activating HIF1α or JunB (Schmidt, Textor et al. 2007).

JunB belongs to the AP-1 family of transcription factors. These family members form homo- or heterodimers able to bind to the AP-1 binding site on the *VEGF-A* promoter. The first evidence for the implication of JunB in angiogenesis dates back to the 90's. JunB-deficient embryos present with severe growth delay and embryonic lethality due to a deficient feto-maternal circulatory system (Schorpp-Kistner, Wang et al. 1999). JunB plays a critical role in VEGF-A expression. It has been shown to induce VEGF-A expression in response to hypoglycemia as well as to regulate tumor progression and angiogenesis (Textor, Sator-Schmitt et al. 2006, Schmidt, Textor et al. 2007). JunB also induces cell invasion and angiogenesis in

renal cell carcinoma via the production of MMPs and C-C motif ligand-2 (CCL2) (Kanno, Kamba et al. 2012). Yet, in a recent paper, Braun and collaborators show that stromal expression of JunB is dispensable for tumor growth and angiogenesis in mouse models of lung cancer and melanoma (Braun, Strittmatter et al. 2014).

Sp1 can be phosphorylated in response to numerous factors, such as HGF, EGF, TGF-β1 or Erk (Arcondeguy, Lacazette et al. 2013). Once phosphorylated, Sp1 binds to the *VEGF-A* promoter and induces transcription (Novak, Metzger et al. 2003). Sp1 inhibition correlates with decreased angiogenesis and impaired tumor progression in a melanoma model (Ishibashi, Nakagawa et al. 2000).

Finally, the transcription factor Stat3 is constitutively activated in a wide range of cancers, notably in breast carcinomas. Niu and collaborators have identified a Stat3 binding site on the *VEGF-A* promoter (Niu, Wright et al. 2002). Constitutive Stat3 activation promotes *VEGF-A* transcription, while Stat3 inhibition has been associated with decreased promoter activity (Wei, Le et al. 2003).

1.3.3. Alternative pro-angiogenic signaling pathways

VEGF-A is a master regulator of angiogenesis. However, this complex process relies on additional signaling pathways. As previously described, the PDGF-β/PDGFRβ axis supports pericyte recruitment and blood vessel maturation. PDGFRβ inhibition counteracts with pericyte chemoattraction and results in blood vessel regression and tumor growth inhibition (Bergers, Song et al. 2003).

Besides VEGF-A, FGF2 plays a significant role in angiogenesis by inducing endothelial cell migration and proliferation, and FGF2 inhibition has been associated with decreased microvessel density and tumor growth in melanoma (Wang and Becker 1997, Beenken and Mohammadi 2009). Similarly, FGF1 supports tumor angiogenesis and tumor growth (Compagni, Wilgenbus et al. 2000).

Recent evidence suggests a high degree of similitude between sprouting endothelial cells and axonal growth cones. Indeed, a vast majority of proteins implicated in neuronal guidance are also implicated in angiogenesis (Carmeliet and Tessier-Lavigne 2005). These are for example netrins, semaphorins, ephrins, neuropilins and ROBO receptors.

The pleiotropic role of VEGF-A in both tumor angiogenesis and stem cell maintenance makes it a prime target in the fight against cancer.

1.4. Angiogenesis: A good target in cancer therapy?

Cancer is an age-old disease still lacking an effective cure. Conventional chemotherapy kills rapidly dividing cancer cells. However, such treatment presents relatively limited efficacy mainly due to the presence of CSCs with low-division rates; they survive chemotherapy and repopulate the tumor as soon as the treatment ceases. Recent decades have seen the development of targeted therapies, i.e. therapies specifically interfering with cancer-related genes without harming normal cells. Anti-angiogenic therapy belongs to this class of therapeutic approaches.

In its Canon of Medicine, Avicenna already suggested that "removal of blood vessels going to the tumor" might be a good therapeutic strategy to combat cancer. Thousand years later, Algire and colleagues highlighted the importance of blood vessels in primary tumor growth (Algire and Chalkley 1945). This discovery has been confirmed by the work of Judah Folkman in the early 70's (Folkman 1971). Indeed, Folkman suggested that tumors required blood vessels in order to survive and grow and proposed that inhibition of blood supply might induce tumor starvation and hence its shrinkage. Together with the identification of VEGF-A in the late 80's, these observations led to the development of therapeutic strategies targeting tumor angiogenesis (Leung, Cachianes et al. 1989, Ferrara, Hillan et al. 2004).

Two strategies can be used to target angiogenesis. The first one consists in specifically killing endothelial cells to prune blood vessels. The second, proposed by Carmeliet, aims to normalize blood vessels. Tumor angiogenesis is a relatively chaotic process that leads to the formation of a leaky, tortous and dilated vasculature. Blood flux in these vessels is far from optimal. Therefore, it has been suggested that blood vessel normalization could improve tumor irrigation and favor the entrance of chemotherapy in the tumor (Carmeliet and Jain 2011). Vessel normalization can be achieved by using VEGF-A inhibitors that inhibit excessive vessel sprouting or by forcing vessel maturation, for example via inhibition of angiopotein-2 binding to Tie2 receptors (Thurston, Suri et al. 1999).

1.4.1. From neutralizing antibodies to tyrosine kinase inhibitors

The first approach to inhibit angiogenesis consists in the use of monoclonal antibodies. Monoclonal antibodies are produced by hybridomas - that result from the fusion between B cells and myelomas. They inhibit the binding of a ligand to its receptor, either by trapping the ligand (e.g. bevacizumab) or by binding to the receptor (e.g ramucirumab or DC-101). Bevacizumab, a humanized antibody neutralizing VEGF-A was rapidly approved in combination with chemotherapy in the treatment of several cancer types, including metastatic breast cancer (Miller, Wang et al. 2007). It is in the treatment of metastatic colon cancer that bevacizumab revealed the greatest efficacy. Indeed, bevacizumab addition to a combination of irinotecan, fluorouracil and leucovorin (IFL) extended progression-free survival of 4.4 months compared to IFL alone (Hurwitz, Fehrenbacher et al. 2004). At the exception of glioblastoma treatment, bevacizumab is always used in combination with chemotherapy. It is used in the treatment of clear cell renal cell carcinoma in combination with interferon-α and in the treatment of non-small cell lung carcinoma in combination with paclitaxel-carboplatin (Sandler, Gray et al. 2006, Escudier, Pluzanska et al. 2007). However, it has been withdrawn for the treatment of metastatic breast cancer, as it failed to improve patient overall survival (Rose 2011). Indeed, after an initial decrease in tumor growth, therapy resistance develops rapidly, mainly driven by the activation of alternative pro-angiogenic signaling pathways such as IL-17, PDGF/R and FGF/R axes (Compagni, Wilgenbus et al. 2000, Casanovas, Hicklin et al. 2005, Ebos, Lee et al. 2007, Bergers and Hanahan 2008, Chung, Wu et al. 2013).

To circumvent these limitations, tyrosine kinase inhibitors (TKIs) simultaneously targeting several pro-angiogenic signaling pathways have been developed and are currently approved for clinical use (Ebos and Kerbel 2011). TKIs are small molecules able to cross the cell membrane and to bind to the ATP-binding pocket of the tyrosine kinase receptors, leading to their inactivation. To quote only the best-known examples, sunitinib and sorafenib are currently used in clinics. In contrast to bevacizumab, TKIs are not used in combination with chemotherapy, since their broad range of signaling targets makes them relatively toxic on their own. Sunitinib - an inhibitor of VEGFRs and PDGFRs - increases progression-free survival for

patients suffering of gastro-intestinal stromal tumors, but does not improve their overall survival (Escudier, Roigas et al. 2009). It also extends progression-free survival and overall survival of metastatic renal cell carcinoma patients - a highly angiogenic tumor type - and is currently used to treat metastatic neuro-endocrine pancreatic cancer (Motzer, Hutson et al. 2007, Motzer, Hutson et al. 2009, Raymond, Dahan et al. 2011). Sorafenib inhibits VEGFRs, PDGFRs and Raf kinases and is used in the treatment of advanced hepatocellular carcinomas and metastatic renal cell carcinomas (Llovet, Ricci et al. 2008, Escudier, Eisen et al. 2009).

1.4.2. Mechanisms of resistance to anti-angiogenic therapy

As previously described, anti-angiogenic therapy increases progression-free survival. However, mainly due to resistance development, it has only a limited effect on overall survival. Some patients are immediately refractory to the treatment and do not even show a transient benefit. This is the case with pancreatic ductal adenocarcinoma, a tumor type which is particularly hypovascularized (Bergers and Hanahan 2008). These patients are intrinsically resistant to anti-angiogenic therapy. Others will initially respond to the treatment and escape during therapy. This type of resistance is referred to as acquired resistance. Most mechanisms of resistance rely on the fine-tuned interplay between tumor cells, blood vessels and the tumor microenvironment.

Several mechanisms of resistance have been described so far, such as activation of alternative pro-angiogenic signaling, recruitment of bone marrow-derived cells, increased pericyte coverage, increased invasiveness, and metabolic adaptation (Figure 6).

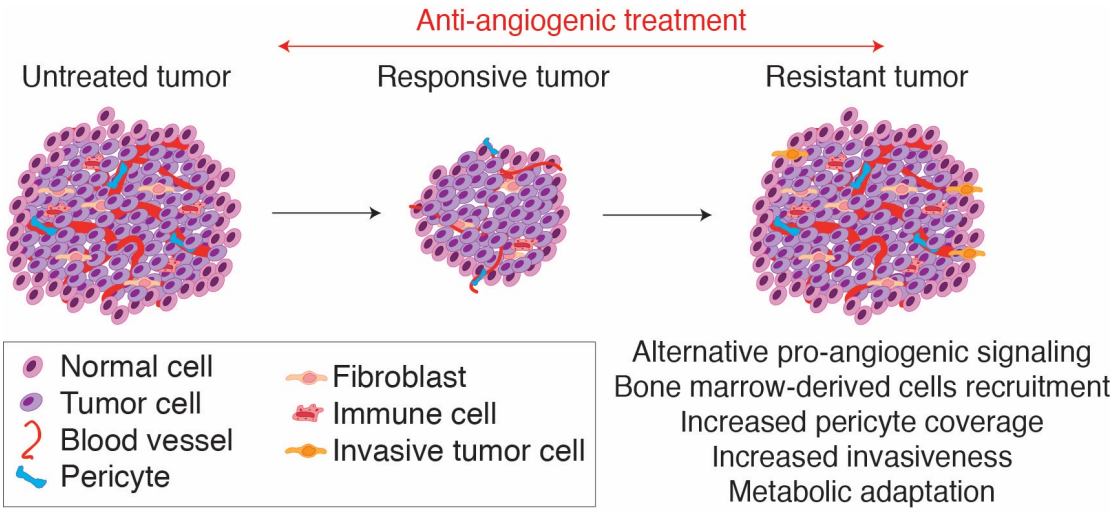

Figure 6: Mechanisms of evasive resistance to anti-angiogenic therapy.
Tumors initial response to anti-angiogenic therapy is associated with decreased vascularization and tumor shrinkage. Tumors can become refractory to anti-angiogenic therapy and resume growth. For this, they can activate alternative pro-angiogenic signaling pathways or recruit bone marrow-derived cells that secrete pro-angiogenic factors. These two mechanisms are associated with revascularization. Alternatively, they can compensate their lack of blood vessel by increasing pericyte recruitment and blood vessel maturation. They can also cope with decreased microvessel density by adjusting their metabolism. Resistance to anti-angiogenic therapy is associated with increased invasiveness and metastatic potential. Figure drawn based on (Bergers and Hanahan 2008).

Activation of alternative pro-angiogenic signaling pathways

Advanced breast cancers do not only rely on VEGF-A but also express an array of additional angiogenesis-promoting factors. FGF2 expression has been proposed to be responsible for the limited response observed in metastatic breast cancers treated with bevacizumab. Activation of alternative pro-angiogenic signaling pathways to overcome VEGF-A inhibition has originally been proposed by Casanovas and collaborators. They observed that RT2 mice treated with DC101, a TKI targeting VEGFR2, overexpress a plethora of pro-angiogenic factors, including FGF1, FGF2, ephrins and angiopoietin1, allowing the tumor to revascularize (Casanovas, Hicklin et al. 2005). Inhibition of FGF signaling reverts resistance development and represses vascularization in this pre-clinical model. Similarly, FGF2 expression has been found increased in the blood of glioblastoma patients treated with a VEGFR inhibitor (Batchelor, Sorensen et al. 2007).

Recruitment of bone marrow-derived cells

Shojaie and colleagues have observed that $CD11b^{+}$ $Gr1^{+}$ monocytes can mediate intrinsic resistance to bevacizumab through the secretion of pro-angiogenic factors (Shojaei, Wu et al. 2007). In another study, bevacizumab treatment has been shown to

promote the recruitment of T helper cells and granulocytes to the tumor. These cells support tumor revascularization through the secretion of VEGF-A-independent pro-angiogenic factors, including Bv8 (Chung, Wu et al. 2013). Similarly, bone marrow-derived fibrocyte-like cells have recently been proposed to mediate resistance to bevacizumab via the production of FGF2 (Mitsuhashi, Goto et al. 2015).

Increased pericyte coverage and vessel maturation

Mature blood vessels are less sensitive to angiogenesis inhibitors (Bergers, Song et al. 2003). Therefore, it has been proposed that targeting pericytes in combination with anti-angiogenic therapy would increase vessel pruning (Sun, Wang et al. 2005). Such an inhibition can be achieved by using pan-TKIs such as sunitinib, which is currently used in the clinics to inhibit VEGFRs and PDGFRs.

Increased invasiveness

Whereas several studies have shown that TKIs significantly reduce primary tumor growth, invasion and metastasis, others have suggested that they might instead promote cell migration and enhance metastatic disease (Padera, Kuo et al. 2008, Ebos, Lee et al. 2009, Paez-Ribes, Allen et al. 2009, Lu, Chang et al. 2012, Sennino, Ishiguro-Oonuma et al. 2012). For example, work from Ebos and collaborators has revealed that despite decreasing primary tumor growth, short-term sunitinib treatment accelerates the development of metastases. Interestingly, treatment of recipient mice with anti-angiogenic therapies prior to tumor cell inoculation has also resulted in significantly enhanced multi-organ metastasis (Ebos, Lee et al. 2009). Anti-angiogenic therapy affects virtually every step of the metastatic cascade (invasion, intravasation, extravasation and colonization of distant tissue). For example, Paez-Ribes and colleagues have reported an increased invasiveness of pancreatic cancer treated with DC101 – a VEGFR2 inhibitor (Paez-Ribes, Allen et al. 2009). Increased tumor invasiveness upon anti-angiogenic therapy can be explained by increased hypoxia observed in treated tumors. Indeed, establishment of a hostile, hypoxic and nutrient-deprived environment has been shown to increase tumor cell invasion through an activation of Met receptor signaling (Pennacchietti, Michieli et al. 2003). Cooke and collaborators have also observed increased metastatic burden after pericyte

depletion, suggesting an increased ability of tumor cells to intra- or extravasate (Cooke, LeBleu et al. 2012).

Metabolic adaptation

More recently, new mechanisms of resistance involving metabolic adaptation processes have been reported. For example, by repressing blood flow in the tumor, anti-angiogenic therapy has been shown to induce hypoxia. HIF1α stabilization induces metabolic reprogramming towards glycolysis that sustains tumor cell survival. Such mechanisms have been associated with the use of bevacizumab in glioblastoma, as well as in ovarian and breast cancer (Keunen, Johansson et al. 2011, Quintieri, Selmy et al. 2014, Curtarello, Zulato et al. 2015). In a similar manner, sunitinib and sorafenib cessation has been associated with increased lipid synthesis and lipogenesis inhibition repressed tumor regrowth and metastasis (Sounni, Cimino et al. 2014).

2. Aim of the study

Angiogenesis is a well-known hallmark of cancer. Its main regulator, Vascular Endothelial Growth Factor A (VEGF-A), plays a central role in tumor progression and has been anticipated to be an appropriate target in cancer therapy. However, despite the approval of several anti-angiogenic therapies, clinical results remain unsatisfactory. Transient benefits are followed by rapid tumor recurrence, associated with increased invasiveness and drug resistance. Therefore a better understanding of the regulation of pro-angiogenic signaling pathways during tumor progression and alternative strategies developed by the tumors to escape anti-angiogenic therapy is urgently required. Gaining insights into these mechanisms will help to open avenues for the development of more efficient therapeutic strategies.

During my Ph.D., I addressed two specific aspects of tumor angiogenesis:

- In one project, I deciphered the molecular mechanisms inducing resistance to anti-angiogenic therapy in a mouse model of breast cancer;

- In a second project, I aimed at identifying the signaling pathways regulating the pro-angiogenic signature acquired during an EMT.

3. Results

3.1. Targeting metabolic symbiosis to overcome resistance to anti-angiogenic therapy

Laura Pisarsky[1*], Ruben Bill[1*], Ernesta Fagiani[1], Sarah Dimeloe[1], Ryan William Goosen[1], Jörg Hagmann[1], Christoph Hess[1], and Gerhard Christofori[1]

[1]Department of Biomedicine, University of Basel, 4058 Basel, Switzerland

*Co-first authors

- Manuscript accepted for publication in Cell Reports -

3.1.1. Abstract

Despite the approval of several anti-angiogenic therapies, clinical results remain unsatisfactory, and transient benefits are followed by rapid tumor recurrence. Here, we demonstrate a potent anti-angiogenic efficacy of the multi-kinase inhibitors nintedanib and sunitinib in a mouse model of breast cancer. However, after an initial regression, tumors resume growth in the absence of active tumor angiogenesis. Gene expression profiling of tumor cells reveals a metabolic reprogramming towards anaerobic glycolysis. Indeed, combinatorial treatment with a glycolysis inhibitor (3PO) efficiently inhibits tumor growth. Moreover, tumors establish metabolic symbiosis, illustrated by the differential expression of MCT1 and MCT4, monocarboxylate transporters active in lactate exchange in glycolytic tumors. Accordingly, genetic ablation of MCT4 expression surmounts the adaptive resistance against anti-angiogenic therapy. Hence, targeting metabolic symbiosis may be an attractive avenue to avoid resistance development to anti-angiogenic therapy in patients.

3.1.2. Introduction

An imbalance between pro and anti-angiogenic factors inducing the formation of new blood vessels from a preexisting vasculature (angiogenesis) has been described as a hallmark of cancer (Hanahan and Weinberg 2011). Hence, targeting angiogenesis might plausibly reduce intra-tumoral levels of oxygen and nutrients, resulting in tumor starvation and thus in reduced tumor growth (Folkman 1971), and anti-angiogenic therapies were rapidly translated with great expectations from preclinical cancer models to clinical practice (Ferrara and Kerbel 2005, Crawford and Ferrara 2009, Carmeliet and Jain 2011). For example, the discovery of Vascular Endothelial Growth Factor (VEGF-A) and its receptors and their identification as a rate-limiting factor for normal and pathological angiogenesis has led to the development of bevacizumab (Avastin®), a humanized monoclonal antibody targeting VEGF-A (Ferrara, Hillan et al. 2004, Ferrara and Kerbel 2005). While some cancer types, such as colorectal (Hurwitz, Fehrenbacher et al. 2004), renal cell (Motzer, Hutson et al. 2007) and pancreatic neuroendocrine carcinoma (PNETs; (Raymond, Dahan et al.

2011), have shown encouraging responses to this therapeutic strategy, numerous other cancer types, in particular breast cancer, seem to be poorly responsive to anti-angiogenic regimens. Indeed, metastatic breast cancer patients treated with standard chemotherapy plus bevacizumab have only benefited from 1-2 months of progression-free survival, and the rapid onset of resistance evidently prevented any overall survival benefit (Miller, Wang et al. 2007, Kerbel 2009, Rose 2011).

These data underline the importance of deciphering the molecular mechanisms underlying intrinsic or adaptive resistance to anti-angiogenic therapy. When blocking the VEGF-A signaling axis in preclinical models, e.g. with bevacizumab, tumors escape by activating alternative pro-angiogenic signaling pathways including fibroblast growth factors (FGFs), platelet-derived growth factors (PDGFs), Bv8/prokineticin, and interleukin-17 (Il-17) (Compagni, Wilgenbus et al. 2000, Casanovas, Hicklin et al. 2005, Bergers and Hanahan 2008, Ferrara 2010, Chung, Wu et al. 2013). In order to counteract the activation of these alternative pro-angiogenic pathways, several multikinase inhibitors and other anti-angiogenic drugs, targeting VEGF-dependent and independent pro-angiogenic signaling pathways, are currently in clinical use or in clinical trials. For example, sorafenib, a multikinase inhibitor targeting RAF, VEGF receptors (VEGFR) 1-3, PDGF receptors (PDGFR) α and β, c-KIT and FLT-3, is currently used for the treatment of hepatocellular carcinoma, and sunitinib, blocking VEGFR1-3, PDGFRα/β, c-KIT and FLT-3, is employed for the treatment of renal cancer. Both inhibitors show significant anti-tumor efficacy in preclinical tumor models and in cancer patients, however, they also suffer from resistance development based on thus far unknown mechanisms (Paez-Ribes, Allen et al. 2009, Raymond, Dahan et al. 2011). Transient benefits are rapidly followed by tumor recurrence, sometimes associated with drug resistance and heightened tumor invasiveness (Bergers and Hanahan 2008, Paez-Ribes, Allen et al. 2009, Ebos and Kerbel 2011, Sennino and McDonald 2012, Singh and Ferrara 2012).

Nintedanib (BIBF-1120) is an even wider-spectrum angiokinase inhibitor targeting VEGFR1-3, PDGFα/β, and FGF receptors (FGFR) 1-4, as well as FLT-3 and SRC family kinases (Hilberg, Roth et al. 2008). Nintedanib has recently shown promising results in pre-clinical models of lung cancer, ductal adenocarcinoma of the pancreas and PNET (Kutluk Cenik, Ostapoff et al. 2013, Awasthi, Hinz et al. 2014, Awasthi, Hinz et al. 2015, Bill, Fagiani et al. 2015). Furthermore, nintedanib has

demonstrated excellent tolerance and potent activity in a phase I clinical trial in early HER2-negative breast cancer (Quintela-Fandino, Urruticoechea et al. 2014) and in a phase III study in combination with chemotherapy in NSCLC leading to its approval as a second-line treatment in combination with docetaxel for advanced NSCLC (Reck, Kaiser et al. 2014, McCormack 2015).

We have therefore assessed the effects of nintedanib in mouse models of cancer. We report that tumors treated with nintedanib or sunitinib do not revascularize during the development of therapy resistance. Instead, the cells located in avascular areas escape the lack of oxygen by shifting their metabolism towards a hyperglycolytic state and by producing lactate, while the cells localized in the vicinity of blood vessels utilize the lactate for oxidative phosphorylation. The data establish metabolic symbiosis (Sonveaux, Vegran et al. 2008, Porporato, Dhup et al. 2011) as an alternative route to develop resistance to anti-angiogenic therapy in mouse models of breast cancer and of insulinoma. Notably, interference with glycolysis or disruption of metabolic symbiosis reinstalls nintedanib's efficacy in repressing tumor growth.

3.1.3. Results

3.1.3.1. Py2T tumors develop evasive resistance to anti-angiogenic therapy

Nintedanib is a potent angiogenesis inhibitor that represses endothelial cell proliferation and induces their apoptosis (EC_{50} < 10nM), yet with limited direct effects on tumor cells (Hilberg, Roth et al. 2008). A stable murine breast cancer cell line (Py2T) established from a breast tumor of an MMTV-PyMT transgenic mouse (Waldmeier, Meyer-Schaller et al. 2012) displayed an EC_{50} of 8 µM *in vitro* which is above the pharmacologically achievable concentration in mice (Hilberg, Roth et al. 2008, Roth, Heckel et al. 2009) (Figure S1A). To study the tumor suppressive efficacy of nintedanib *in vivo*, Py2T cells were orthotopically implanted into the mammary fat pad of immune-competent syngeneic FVB/N female mice. When tumors reached a volume of 15-20 mm^3, where the angiogenic switch had already taken place (Figure S1B), daily treatment with nintedanib was initiated (50 mg/kg, p.o.). During the first week of treatment (short term treatment; ST), tumor volumes as well as tumor weights in nintedanib-treated animals were significantly reduced

(Figure 1A, B). This nintedanib-responsive phase was associated with decreased cell proliferation and increased apoptosis (Figure 1C-F). However, after three weeks of treatment (long term treatment; LT), tumors escaped this therapeutic effect and showed an enhanced tumor growth with increased cell proliferation and reduced apoptosis (Figure 1A, C-F). Apparently, Py2T breast cancer cells escaped nintedanib treatment despite its broad range of inhibitory activities.

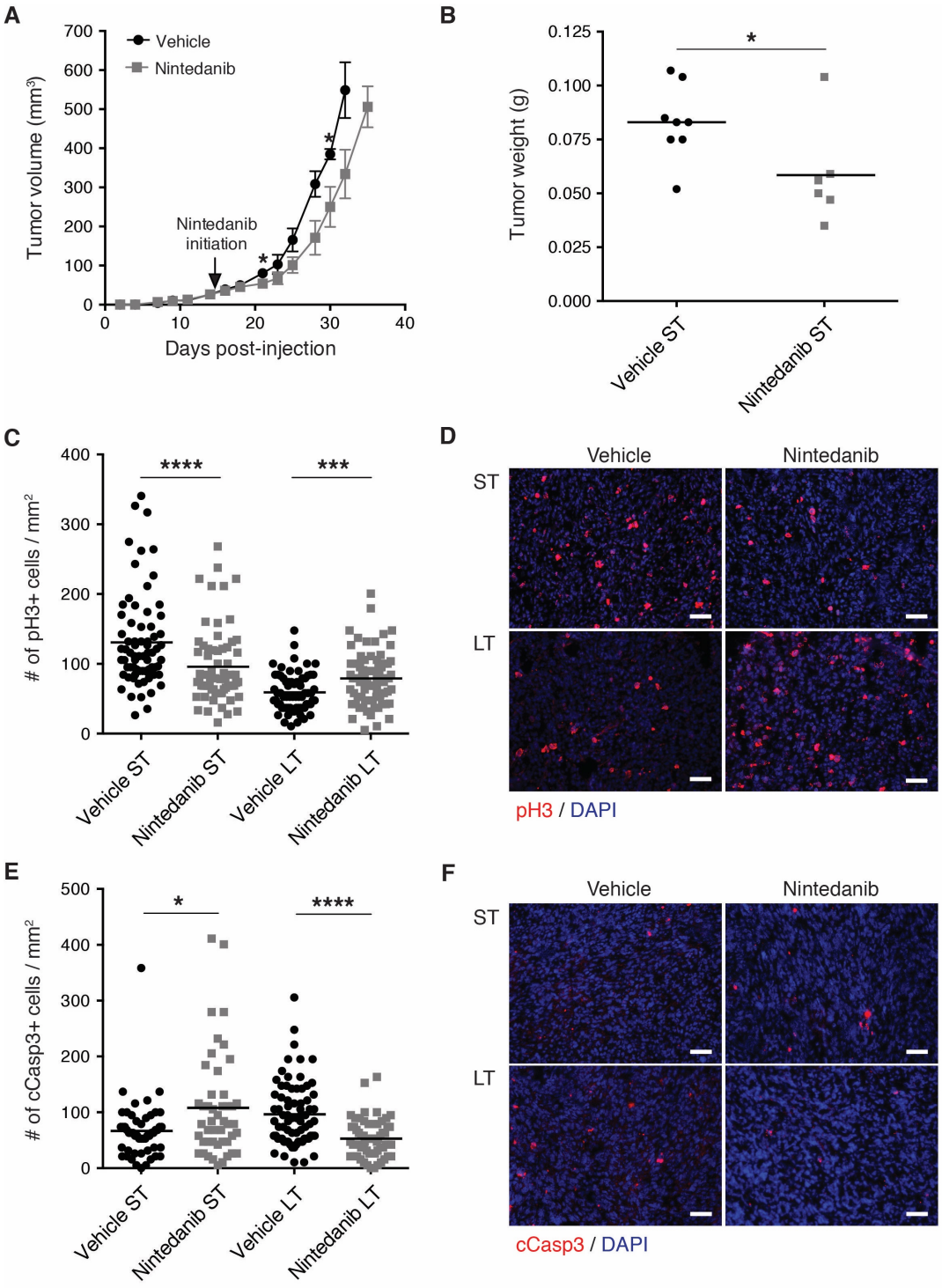

Figure 1. Evasive resistance to anti-angiogenic therapy. Py2T murine breast cancer cells were implanted into the mammary fat pad of FVB/N mice, and treated with nintedanib (50mg/kg daily p.o.) or vehicle control from day 14 after tumor cell implantation.
(A) Primary tumor growth was monitored by assessing tumor volumes over the time of therapy. Values represent mean ± SEM. N=13 mice per group.
(B) Tumor weights were determined after 7 days of nintedanib short-term (ST) treatment. N=6-8 mice per group.
(C-F) Cell proliferation (C, D) and the incidence of apoptosis (E, F) were quantified by immunofluorescence staining for phospho-histone 3 (pH3; red) and cleaved caspase-3 (cCasp3; red), respectively, of tumor sections from short-term (ST) and long-term (LT) vehicle or nintedanib-treated mice. Representative immunofluorescence microscopy pictures are shown in D and F. DAPI was used to visualize cell nuclei. Values represent the number of pH3 positive (C) and cCasp3 positive (E) cells per area of each microscopic field of view. N=5-8 mice per group. Mann–Whitney *U* test. *, $P < 0.05$; ***, $P < 0.001$; ****, $P < 0.0001$. Scale bars, 50 µm. (See also Figure S1).

3.1.3.2. Evasive resistance is not associated with tumor revascularization

We next investigated whether angiogenesis had been reactivated in LT treated Py2T tumors, thereby escaping nintedanib treatment. Intriguingly, microvessel density was found decreased both after ST and LT nintedanib regimen, indicating a potent and stable anti-angiogenic effect of nintedanib, even in a phase of drug-refractory exponential tumor growth (Figure 2A, B; Figure S2A). The numbers of blood vessels became more variable following LT nintedanib treatment, potentially indicating an initiation of revascularization. However, immunofluorescence co-staining for CD31 and cleaved Caspase 3 (cCasp3) revealed increased apoptosis in endothelial cells after ST and LT nintedanib treatment, demonstrating the sustained anti-angiogenic efficacy of nintedanib even after LT treatment (Figure 2C, D). This therapy-resistant tumor growth was not specific for the multi-kinase inhibitor nintedanib; in a head-to-head comparison, Py2T tumors treated with nintedanib and sunitinib displayed comparable tumor growth and reduced microvessel densities after LT treatment (Figure S2B-D).

We next assessed whether Py2T tumors compensate for the lack of blood vessels with increased pericyte coverage. Pericytes promote the maturation and stabilization of blood vessels through PDGFR signaling and thus influence the responsiveness to anti-angiogenic therapy (Hellstrom, Kalen et al. 1999). Interestingly, despite its inhibitory activity on PDGFR signaling, nintedanib did not affect the pericyte coverage of blood vessels resisting nintedanib treatment (Figure 2E; Figure S2E). Nintedanib also did not affect the functionality of the remaining blood vessels as determined by the injection of fluorescence-labeled lectin (Figure 2F; Figure S2F). Consistent with decreased tumor perfusion, pimonidazole staining revealed a significant increase in tumor hypoxia not only in the ST-treated,

nintedanib-responsive tumors but also in the LT-treated, nintedanib-resistant tumors (Figure 2G, H). These data demonstrate a potent anti-angiogenic activity of nintedanib and suggest a new mechanism of therapy resistance by which tumors escape anti-angiogenic therapy in the absence of any revascularization.

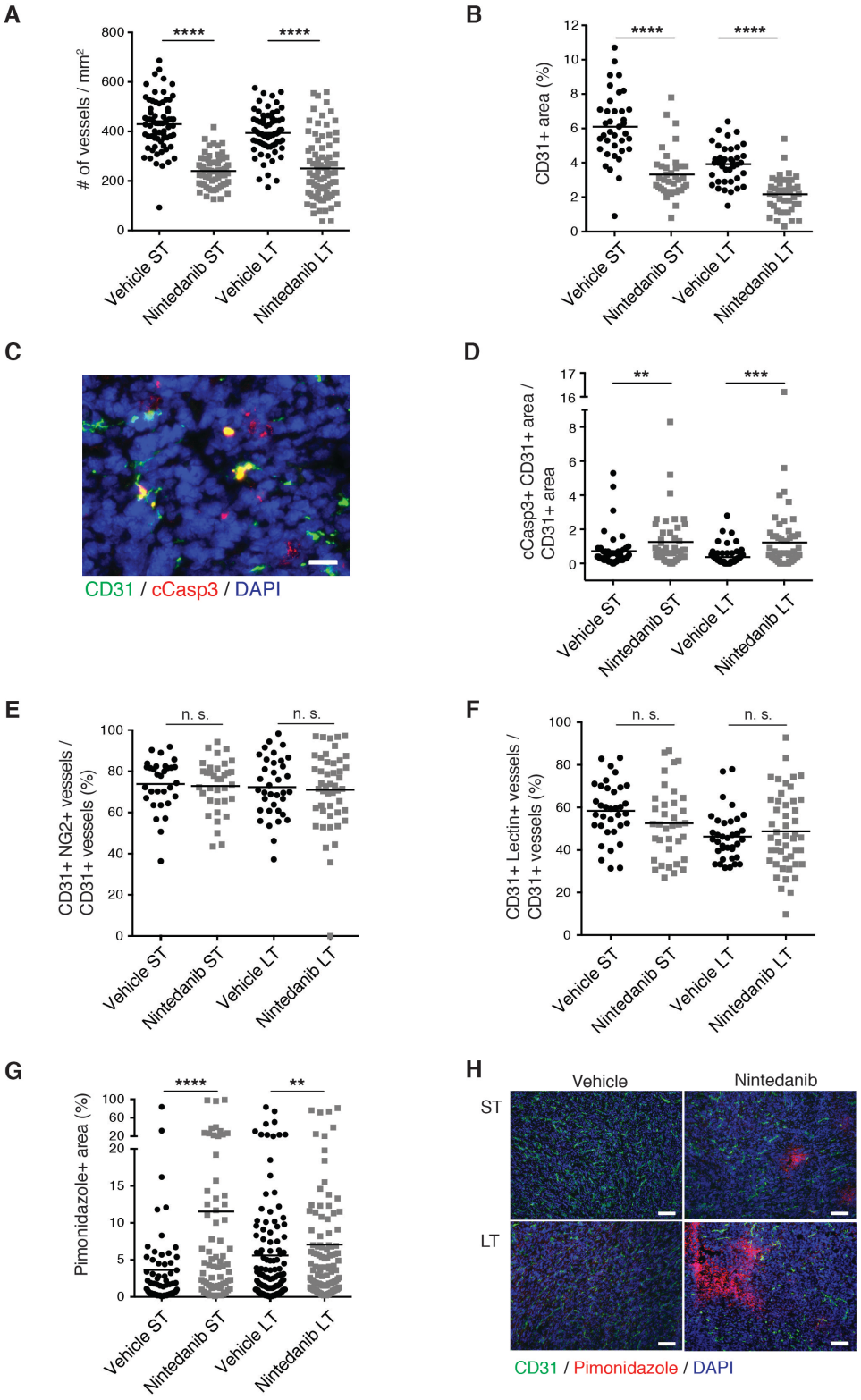

Figure 2. **Lack of tumor revascularization during resistance against nintedanib therapy.**
(A, B) Microvessel densities (A) and CD31-positive area fractions (B) were quantified in Py2T tumors from mice treated for 1 week (ST) or 3 weeks (LT) with vehicle or nintedanib.
(C) Endothelial cell apoptosis (CD31, green; cCasp3, red) is shown on representative immunofluorescence picture of a tumor from a 1 week (ST) nintedanib-treated mouse. DAPI was used to visualize cell nuclei. Scale bars, 20 μm.
(D) Quantification of endothelial cell apoptosis by immunofluorescence co-staining for cCasp3 and CD31 in tumors from ST and LT vehicle or nintedanib-treated mice.
(E) Quantification of the percentage of CD31-positive blood vessels that were in contact with NG2-positive perivascular cells in Py2T tumors from ST and LT vehicle or nintedanib-treated mice.
(F) The functionality of blood vessels was assessed by i.v. injection of FITC-Lectin into Py2T tumor-bearing mice following ST or LT vehicle or nintedanib-treatment. Patent, perfused blood vessels were identified by immunofluorescence staining for CD31 and detection of FITC-Lectin and quantified by counting CD31 and lectin double-positive blood vessels.
(G) Hypoxic areas were identified and quantified by immunofluorescence staining for pimonidazole adducts in Py2T tumors from ST and LT vehicle or nintedanib-treated mice.
(H) Representative pictures of the immunofluorescence co-staining for pimonidazole adducts (red) and CD31 (green) on histological sections of tumors from ST and LT vehicle or nintedanib-treated mice. DAPI staining visualizes cell nuclei. Scale bars, 100 μm.
N = 6-8 mice per group. Mann–Whitney U test. n. s., non significant; **, $P < 0.01$; ***, $P < 0.001$; ****, $P < 0.0001$. (See also Figure S2).

3.1.3.3. Tumor cells become hyperglycolytic to survive hypoxia

To investigate the molecular mechanisms underlying the resistance against nintedanib treatment, we isolated by flow cytometry endothelial and tumor cells from nintedanib-treated and untreated tumors at different time points of resistance development. To facilitate the isolation of tumor cells, Py2T cells were transduced with a retroviral construct expressing a truncated, non-functional form of murine CD8α (Misteli, Wolff et al. 2010). A $CD45^-CD8^+$ population could only be identified in Py2T-$CD8\alpha^+$ tumors and not in wild-type Py2T tumors (Figure S3A). After ST (1 week) and LT (3 weeks) treatment with nintedanib, $CD45^-CD8\alpha^+$ tumor cells and $CD45^-CD8\alpha^-CD31^+$podoplanin$^-$ endothelial cells were sorted by flow cytometry (Figure S3B-D), and changes in gene expression were assessed by DNA oligonucleotide microarray analysis. Surprisingly, endothelial cell gene expression profiles between ST and LT nintedanib-treated tumors did not markedly differ, mainly reflecting endothelial cells undergoing apoptosis (data not shown).

In contrast, gene expression analysis of isolated tumor cells revealed a marked difference between untreated and treated groups. The genes resulting from the comparison between LT nintedanib-treated and untreated tumor cells were subjected to KEGG-pathway analysis which showed an enrichment of metabolic pathways, in particular glycolysis (Figure 3A). Gene Set Enrichment Analysis (GSEA) (Subramanian, Tamayo et al. 2005) also showed an enrichment of glycolysis gene

expression, especially when comparing the gene expression profiles of LT vs. untreated tumor cells, yet also when comparing ST vs. untreated tumor cells (Figure 3B). Glycolysis gene-enrichment also became evident when the gene expression profiles associated with a core set of glycolytic enzymes were visualized using a heat map. Indeed, hierarchical clustering correctly interrelated the three different treatment conditions (Figure 3C). Quantitative RT-PCR analysis confirmed the upregulated expression of most of the glycolytic enzymes upon ST and LT nintedanib treatment, while the expression of genes implicated in mitochondrial biogenesis and oxidative phosphorylation were unaffected (Figure 3D, E).

Because nintedanib-treated tumors exhibited enhanced hypoxia compared to size-matched vehicle-treated tumors (Figure 2G, H), we hypothesized that hypoxia could be a determinant of tumor cell heterogeneity and a direct inducer of the glycolytic shift. As expected, when compared with normoxic cultures, Py2T cells cultured for 3 days in hypoxic conditions (1% O_2) exhibited a significantly increased expression of nine out of ten glycolysis-related transcripts analyzed (Figure S3E).

Together, the data suggest a metabolic adaptation to anti-angiogenic therapy, in which hypoxic tumor cells shift to a hyperglycolytic state to survive and proliferate at reduced oxygen and nutrient supply.

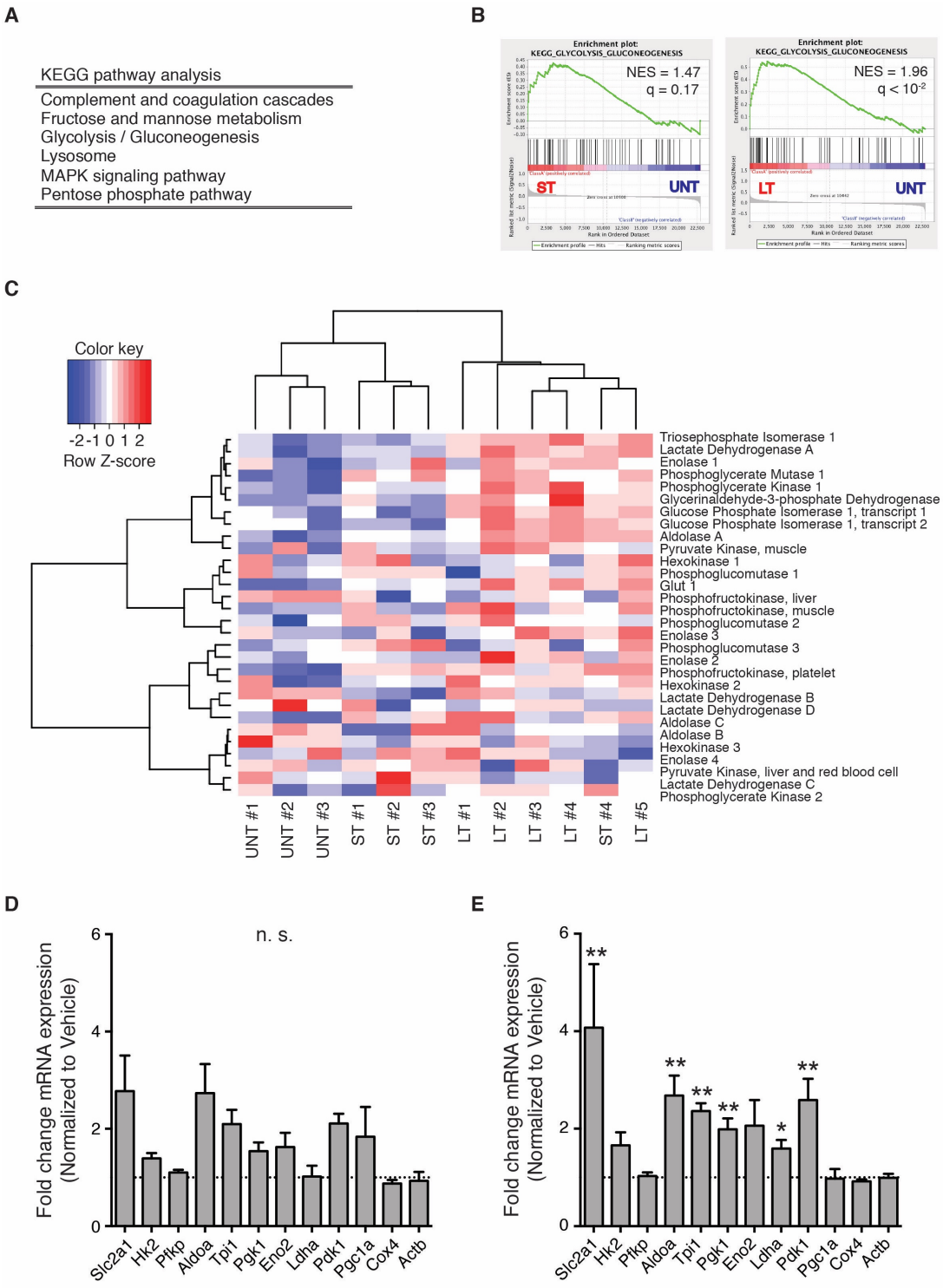

Figure 3. Tumor cells become hyperglycolytic during nintedanib treatment.
(A) Differential gene expression between flow cytometry-isolated LT nintedanib and untreated tumor cells was assessed by Affymetrix microarray analysis. The list of differentially expressed genes was subjected to KEGG pathway analysis.
(B) Gene set enrichment analysis (GSEA) between gene expression profiles of either ST or LT nintedanib and untreated tumor cells. Shown are the normalized enrichment score (NES) and the FDR q-value.
(C) A set of core glycolysis enzymes was used to perform hierarchical clustering of gene expression profiles derived from LT and ST nintedanib and untreated controls.
(D, E) Expression of different glycolysis and mitochondrial activity-related transcripts in ST (D) and LT (E) nintedanib-treated tumors analyzed by quantitative RT-PCR is shown. Data are normalized to

untreated tumors. Shown are mean ± SEM. N = 4 mice per group. Mann–Whitney U test. n. s.: non significant; *, P < 0.05; **, P < 0.01. (See also Figure S3).

3.1.3.4. Therapy resistance establishes metabolic symbiosis

Considering the highly glycolytic phenotype of nintedanib-treated tumor cells, we analyzed lactate production in Py2T tumors. Total lactate production was not increased in nintedanib-treated tumors compared to vehicle-treated tumors (Figure S4A), possibly explained by a fast metabolic utilization of lactate. The alternation between highly hypoxic and normoxic areas in nintedanib-treated tumors (Figure 2H), together with comparable levels of lactate between nintedanib and vehicle-treated tumors, suggested the establishment of lactate-based metabolic symbiosis (Sonveaux, Vegran et al. 2008). In such symbiosis, hypoxic glycolytic cells use glucose to produce high levels of lactate that is rapidly exported through monocarboxylate transporter 4 (MCT4), mainly a lactate exporter. Oxidative cells located in perfused areas express MCT1, mainly a lactate importer, allowing them to take up lactate and directly fuel their Krebs cycle. These cells do not rely on glycolysis, and glucose can bypass them and diffuse to hypoxic areas, where it is taken up by glycolytic cells expressing high levels of hypoxia-induced Glut1 to produce lactate (Sonveaux, Vegran et al. 2008)(Sonveaux, Vegran et al. 2008)(Sonveaux, Vegran et al. 2008)(Sonveaux, Vegran et al. 2008)(Sonveaux, Vegran et al. 2008)(Sonveaux, Vegran et al. 2008).

We assessed the establishment of metabolic symbiosis during the development of resistance against nintedanib-mediated anti-angiogenic therapy in the Py2T transplantation model of breast cancer. Immunofluorescence staining for MCT1 and MCT4 demonstrated a diffuse baseline expression of MCT1 that remained unchanged during nintedanib treatment, whereas MCT4 was highly expressed in non-vascularized areas of LT nintedanib-treated tumors and to a lesser extent in ST-treated tumors (Figure 4A; Figure S4B-D). Similar results were observed in sunitinib-treated tumors (Figure S4E). To assess the generality of our findings, we analyzed microvessel densities and MCT4 expression in tumors of Rip1Tag2 transgenic mice that have been treated with nintedanib (Bill, Fagiani et al. 2015). The Rip1Tag2 transgenic mouse model of pancreatic neuroendocrine carcinoma is highly sensitive to anti-angiogenic therapies and has been instrumental for compound testing and

subsequent successful translation to the treatment of patients with pancreatic neuroendocrine tumors (PNETs) (Tuveson and Hanahan 2011). With Rip1Tag2 mice, nintedanib treatment was initiated at 10 weeks of age, which prolonged median survival from 24 days in control-treated animals to 55 days in nintedanib-treated animals. Comparable to the Py2T breast cancer model, Rip1Tag2 mice also developed resistance to nintedanib therapy and did not display any revascularization in therapy-refractory tumors (Figure S4F), and MCT4 expression was also only found in tumors after prolonged nintedanib treatment (Figure S4G).

To further assess the establishment of metabolic symbiosis in nintedanib therapy-resistant tumors we assessed by immunofluorescence microscopy analysis the expression and localization of markers for hypoxia (pimonidazole), glucose uptake (Glut1), lactate export (MCT4), mitochondrial biogenesis and oxidative phosphorylation (PGC1α, COX IV) (Wu, Puigserver et al. 1999, LeBleu, O'Connell et al. 2014). Notably, the mean shortest distance between MCT4-expressing cells and the nearest blood vessel was increased in LT tumors, although not with statistical significance (Figure 4B), indicating the expression of MCT4 in hypoxic areas. Indeed, the expression of hypoxia-induced glucose transporter 1 (Glut1) correlated with the expression of hypoxia-induced MCT4 and with the hypoxia-marker pimonidazole in the hypoxic areas of nintedanib LT tumors (Figure 4C-G and S4H-I). The expression of MCT4 co-localized with pimonidazole as well (Figure 4H, I and S4J). On the other hand, the expression of PGC1α and COXIV did not specifically localize with vascularized or non-vascularized areas, yet increased in ST and LT nintedanib-treated tumors (Figure S4K, N). Curiously, the co-expression of MCT4 with PGC1α and COX IV was decreased and unchanged, respectively, in ST nintedanib-treated tumors, yet it was unchanged with PGC1α and increased with COX IV comparing LT vehicle and nintedanib-treated tumors (Figure S4L, M, O, P). These results suggest a first wave of tumor hypoxia and glycolysis followed by a homeostasis of metabolic symbiosis between anaerobic glycolysis and aerobic oxidative phosphorylation during prolonged anti-angiogenic therapy.

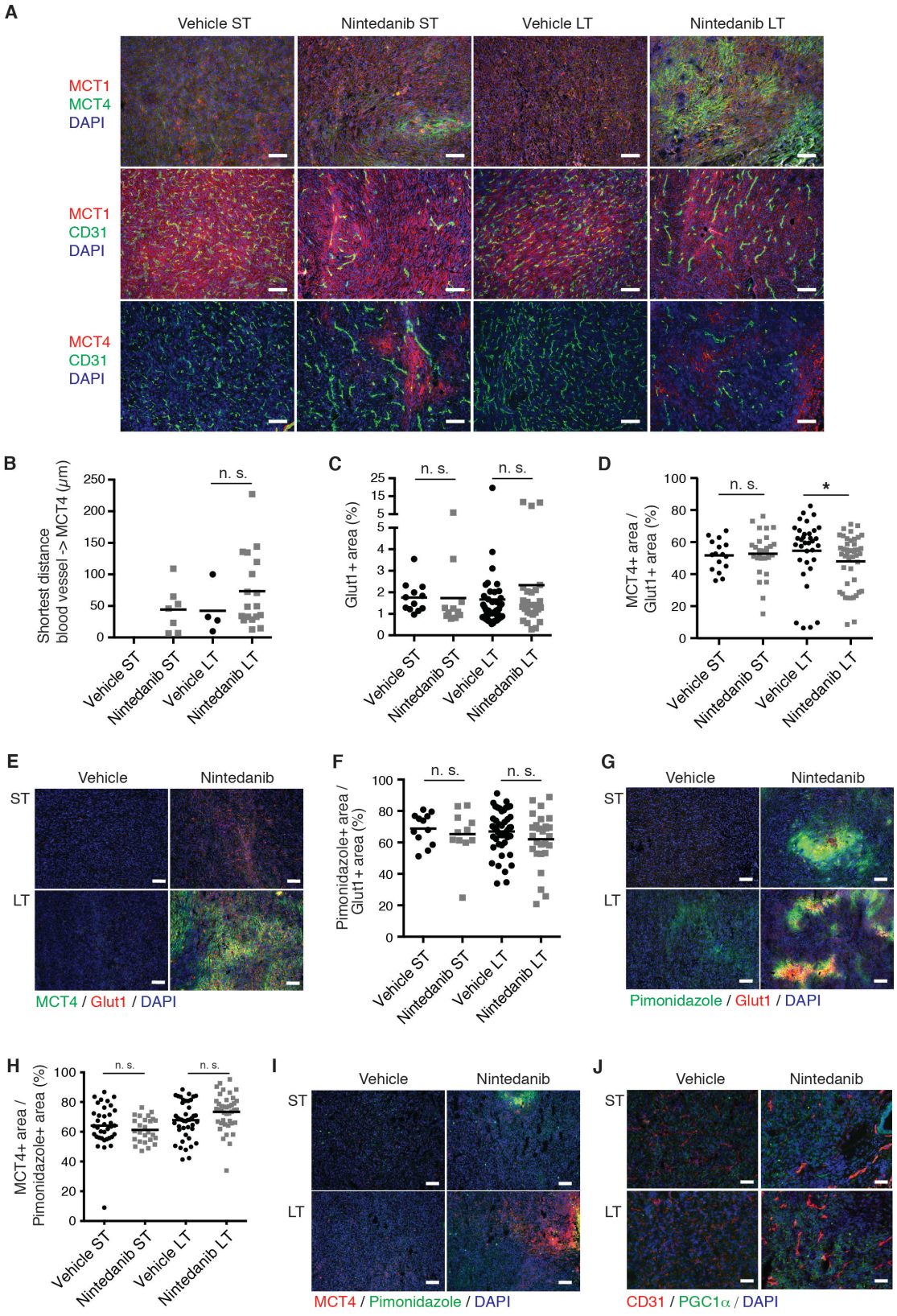

Figure 4. Tumors establish metabolic symbiosis to overcome nintedanib treatment.
(A) Representative pictures of combinatorial immunofluorescence staining for MCT1, MCT4 and CD31 on histological sections of tumors from mice treated with either vehicle or nintedanib (50 mg/kg/day) are shown, as indicated. DAPI was used to visualize cell nuclei. Scale bars, 100 µm.
(B) Quantification of the closest distance separating blood vessels from MCT4+ areas by immunofluorescence co-staining for MCT4 and CD31 on Py2T tumors from ST and LT vehicle or

nintedanib-treated mice. Note that in ST vehicle-treated tumors MCT4 was not significantly expressed and thus the distance to blood vessels could not be determined.
(C, D) Quantification of the Glut1+ area fraction (C) and the MCT4+ area fraction within Glut1+ areas (D) by immunofluorescence co-staining for MCT4 and Glut1 on Py2T tumors from ST and LT vehicle or nintedanib-treated mice.
(E) Representative microphotographs of immunofluorescence co-staining for MCT4 and Glut1 on histological sections of tumors from ST and LT vehicle or nintedanib-treated mice. DAPI is used to visualize cell nuclei. Scale bars, 100 µm.
(F) Quantification of the hypoxic (pimonidazole+) area fraction within Glut1+ areas by immunofluorescence co-staining for pimonidazole and Glut1 on Py2T tumors from ST and LT vehicle or nintedanib-treated mice.
(G) Representative microphotographs of immunofluorescence co-staining for pimonidazole and Glut1 on histological sections of tumors from ST and LT vehicle or nintedanib-treated mice. DAPI was used to visualize cell nuclei. Scale bars, 100 µm.
(H) Quantification of the MCT4+ area fraction within pimonidazole+ areas by immunofluorescence co-staining for MCT4 and pimonidazole on Py2T tumors from ST and LT vehicle or nintedanib-treated mice.
(I) Representative microphotographs of immunofluorescence co-staining for MCT4 and pimonidazole on histological sections of tumors from ST and LT vehicle or nintedanib-treated mice. DAPI is used to visualize cell nuclei. Scale bars, 100 µm.
(J) Representative microphotographs of immunofluorescence co-staining for PGC1α and CD31 on histological sections of tumors from ST and LT vehicle or nintedanib-treated mice. DAPI is used to visualize cell nuclei. Scale bars, 50 µm.
N = 4 mice per group. Mann–Whitney U test. n.s., non significant; *, $P < 0.05$; **, $P < 0.01$. (See also Figure S4).

3.1.3.5. Targeting glycolysis or metabolic symbiosis delays resistance development

The small molecule 3-(3-pyridinyl)-1-(4-pyridinyl)-2-propen-1-one (3PO) inhibits the glycolytic activator phosphofructokinase-2/fructose-2,6-bisphosphatase 3 (PFKFB3) in endothelial cells (Schoors, De Bock et al. 2014). Its combined activity as a glycolysis and endothelial cell inhibitor made it a prime compound to overcome glycolysis-induced resistance to anti-angiogenic therapy (Rivera and Bergers 2014)(Rivera and Bergers 2014)(Rivera and Bergers 2014)(Rivera and Bergers 2014)(Rivera and Bergers 2014)(Rivera and Bergers 2014). While single treatment with nintedanib significantly repressed tumor growth in Py2T-transplanted mice, single treatment with 3PO only marginally delayed it (Figure 5A, B). Notably, the combined treatment with nintedanib and 3PO showed an additive effect on tumor growth inhibition. This combined effect was not mediated by an additive anti-angiogenic effect, since the microvessel densities between the nintedanib single and the nintedanib plus 3PO combination treatments were not significantly altered (Figure 5C). Consistent with its ability to normalize blood vessels single treatment with 3PO significantly increased pericyte coverage and thus vessel

functionality, possibly explaining the limited repression of tumor growth despite the significant decrease in microvessel density (Figure 5D) (Schoors, De Bock et al. 2014). This effect was abrogated upon combined 3PO and nintedanib treatment.

To determine the early effects of 3PO treatment on nintedanib-treated tumors, Py2T transplanted mice were first treated with nintedanib for eight days and then subjected to treatment with 3PO and nintedanib for subsequent five days. While nintedanib significantly repressed tumor growth upon short-term treatment, 3PO treatment did not add further tumor repression (Figure S5A, B). However, the extent of tumor hypoxia and the rate of tumor cell apoptosis specifically in the hypoxic tumor areas significantly increased upon combined nintedanib/3PO treatment (Figure S5C-E). Collectively, these results suggest that the inhibition of glycolysis is one avenue of overcoming resistance to anti-angiogenic therapy with multi-kinase inhibitors.

To determine whether the inhibition of metabolic symbiosis could overcome the development of resistance against anti-angiogenic therapy, we generated Py2T cell lines that were devoid of MCT4 by CRISPR/Cas9-mediated knockout of the *Slc16a3* gene (MCT4 is known as Solute carrier 16 a3; Slc16a3). Two stable cell clones (CRISPR MCT4 #1 and #2), which showed targeted recombination in the *Slc16a3* gene and did not express MCT4 protein anymore were used for further experimentation (Figure S5F). The loss of MCT4 expression in these clones significantly repressed tumor growth as compared to wild type cells under treatment with nintedanib treatment leading to an additive effect in repressing tumor growth kinetics and final tumor weights (Figure 5E, F). These results were confirmed by shRNA-mediated ablation of MCT4 expression (shMCT4) in Py2T cells (Figure S5G). The loss of MCT4 expression in shMCT4 cell lines significantly retarded tumor growth kinetics and final tumor weights under treatment with nintedanib as compared to shCtrl cells (Figure S5G, H, I). However, after a first delay, shMCT4 tumors resumed growth. Immunofluorescence staining for CD31 did not reveal any increase in microvessel density in nintedanib-treated shMCT4 tumors, excluding an escape route by revascularization (Figure S5J). Instead, we observed an increase of MCT4 expression both at the protein and mRNA level in nintedanib-treated shMCT4 tumors (Figure S5K, L), suggesting that cells with poor shRNA-mediated knockdown efficiency developed a selective growth advantage and elicited tumor recurrence.

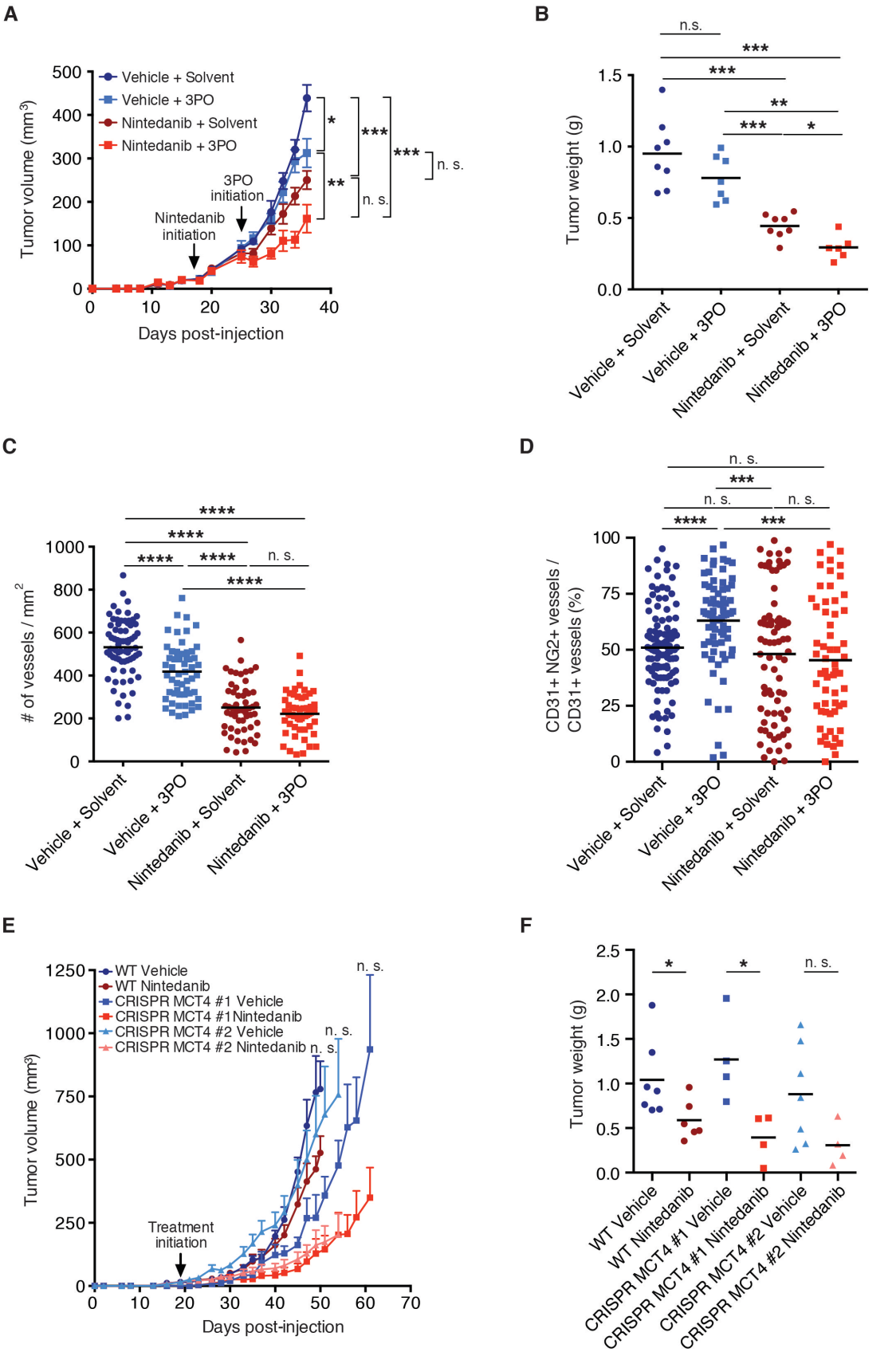

Figure 5. Targeting glycolysis or metabolic symbiosis in combination with nintedanib treatment delays tumor growth.

(A, B) Primary tumor growth over time (A) and tumor weights at the experimental end point (B) of mice treated with either vehicle or nintedanib (50 mg/kg/day) in combination with 3PO (70 mg/kg/day)

or solvent are shown. 3PO treatment was initiated 8 days after the initiation of nintedanib treatment and then continued as combinatorial treatment (long-term treatment). In (A), data are displayed as mean tumor volumes ± SEM.
(C) Quantification of microvessel densities by immunofluorescence staining for CD31 on histological tumor sections from long-term nintedanib and 3PO-treated mice. Values represent the number of counts per each area of microscopic field of view and means are displayed. N = 6-8 mice per group.
(D) Pericyte coverage was assessed by immunofluorescence staining for CD31 and NG2 on histological tumor sections from long-term nintedanib and 3PO-treated mice. Values represent the percentage of NG2+ blood vessels and means are displayed. N = 4-5 mice per group.
(E, F) Primary tumor growth over time (E) and tumor weights at the experimental end point (F) of mice injected with Py2T WT or Py2T CRISPR MCT4 #1 and #2 cells and treated with either vehicle control or nintedanib (50 mg/kg/day) are shown. Nintedanib treatment was initiated 19 days after tumor cell injection, once the tumors were palpable. Mice injected with CRISPR MCT4 #1 cells presented a delayed tumor onset and were therefore treated once the tumors became palpable (days 27-38). In (E), data are displayed as mean tumor volumes ± SEM. N = 4-7 mice per group.
Mann–Whitney U test. n.s., non significant; *, $P < 0.05$; **, $P < 0.01$; ***, $P < 0.001$; ****, $P < 0.0001$. (See also Figure S5).

3.1.3.6. Hypoxia-induced glycolysis is reverted by 3PO and loss of MCT4

The results presented above beg the question whether in Py2T tumor cells hypoxia-induced glycolysis is directly affected by treatment with nintedanib and 3PO or the loss of MCT4 expression. Thus, we performed extracellular flux analysis by 'Seahorse' methodology to determine the oxygen consumption rate (OCR) as a measure of oxidative phosphorylation and the extracellular acidification rate (ECAR) as a measure of glycolysis. As expected, under hypoxic conditions, Py2T cells exhibited increased ECAR (glycolysis) and decreased OCR (oxidative phosphorylation) as compared to normoxic conditions (Figure 6A, B). When directly quantified, hypoxic cells had reduced ATP-coupled OCR, increased ECAR, unchanged glycolytic capacity, and decreased glycolytic reserve as compared to cells cultured under normoxia (Figure 6C-F). To determine any effects of therapeutic treatments on the rates of glycolysis and oxidative phosphorylation, the ratios between ECAR and OCR were determined in wild type or MCT4 knockout Py2T cells cultured under normoxia or hypoxia and treated with solvent, nintedanib or 3PO. These experiments revealed that nintedanib did not affect the ratio between ECAR and OCR (Figure 6G), while 3PO reduced this ratio, i.e. it decreased glycolysis and increased oxidative phosphorylation, under hypoxic but not under normoxic conditions (Figure 6H). The genetic ablation of MCT4 expression also reduced ECAR/OCR only under hypoxic growth conditions (Figure 6I), which also resulted into increased tumor cell apoptosis and cell cycle arrest (Figure 6J, K).

Taken together, the data show that anti-angiogenic resistance can occur via the establishment of metabolic symbiosis and that interfering with metabolic symbiosis can overcome resistance to anti-angiogenic therapy with multi-kinase inhibitors.

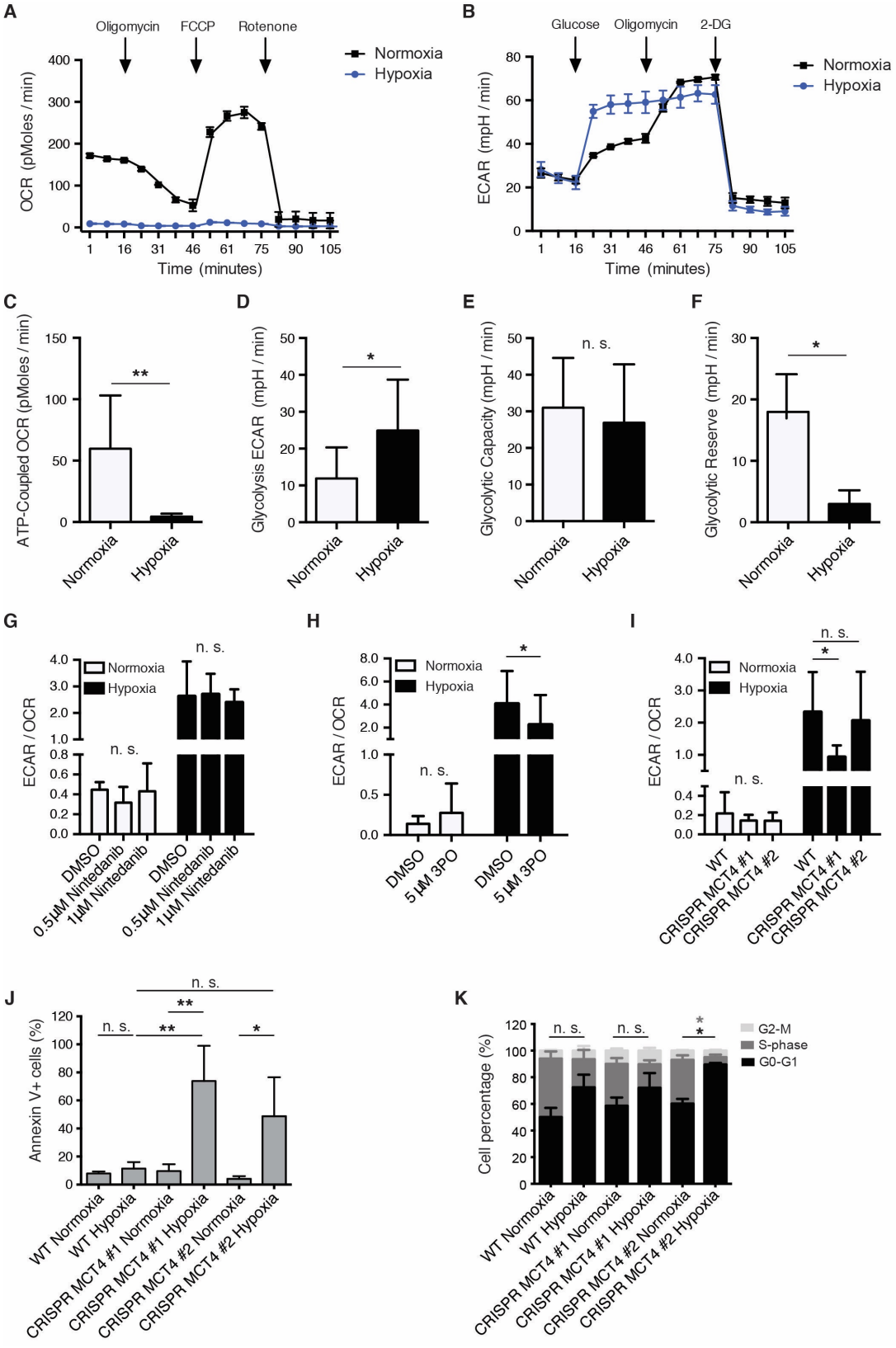

Figure 6. Glycolysis induced by hypoxia can be reverted by treatment with 3PO or the loss of MCT4.
(A, B) Shown are the measurements of representative oxygen consumption rates (A; OCR) and extracellular acidification rates (B; ECAR) of Py2T cells cultured in normoxic or hypoxic conditions. N = 5.
(C-F) Quantification of ATP-coupled respiration (C), glycolysis (D), glycolytic capacity (E) and glycolytic reserve (F) of Py2T cells cultured under normoxic or hypoxic conditions. See Supplemental Experimental Procedures for details). Data are displayed as mean ± SD. N = 5 (glycolytic reserve: N=4). Statistical significance was calculated using 2-way ANOVA test.
(G-H) ECAR/OCR ratio of Py2T cells cultured under normoxic or hypoxic conditions and treated with DMSO, 0.5 μM or 1 μM nintedanib (G) or 5 μM 3PO (H). Data are displayed as mean ± SD. N = 4. 2-way ANOVA test.
(I) ECAR/OCR ratio of Py2T WT cells or Py2T CRISPR MCT4#1 and #2 cells cultured under normoxic or hypoxic conditions. Data are displayed as mean ± SD. N = 4. 2-way ANOVA test.
(J) The percentages of apoptotic Py2T WT cells or Py2T CRISPR MCT4 #1 and #2 cells cultured under normoxic or hypoxic conditions were assessed using flow cytometry analysis of Annexin V-expressing cells. Data are displayed as mean ± SD. N = 3. 1-way ANOVA test.
(K) Cell cycle analysis for Py2T WT cells or Py2T CRISPR MCT4 clones #1 and #2 cultured under normoxic or hypoxic conditions was performed using EdU staining. Data are displayed as mean ± SD. N = 3. 2-way ANOVA test.
n.s., non significant; *, $P < 0.05$; **, $P < 0.01$.

3.1.4. Methods

Mice

FVB/N mice were kept and bred under specific pathogen-free (SPF) conditions. The generation and characterization of Rip1Tag2 transgenic mice has been described elsewhere (Hanahan 1985). All experiments were performed following the rules and legislations of the Cantonal Veterinary Office, Basel-Stadt, Switzerland and the Swiss Federal Veterinary Office (SFVO) under licence numbers 1878, 1907 and 1908.

Cell lines and orthotopic tumor cell transplantation

Py2T murine breast cancer cells were cultured as previously described (Waldmeier, Meyer-Schaller et al. 2012). $5x10^5$ cells were orthotopically injected into the mammary gland number 9 of 7-11 weeks old female FVB/N mice under isoflurane/oxygen anesthesia. Tumor length (l) and width (w) were assessed 3 times per week using a vernier caliper and tumor volume (V) was calculated using the formula $V=0.543*l*w^2$.

Therapy studies, RNA isolation, Quantitative RT-PCR, Immunofluorescence microscopy analysis, Flow cytometry, Microarray analysis and Bioinformatical analysis

See Supplemental Experimental Procedures

Establishment of CRISPR MCT4 cell lines

Subconfluent Py2T cells were transfected with 2 µg of MCT4 CRISPR/Cas9 KO plasmid and 2 µg of MCT4 HDR plasmid (Santa Cruz, sc-429828 and sc-429828HDR, respectively). Successfully transfected cells were selected by puromycin treatment (5 µg/ml) and FACS-sorted based on their RFP expression. Single clones were derived and validated using PCR primers flanking the sequences targeted by the gRNAs, subsequent sequencing and Western blot analysis. Prior to *in vivo* experiments, the RFP and puromycin resistance cassettes were removed using infection with adenovirus expressing Cre recombinase (Ad-Cre).

Extracellular metabolic flux analysis

For details see Supplemental Information.

Statistical analysis

Data analysis and graph generation was performed using GraphPad Prism 6 (GraphPad Prism Software Inc.).

3.1.5. Discussion

In this and in the accompanying reports by Hanahan and colleagues (Allen et al.) and Casanovas and colleagues (Jimenez-Valerio et al.), we report the intriguing finding that a glycolytic shift underlies the development of resistance to anti-angiogenic therapy with multi-kinase inhibitors. Notably, in response to the efficient repression of tumor angiogenesis, tumors compartmentalize into hypoxic regions at a distance from blood perfusion and into normoxic regions in the vicinity of mature and functional blood vessels. The hypoxic tumor cells exhibit high glucose uptake by the hypoxia-induced expression of Glut1 and they efficiently generate and export lactate by the hypoxia-induced expression of the lactate exporter MCT4. Conversely, the normoxic tumor cells take up the lactate produced by the hypoxic tumor cells and oxygen from nearby blood vessels and fuel both into oxidative phosphorylation (Figure 7). Such aspect of metabolic intra-tumoral heterogeneity is portrayed by the concept of metabolic symbiosis (Sonveaux, Vegran et al. 2008).

Here, we have analyzed the efficacy of the angiokinase inhibitors nintedanib and sunitinib in a preclinical mouse model of breast cancer and in the Rip1Tag2 transgenic mouse model of pancreatic neuroendocrine cancer. Treatment of Py2T tumor-bearing mice and of Rip1Tag2 mice with the angiogenesis inhibitors has lead to a significant therapeutic response, characterized by increased tumor and endothelial cell apoptosis, decreased tumor cell proliferation and reduced tumor size. However, despite the potent anti-angiogenic efficacies, the treated tumors rapidly escape therapy. Evasive resistance to anti-angiogenic therapy has previously been reported to rely partially on the redundancy of pro-angiogenic growth factors leading to tumor revascularization (Bergers and Hanahan 2008, Ferrara 2010, Chung, Wu et al. 2013). Intriguingly, the nintedanib and sunitinib-resistant tumors do not show any evidence of revascularization. Rather, with the reduction in tumor perfusion, hypoxia is increased in resistant tumors, and microarray gene expression analysis reveals a metabolic shift to glycolysis in the resistant tumor cells. Indeed, glycolysis and glucose transport-related genes are well known targets of hypoxia-induced cellular adaptations (Harris 2002), and glycolysis induction has been recently described in response to VEGF-inhibitors (Kumar, Wigfield et al. 2013, Curtarello, Zulato et al. 2014).

The tumor cells′ shift to glycolysis as a mechanism underlying resistance against anti-angiogenic therapy offers the opportunity of defeating therapy-resistance by interfering with glycolysis. Indeed, in this and in the accompanying reports (Allen et al; Jimenez-Valerio et al.), combination therapy involving angiokinase inhibitors with 3PO (our work), a glycolytic flux inhibitor (Clem, Telang et al. 2008, Schoors, De Bock et al. 2014), or with rapamycin, an mTOR and glycolysis inhibitor (presented in the accompanying papers), surmounts resistance to treatment. However, combination treatment of nintedanib with 2-deoxyglucose, a competitive inhibitor of the production of glucose-6-phosphate from glucose (Wick, Drury et al. 1955), did not delay tumor growth, most likely due the fact that we have been unable to supply the very high concentrations of 2-deoxyglucose in tumors that would be pharmacologically active (data not shown). Dichloroacetate (DCA), a drug inhibiting pyruvate dehydrogenase kinase and thus promoting glucose oxidation over glycolysis by increasing the pyruvate flux into mitochondria (Michelakis, Sutendra et al. 2010), also has not shown any effect on tumor growth (data not shown). Hence, the

pharmacological targeting of glycolysis in the context of anti-angiogenic therapy may be more complex than anticipated.

Along these lines, despite a clear hypoxia-response pattern to nintedanib therapy, high-throughput metabolomic analysis of tumor lysates from treated mice has failed to show any significant differences in central carbon metabolism between nintedanib LT and untreated tumors (data available upon request). However, according to the hypothesis of a metabolic symbiosis and based on our detailed *in situ* analysis of the expression of markers of glycolysis and oxidative phosphorylation, the metabolomic analysis of tumors *ex vivo* may be obscured by the concomitant presence of cells using hypoxia/glycolysis or oxidative phosphorylation in the same tumor. We have thus directly analyzed the hypoxia-induced metabolic shift between glycolysis and oxidative phosphorylation in cultured tumor cells by 'Seahorse' technology and have found that inhibition of glycolysis by 3PO as well as the genetic ablation of MCT4 expression repress hypoxia-induced glycolysis and induce cell cycle arrest and apoptosis.

Regions with higher oxygen partial pressure metabolize lactate produced in hypoxic areas and thus increase the diffusion capacity of oxygen and glucose. Indeed, increased expression of MCT4 has been correlated with poor prognosis in melanoma and breast cancer (Ho, de Moura et al. 2012, Doyen, Trastour et al. 2014). Accordingly, the genetic ablation of MCT4 expression in Py2T tumors treated with nintedanib show significantly delayed tumor growth. Our data therefore suggest that i) despite the broad range activities of the multi-kinase inhibitors nintedanib and sunitinib, tumors can still escape treatment; ii) nintedanib and sunitinib resistance does not occur via tumor revascularization but is induced by a metabolic shift towards glycolysis and the establishment of metabolic symbiosis; iii) nintedanib and sunitinib treatment should be used in combination with glycolysis/metabolic symbiosis inhibitors for long-term efficacy (Figure 7). Along these lines, it has been recently reported that the genetic disruption of MCT1 or MCT4 represses breast tumor growth (Morais-Santos, Granja et al. 2015) and sensitizes glycolytic tumor cells to treatment with phenformin, an inhibitor of mitochondrial complex I (Marchiq and Pouyssegur 2015). However, complicating things, a recent investigation of metabolic changes in tumors after cessation of sunitinb or sorafenib therapy has revealed a metabolic shift

to lipid synthesis, and blockade of lipidogenesis has inhibited tumor regrowth (Sounni, Cimino et al. 2014).

In conclusion, the data presented here and in the accompanying reports underscore the variety of evasive responses to anti-angiogenic and likely to other targeted therapies. The establishment of metabolic symbiosis adds not only another level of complexity but also a number of novel drugable targets to the design of combinatorial therapies. The results also emphasize the importance of intra-tumoral heterogeneity as therapy response, in particular with regard to oxygen and nutrient availability. Such heterogeneity likely masks critical adaptation mechanisms when performing cross-sectional analysis without spatial resolution.

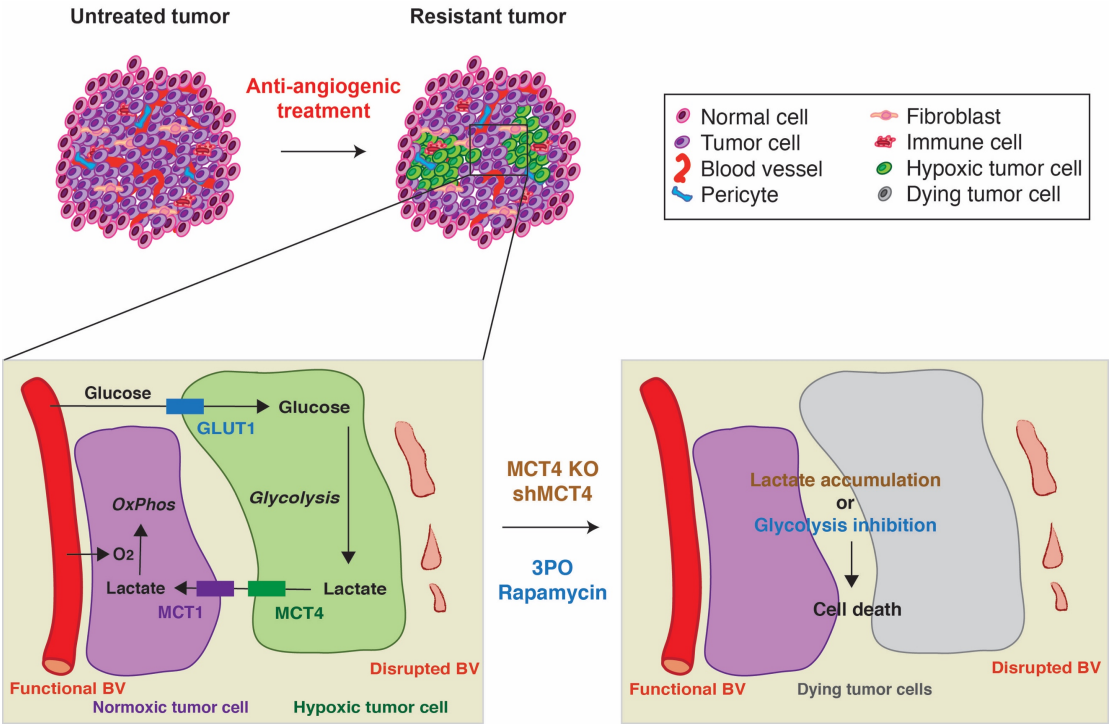

Figure 7. Targeting metabolic symbiosis overcomes resistance to anti-angiogenic therapy. Anti-angiogenic therapy induces hypoxia and reduces the supply of nutrients. As a result, tumor cells shift their metabolism towards a hyperglycolytic state and establish metabolic symbiosis: tumor cells in hypoxic areas upregulate glycolysis, increase lactate production and export lactate via MCT4. On the other hand, lactate is taken up by tumor cells in more oxygenated regions of the tumor and is directly fueling the citric acid cycle and thus oxidative phosphorylation. As a consequence, tumor cells in normoxic tumor regions reduce glucose consumption, which increases its diffusion distance. Ablating MCT4 expression (MCT4 KO or shMCT4) or inhibition of glycolysis (3PO) disrupts this homeostatic interplay and decreases tumor growth.

3.1.6. Supplemental information

Supplemental Figures

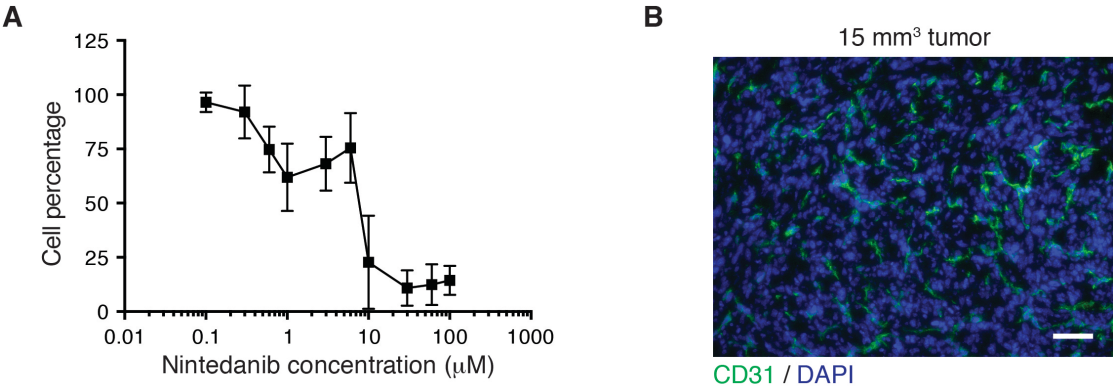

Figure S1. Related to Figure 1. Nintedanib treatment of Py2T cells *in vitro*.
(A) The inhibitory effect of increasing concentrations of nintedanib after 72 hours of treatment on Py2T tumor cell numbers has been determined by using an MTT assay *in vitro*. Data are shown as mean cell number normalized to control cells ± SD from three independent experiments.
(B) Representative immunofluorescence microphograph showing CD31-positive blood vessels in a tumor with a volume of 15 mm^3 representing the time point at which treatments were generally initiated. DAPI was used to visualize cell nuclei. Scale bar, 50 µm.

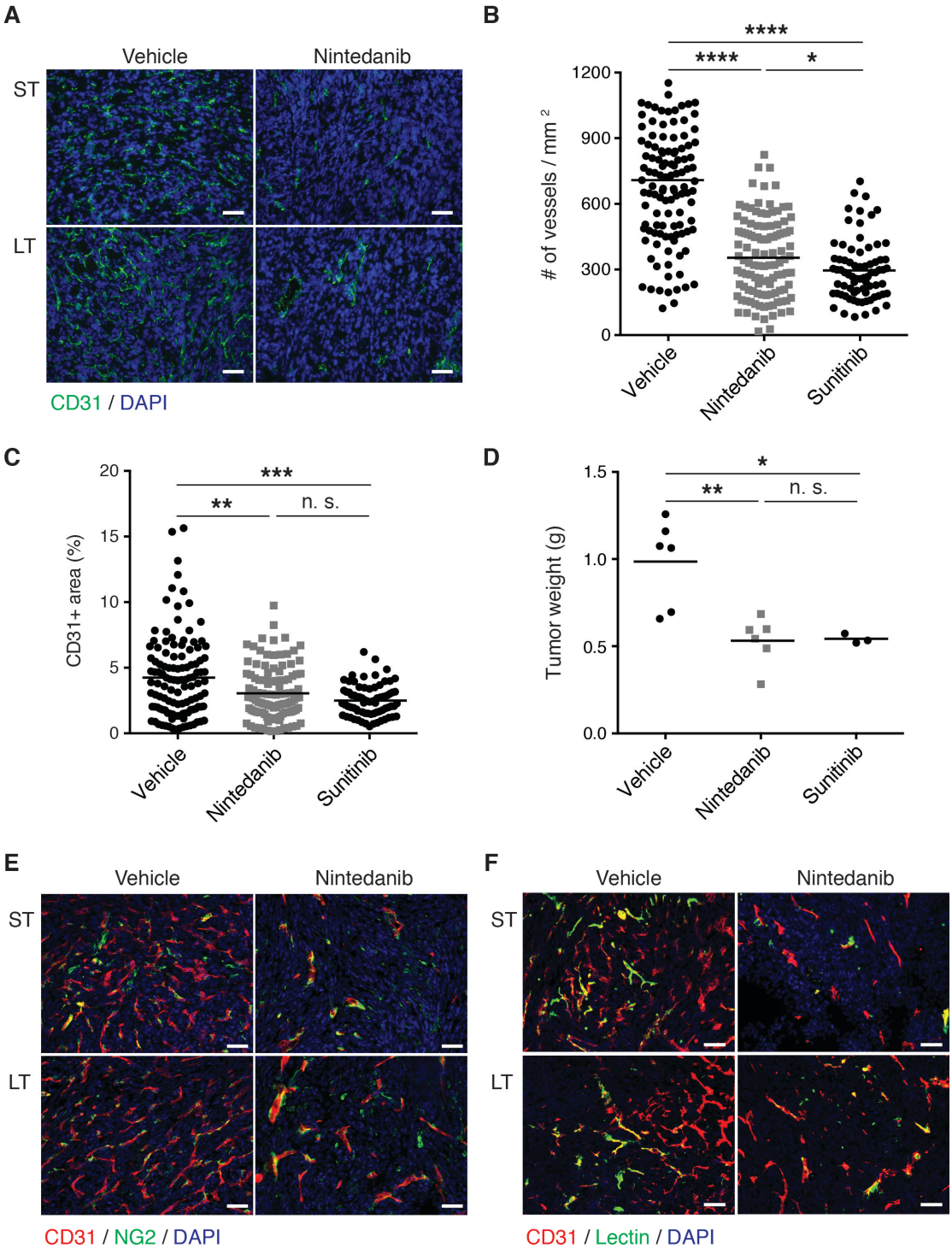

Figure S2. Related to Figure 2. Nintedanib and sunitinib treatments demonstrate potent anti-angiogenic effects.

(A) Representative images of immunofluoresecence stainings of tumor sections from ST and LT vehicle or nintedanib-treated mice with antibodies against CD31 are shown (C; green). DAPI was used to visualize cell nuclei. Scale bars, 50µm.

(B-D) Py2T tumor-bearing mice were treated with nintendanib or sunitinib during 21 days, and mice were sacrificed at day 35 post tumor cell injection. Microvessel densities (B) and CD31-positive area fractions per field of view (C) determined by immunofluorescence staining are shown. Tumor weights at the experimental end point are depicted in (D). N = 3-6 mice per group. Statistical significance was calculated using Mann–Whitney U test. n. s., non significant; *, $P < 0.05$; **, $P < 0.01$; ***, $P < 0.001$; ****, $P < 0.0001$.

(E) Blood vessel (CD31, red) coverage by perivascular cells (NG2, green) is shown on representative immunofluorescence pictures of tumors from ST and LT vehicle or nintedanib-treated mice. DAPI staining visualizes cell nuclei. Scale bars, 100µm.
(F) Blood vessel (CD31, red) perfusion (lectin, green) is shown on representative immunofluorescence pictures of tumors from ST and LT vehicle or nintedanib-treated mice. DAPI was used to visualize cell nuclei. Scale bars, 100µm.

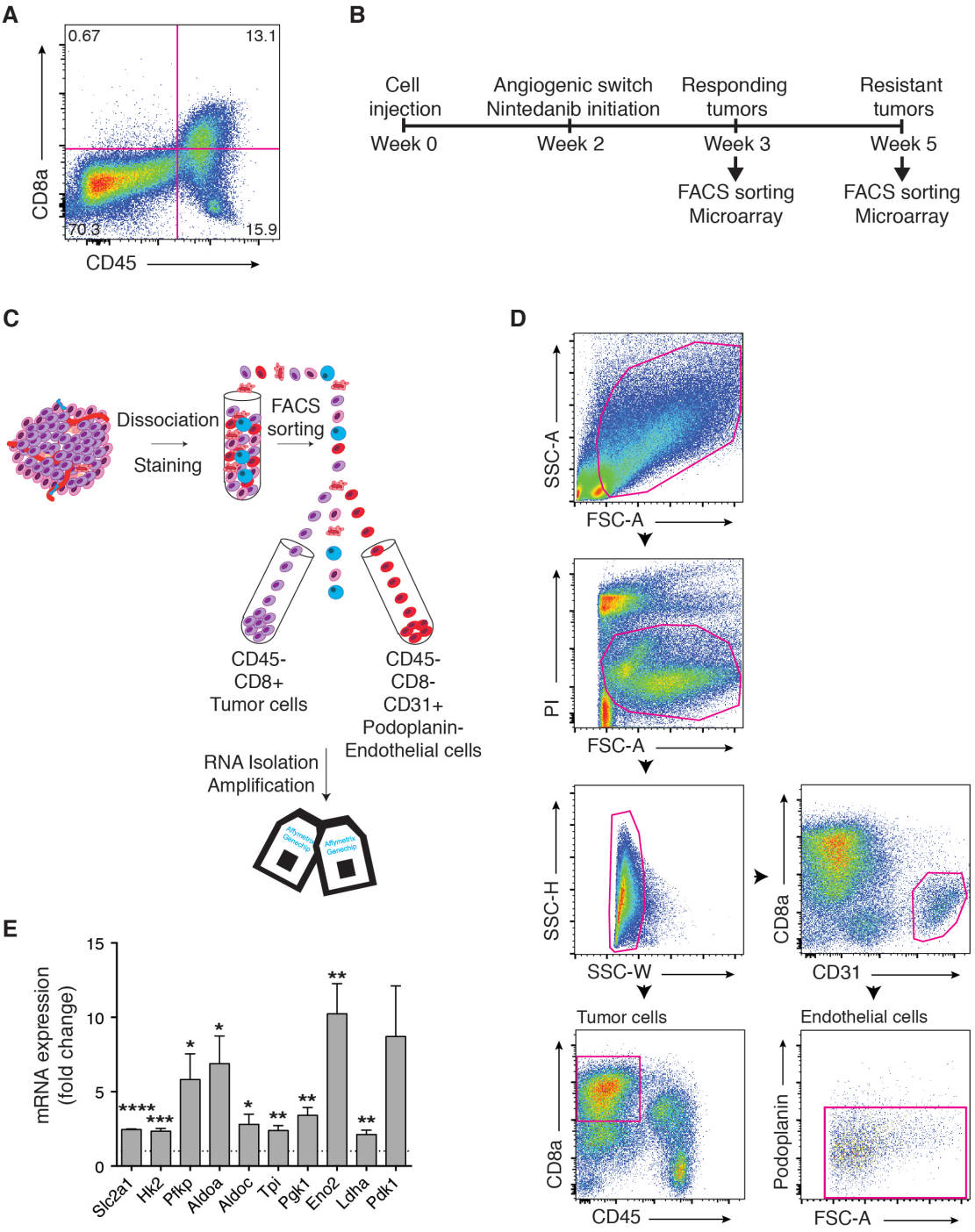

Figure S3. Related to Figure 3. Flow cytometry cell sorting strategy.
(A) Representative flow cytometric analysis of a wild-type Py2T tumor confirming the absence of a CD8α-positive CD45-negative cell population. Relative frequencies of gated populations are shown.
(B) Schematic representation of the experimental setup. Py2T-CD8α cells were orthotopically injected into the mammary fat pad of FVB/N female mice. Two weeks later, after the angiogenic switch had

occurred, nintedanib (50 mg/kg/day) treatment was initiated. One (ST) or three weeks (LT) after nintedanib initiation, corresponding ST and resistant LT-treated tumors, respectively, were harvested for cell isolation by flow cytometry.

(C) Schematic representation of the flow cytometry sorting strategy. Cells from dissociated tumors were separated by flow cytometry: tumor cells were identified by gating on the $CD45^-CD8\alpha^+$ population, whereas endothelial cells were identified by gating on $CD45^-CD8\alpha^-CD31^+$podoplanin$^-$ blood vessel endothelial cells.

(D) Representative results of cell sorting by flow cytometry. Cells were first gated for forward scatter (FSC) and sideward scatter (SSC), and propidium iodide-positive (PI) dead cells and cell doublets were excluded. Then, tumor cells were sorted by gating on the $CD45^-CD8\alpha^+$ population, whereas endothelial cells were sorted by gating on $CD45^-CD8\alpha^-CD31^+$podoplanin$^-$ blood vessel endothelial cells.

(E) Expression of different glycolysis genes in Py2T cells cultured in hypoxic conditions analyzed by quantitative RT-PCR. Data are normalized to cells cultured in normoxic conditions. Shown are means ± SEM. N = 4. Statistical significance was calculated using Student t test. *, $P < 0.05$; **, $P < 0.01$; ***, $P < 0.001$; ****, $P < 0.0001$.

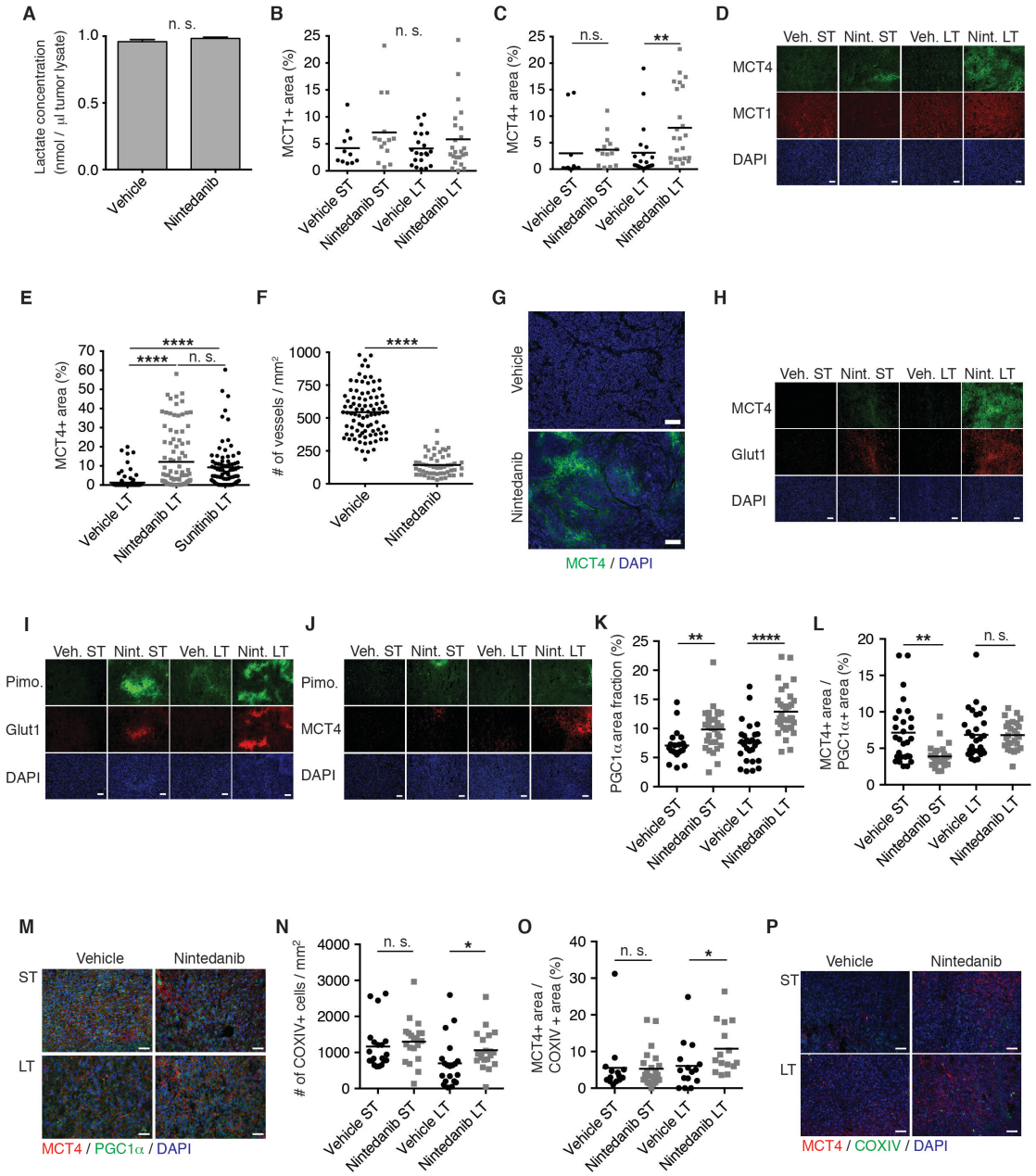

Figure S4. Related to Figure 4. Nintedanib treatment leads to the establishment of metabolic symbiosis.
(A) Lactate levels have been quantified in lysates of tumors from LT vehicle or nintedanib-treated mice, and are shown as mean ± SEM. N = 5 mice per group.
(B, C) Quantification of MCT1 (B) and MCT4 (C) expression by immunofluorescence staining on histological tumor sections from ST and LT vehicle or nintedanib-treated mice is shown. Mean MCT4 positive area fractions per each field of view are shown. N = 4 mice per group.
(D) Single channels corresponding to the MCT4/MCT1 costaining presented in Figure 4A. Veh., vehicle; Nint., nintedanib. Scale bars, 100 μm.
(E) MCT4 expression in tumors derived from LT vehicle, nintedanib or sunitinib-treated mice was assessed by immunofluorescence staining. Values represent the MCT4-positive area fraction per each field of view. N = 5-6 mice per group.
(F, G) Shown are microvessel densities (F) and representative immunofluorescence stainings for MCT4 (G) in tumors of Rip1Tag2 transgenic mice treated for 3 weeks (LT) with nintedanib. DAPI was used to visualize cell nuclei. N = 8-9 mice per group. Scale bars, 100 μm.
(H-J) Single channels corresponding to MCT4/Glut1, pimonidazole/Glut1 and pimonidazole/MCT4 costainings presented in Figure 4E, 4G and 4I, respectively. Pimo., pimonidazole; Veh., vehicle; Nint., nintedanib. Scale bars, 100 μm.
(K) Mitochondrial biogenesis was identified and quantified by immunofluorescence staining for PGC1α in Py2T tumors from ST and LT vehicle or nintedanib-treated mice. N = 4 mice per group.
(L, M) Quantification of MCT4 expression in PGC1α+ area (L) by immunofluorescence staining on histological tumor sections from ST and LT vehicle or nintedanib-treated mice is shown together with some representative pictures (M). N = 4 mice per group. Scale bars, 50 μm.
(N) COX IV+ cell number was assessed by immunofluorescence staining on histological tumor sections from ST and LT vehicle or nintedanib-treated. N = 4 mice per group.
(O, P) Quantification of MCT4 expression in COX IV+ area (O) by immunofluorescence staining on histological tumor sections from ST and LT vehicle or nintedanib-treated mice is shown together with some representative pictures (P). N = 4 mice per group. Scale bars, 50 μm.
Statistical significance was calculated using Mann–Whitney U test. n.s., non significant; *, $P < 0.05$; **, $P < 0.01$; ***, $P < 0.001$; ****, $P < 0.0001$.

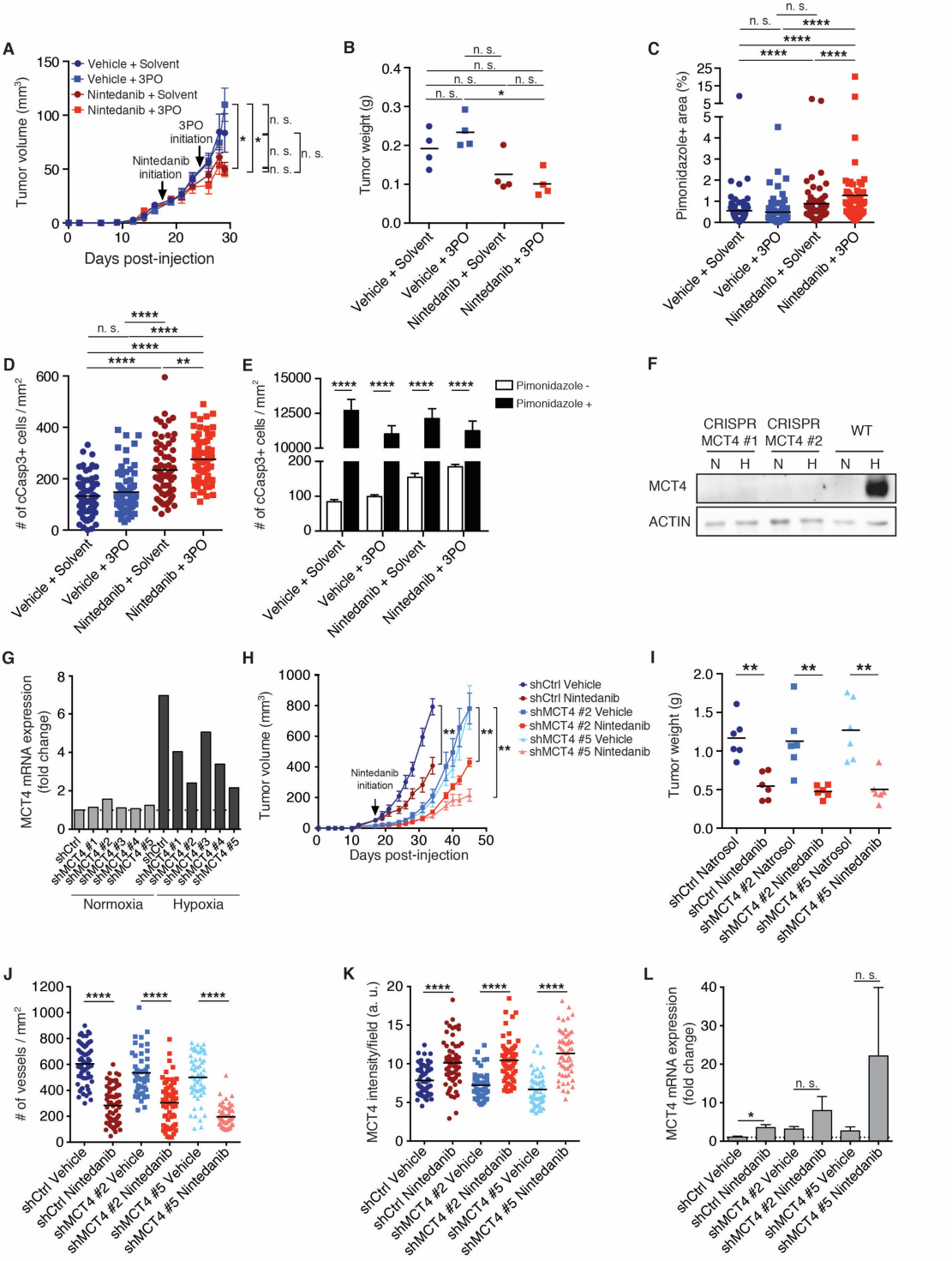

Figure S5. Related to Figure 5. Targeting glycolysis and metabolic symbiosis overcomes anti-angiogenic resistance.

(A, B) Primary tumor growth over time (A) and tumor weights at the experimental end point (B) of mice treated with either vehicle or nintedanib (50 mg/kg/day) in combination with 3PO (70 mg/kg/day) or solvent are shown. The mice were treated with 3PO 8 days after the initiation of nintedanib treatment and were analyzed 5 days later to determine early effects of 3PO therapy (short-term nintedanib and 3PO-treated mice). In (A), data are displayed as mean tumor volumes ± SEM.

(C) Hypoxic areas were identified and quantified by immunofluorescence staining for pimonidazole adducts in Py2T tumors treated as described in (A). Values represent the pimonidazole+ area fraction for each microscopic field of view and means are displayed.

(D, E) Quantification of total (D) and hypoxia- or normoxia-related (E) apoptosis by immunofluorescence co-staining for cCasp3 and pimonidazole in tumors from short-term nintedanib and 3PO-treated mice.
N = 4 mice per group.
(F) Representative western blot analysis of MCT4 expression in Py2T WT cells or Py2T CRISPR MCT4 Clones #1 and #2 cultured for 72h under normoxic or hypoxic condition.
(G) The efficiency of shRNA-mediated knockdown of MCT4 expression was determined by measuring the MCT4 mRNA levels of shCtrl or shMCT4 Py2T cells cultured in hypoxic or normoxic conditions by quantitative RT-PCR. Data are normalized to shCtrl Py2T cells cultured in normoxic conditions.
(H, I) Primary tumor growth (H) and terminal tumor weights (I) of mice following orthotopic injection of Py2T shCtrl or Py2T shMCT4 #2 and #5 cell lines treated with either vehicle or nintedanib (50 mg/kg/day) have been quantified. The time points for animal sacrifice were chosen for all three cell lines individually such that all the tumors of the corresponding vehicle-treated groups were size matched. In (B), mean ± SEM is depicted.
(J) Quantification of microvessel densities by immunofluorescence staining for CD31 on Py2T shMCT4 tumors from LT vehicle or nintedanib-treated mice. N = 6 mice per group.
(K) Quantification of MCT4 expression by immunofluorescence staining on histological sections from shCtrl or shMCT4 Py2T tumors treated either with nintedanib or vehicle is shown. Data displayed represents mean values per each field of view. N = 6 mice per group.
(L) MCT4 mRNA expression levels were analyzed by quantitative RT-PCR in shCtrl or shMCT4 Py2T tumors treated with either nintedanib or vehicle, and values are displayed as mean ± SEM. Data are normalized to shCtrl vehicle-treated tumors. N = 3 mice per group.
Statistical significance was calculated using Mann–Whitney *U* test. n. s., non significant; *, $P < 0.05$; **, $P < 0.01$; ****, $P < 0.0001$.

Supplemental Experimental Procedures

Therapy studies

Treatment of Py2T tumor-bearing mice was initiated when tumors reached a measurable size (15-20mm^3) to allow a thorough stratification into experimental groups with similar mean tumor volumes. Nintedanib (kindly provided by Boehringer Ingelheim) was formulated in 0.5% natrosol hydroxyethylcellulose (Boehringer Ingelheim) and administered daily at 50 mg/kg body weight (BW) by oral gavage. Rip1Tag2 transgenic mice were treated with the same regimen from 10 weeks of age onwards (Bill, Fagiani et al. 2015). Sunitinib L-malate (LC Laboratories) was administered at 40 mg/kg in carboxymethylcellulose daily by oral gavage as described (Paez-Ribes, Allen et al. 2009). 3-(3-pyridinyl)-1-(4-pyridinyl)-2-propen-1-one (3PO; Axon Medchem, 2175) was dissolved in a 10% EtOH, 40% PEG, 50% PBS solution and administered at 70 mg/kg daily by intraperitoneal (i.p) injection. Treatment was initiated at day 8 of nintedanib treatment.

Animals of the experimental arms were euthanized by CO_2 (or cervical dislocation for hypoxia studies), either time- or size-matched to the control treatment. Primary tumors were dissected and processed for further analyses.

RNA isolation

RNA of sorted endothelial cells was isolated using the Absolutely RNA Nanoprep Kit (Stratagene) following the manufacturer's recommendations. RNA of sorted tumor cells was isolated using TRIzol® LS reagent (Ambion®) and RNA Easy Micro Kit (Qiagen). To isolate RNA from whole tumors, previously snap frozen tissues were homogenized in Tri Reagent (Sigma-Aldrich) using a POLYTRON® (Kinematica) and isolated following the manufacturer's recommendations.

Quantitative RT-PCR

RNA was reverse transcribed using M-MLV reverse transcriptase (Promega) and quantitative PCR was performed using SYBR-green PCR MasterMix (Applied Biosystems) in a StepOne Plus PCR machine (Applied Biosystems). Fold change expression was determined by the comparative Ct method ($\Delta\Delta C_t$) normalized to 60S Ribosomal protein L19 expression. Primers for quantitative PCR are listed in Table

S1.

Lactate assay

Lactate concentration was determined on tumor lysate by using the L-Lactate Assay Kit from Abcam (ab65331) following the manufacturer's recommendations.

Immunoblotting

Immunoblotting has been performed as previously described (Zumsteg et al., 2012). The following antibodies were used: MCT4 (Santa Cruz Biotechnology, sc-50329, 1:200) and actin (Santa Cruz Biotechnology, sc-1616, 1:1000).

Lentiviral infection

Lentiviral plasmids containing short-hairpin RNAs #1-5 (shRNA) against mouse MCT4 were purchased from Sigma-Aldrich (Mission Non-Targeting shRNA control vector: SHC002; shMCT4 #1: TRCN0000079653, shMCT4 #2: TRCN0000079654, shMCT4 #3: TRCN0000079655, shMCT4 #4: TRCN0000079656, shMCT4 #5 TRCN0000079657). In order to produce lentiviral particles, HEK293T cells were transfected with the shRNA containing plasmids, the helper vectors pMDL and pREV and the envelope encoding plasmid pVSV using FugeneHD. Virus containing supernatant was conditioned for 2 days, filtered through a 0.45 µm filter, gently mixed with Lenti-X Concentrator (Clontech), and followed by an overnight incubation at 4°C and subsequent centrifugation the next day. The virus-containing pellet was resuspended in fresh complete DMEM medium, 8 ng/ml polybrene was added and Py2T cells were infected. Successfully transfected cells were selected by puromycin treatment (5 µg/ml). Knockdown efficiency was determined by measuring hypoxia-induced (96h, 1% O_2) MCT4 mRNA expression by quantitative RT-PCR.

Hypoxia and vessel functionality

To assess functional blood vessel perfusion, 100 µg of fluorescein-labeled Lycopersicon esculentum (tomato) lectin (Vector Laboratories, GL-1171) was injected into the tail vein. Two minutes later, mice were terminally anaesthetized and five minutes later perfused via the left cardiac ventricle first with cold 4% PFA and subsequently with cold PBS.

To identify hypoxic tumor areas, 60 mg/kg pimonidazole-HCl (Hypoxyprobe Omni Kits, Hypoxyprobe, Inc.) dissolved in PBS was injected i.p. 1 hour before euthanizing the animals by cervical dislocation.

Immunofluorescence microscopy analysis

Tumors were fixed in 4% PFA for 2 hours followed by overnight incubation in 20% sucrose to cryopreserve the tissue, both at 4°C. Then, tumors were snap frozen in Tissue-Tek OCT compound (Thermo Scientific) and stored at -80°C. Eight µm thick tumor sections were cut, dried for 30 minutes, rehydrated with PBS, permeabilized with 0.2% Triton X-100 for 20 minutes and blocked with 5% normal goat serum (NGS; Sigma-Aldrich) for 1 hour. As an exception, when performing stainings with anti-cCasp3 antibodies, blocking was performed using 20% NGS. When using a goat primary antibody, sections were blocked with 5% bovine serum albumin. Subsequently, primary and secondary antibodies were diluted in blocking solution and incubated overnight at 4°C and 1 hour at room temperature, respectively. Images were acquired with a Leica DMI 4000 microscope.

Antibodies used: rabbit anti-cleaved Caspase-3 (cCasp3; Cell Signaling, 9664, 1:50), rat anti-CD31 (BD Pharmingen, 550274, 1:50), rabbit anti-NG2 (Chemicon, AB5320, 1:100), rabbit anti-phospho Histone H3 (pH3; Millipore, 06-570, 1:200), rabbit anti-pimonidazole (Hypoxyprobe, 1:25), mouse anti-pimonidazole-FITC (Hypoxyprobe, 1:25), goat anti-MCT1 (Santa Cruz, sc-14917, 1:50), rabbit anti-MCT4 (Santa Cruz, sc-50329, 1:50), goat anti-MCT4 (Santa Cruz, sc-14930, 1:50), goat anti-Glut1 (Santa Cruz, sc-1605, 1:50), rabbit anti-CoxIV (Cell Signaling, 4850, 1:100) and rabbit anti-PGC1α (Millipore, AB3242, 1:300). Primary antibody binding was detected by incubating the histological sections with secondary antibodies directed against the respective species of the primary antibodies for 1 hour at room temperature, diluted 1:200 in blocking solution. Secondary antibodies were fluorescently tagged with Alexa 488, Alexa 568 or Alexa 633 (Molecular probes). Subsequently, nuclei were stained with 4′,6-Diamidin-2-phenylindol (DAPI; Sigma-Aldrich; 1:10,000) followed by mounting the slides with Dako mounting medium (Dako).

Flow cytometry

Freshly dissected Py2T primary tumors were immediately minced into small pieces and digested for 30 minutes at 37°C on a bacterial shaker in DMEM (Sigma-Aldrich) supplemented with Nu-Serum Growth Medium Supplement (6%; Corning), DNase I (200 µg/ml; Roche), Dispase II (1.2mg/ml; Roche) and Collagenase D (1.2 mg/ml; Roche). To achieve a single cell suspension, the digested tissue was first passed through a 70 µm and subsequently through a 40 µm cell strainer (Corning). Cells were washed in FACS-buffer (5% fetal bovine serum in PBS; Sigma-Aldrich). Fc-receptors were blocked with an antibody against CD16/CD32 (BioLegend, 101302, 1:100) diluted in FACS-buffer for 30 minutes at 4°C. Then, cells were incubated for 45 minutes on ice with the following antibodies: hamster anti-mouse podoplanin (Hybridoma supernatant clone 8.1.1, 1:10), anti-CD8α-FITC (BioLegend, 100705, 1:150), anti-CD31-APC (BioLegend, 102409, 1:200), anti-CD45-APC-Cy7 (BioLegend, 103116, 1:500). Staining for podoplanin was achieved by subsequently incubating the cells for 30 minutes on ice with an anti-hamster PE-labeled secondary antibody (eBioscience, 12-4112-83, 1:200). Immediately before sorting with a FACSAriaII (BD Bioscience), cells were filtered through a 40 µm mesh and propidium iodide (PI) was added to exclude dead cells. Tumor cells were sorted into FACS-buffer by gating on $CD8\alpha^{+}/CD45^{-}$ cells (Figure S3D). Endothelial cells were directly sorted into the lysis buffer of the Absolutely RNA Nanoprep Kit (Stratagene) by gating on $CD31^{+}/CD45^{-}/Podoplanin^{-}$ cells (Figure S3D).

Annexin V staining

Py2T WT cells or Py2T CRISPR MCT4 clones #1 and #2 were cultured for 3 days under normoxic or hypoxic conditions. Both floating and attached cells were collected and washed in PBS. 1.10^{6} cells were resuspended in 1X binding buffer and stained using Cy5 AnnexinV (BD Pharmingen, # 559934, dilution 1/20) and 2 µg/ml DAPI for 20 min in the dark. 50,000 cells/sample were analyzed by flow cytometry (FACS Canto, Becton Dickinson).

EdU staining

Py2T WT cells or Py2T CRISPR MCT4 clones #1 and #2 were cultured for 3 days under normoxic or hypoxic conditions. Cells were incubated with 10 µM EdU for 30

min. After trypsinization 1.10^6 cells were stained using EdU-Flow cytometry 488 Kit (Base-Click, BCK-FC488) following manufacturer's instruction. Prior to FACS acquisition cells were incubated 2h at 37°C in presence of 10 µg/ml RNAse (Roche, 11119915001) and 50 µg/ml propidium iodide (Sigma-Aldrich, 81845). 50,000 cells/sample were analyzed by flow cytometry (FACS Canto, Becton Dickinson).

Extracellular metabolic flux analysis

For analysis of the OCR (in pmol/min) and ECAR (in mpH/min), the Seahorse XFe-96 metabolic extracellular flux analyzer was used (Seahorse Bioscience, North Billerica, MA, USA). Py2T WT cells or Py2T CRISPR MCT4 clones #1 and #2 were plated at a density of 2,500 cells per well and expanded for 48 hours under normoxic (21% O_2) or hypoxic (1% O_2) conditions. Cells were treated with nintedanib for 48h or with 3PO for 3h. Prior to performing the metabolic assays, medium was exchanged for serum-free unbuffered RPMI-1640 medium (Sigma-Aldrich). Perturbation profiling of mitochondrial respiratory parameters was performed by the addition of oligomycin (1 µM), Carbonyl cyanide-4-(trifluoromethoxy)phenylhydrazone (FCCP) (2 µM) and rotenone (1 µM) and measuring changes in OCR. Glycolytic parameters were assessed independently in parallel wells by the sequential addition of glucose (10 mM), oligomycin (1 µM) and 2-deoxyglucose (2-DG, 50 mM, all Sigma-Aldrich) to cells maintained in glucose-free unbuffered RPMI-1640 medium (Sigma-Aldrich). Metabolic parameters were calculated following the manufacturer's recommandation. Additionally, OCR and ECAR were assessed under hypoxic conditions (1% O2) using the Seahorse XFe-96 metabolic extracellular flux analyzer placed in a Hypoxia Workstation (SCI-tive, Ruskinn Technology, Bridgend, UK). Unbuffered medium (± glucose) was equilibrated to hypoxia overnight and layered onto) Py2T WT cells or Py2T CRISPR MCT4 clones #1 and #2 plated as described above. Metabolic parameters were assessed as per under normoxic conditions and there were additional control wells where 1 M sodium sulfite was injected into calibrant fluid to provide a 'zero' oxygen reference parameter for the software algorithm to calculate OCR.

The different parameters have been calculated as follows: ATP-coupled respiration = [OCR(basal-non corrected basal OCR)] - [OCR(oligomycin)]; glycolysis = [ECAR(glucose)] − [ECAR(basal-non corrected basal ECAR)]; glycolytic capacity =

[ECAR(oligomycin)] − [ECAR(basal-non corrected basal ECAR)]; glycolytic reserve = [ECAR(oligomycin)] − [ECAR(glucose)].

Microarray analysis

Total RNA preparations of flow cytometry-sorted tumor and endothelial cells were analyzed using an Agilent 2100 bioanalyzer. Target synthesis was performed using the following suite of kits provided by Nugen (San Carlos, USA): WT-Ovation Pico (Cat# 3300), WT-Ovation Exon (Cat# 2000) and FL-Ovation Biotin V2 (Cat# 4200). The hybridization cocktail (200µl) containing fragmented biotin-labeled target DNA at a final concentration of 25ng/µl was transferred into Affymetrix GeneChip MoGene-1_0-st-v1 (Affymetrix) and incubated at 45°C on a rotator in a hybridization oven 640 (Affymetrix) for 17 h at 60 rpm. The arrays were washed and stained on a Fluidics Station 450 (Affymetrix) by using the Hybridization Wash and Stain Kit (Affymetrix, Cat# 900720) and the Fluidics Procedure FS450_0001. The GeneChips were processed with an Affymetrix GeneChip® Scanner 3000 7G (Affymetrix). DAT image files of the microarrays were generated using Affymetrix GeneChip Command Console (AGCC, version 0.0.0.676, Affymetrix).

Bioinformatical analysis

All microarray data were preprocessed and analyzed using R (software environment for statistical computing and graphics) version 3.1.0 (2014-04-10) and packages provided by the Bioconductor package library. Raw Affymetrix CEL files were subjected to background correction and normalization using the Robust Multichip Average (RMA) algorithm (rma method, oligo package). Differential gene expression was determined using the limma package (Smyth, Michaud et al. 2005) with and without a p-value cutoff of 0.05 and a range of fold-change values (FC = 1.2 to 1.7). The results of differential gene expression were used to conduct pathway enrichment analysis provided by The Database for Annotation, Visualization and Integrated Discovery (DAVID) v6.7 (Huang da et al., 2009), with a particular focus on pathways defined in the Kyoto Encyclopedia of Genes and Genomes (KEGG) database.

The background-corrected and normalized gene expression datasets associated with the placebo-treated (UT), 1 week-treated (ST), and 3 week-treated (LT) samples were subjected to Gene Set Enrichment Analysis (GSEA) using GSEA V2.1.0. Three sets

of analyses were conducted: ST *versus* UT, LT *versus* UT and ST *versus* LT. In all cases the default run-time arguments were used except for the "Permute" parameter that was set to "gene_set" (in order to accommodate less than 7 samples per class). In addition, analyses were conducted against the "MoGene_1_0_st.chip" microarray annotation and the following gene set libraries: "c2.cp.kegg.v4.0.symbols.gmt" and "c2.cp.reactome.v4.0.symbols.gmt" (Mootha, Lindgren et al. 2003, Subramanian, Tamayo et al. 2005).

Heat maps were generated using the heatmap.2 method provided by the gplots package. Boxplots were generated using the default boxplot method provided in R and based on the median background corrected and normalized expression value for each gene with respect to all samples within each sample class (UT, ST and LT). Additional statistical analyses were also carried out using GraphPad Prism 6 (GraphPad Prism Software Inc.).

The microarray data has been deposited on Gene Expression Omnibus platform under the accession number GSE78698.

Primers for qRT-PCR

Name	**Sequence (5′ - 3')**
Glut1 (Slc2a1)	gaccctgcacctcattgg
	gatgctcagataggacatccaag
Hexokinase 2 (Hk2)	gctgaaggaagccattcg
	tcccaactgtgtcatttaccac
Phosphofructokinase, platelet (Pfkp)	gctatcggtgtcctgacca
	actttggcccccgtgtag
Aldolase A (Aldoa)	aaggaagaggttcctctaaagacc
	aatgcggtgagcgatgtc
Triosephosphate isomerase 1 (Tpi1)	ttcgagcaaaccaaggtcat
	ccggagcttctcgtgtactt
Phosphoglycerate kinase 1 (Pgk1)	gaagtcgagaatgcctgtgc
	ccggctcagctttaaccttt
Enolase 2 (Eno2)	aacagcgttacttaggcaaagg
	ccaccacggagatacctgag
Lactate dehydrogenase A (Ldha)	ggcactgacgcagacaag
	tgatcacctcgtaggcactg
Pyruvate dehydrogenase kinase 1 (Pdk1)	gttgaaacgtcccgtgct
	gcgtgatatgggcaatcc
β-actin (Actb)	ctaaggccaaccgtgaaaag
	accagaggcatacagggaca
Peroxisome proliferator-activated receptor gamma coactivator 1 alpha (Pgc1a)	tgaggaccagcctctttgccca
	cgctacaccacttcaatccaccc
Cytochrome c oxidase subunit IV isoform 1 (Cox4i1)	tacttcggtgtgccttcga
	tgacatgggccacatcag
Monocarboxylate transporter 4 (Scl16a3)	gctcacctcctcccttgtg
	ctcttcctcttcccgatgc
60 ribosomal protein L19 (Rpl19)	ctcgttgccggaaaaaca
	tcatccaggtcaccttctca

3.2. Deciphering the EMT-induced pro-angiogenic signature

3.2.1. Abstract

Vascular Endothelial Growth Factor A (VEGF-A) plays a central role in tumor progression. Besides its role in promoting angiogenesis, several autocrine functions have been revealed in tumor cells, improving their survival, migration, invasion and transmigration abilities. We have recently shown that murine breast cancer cells undergoing an epithelial-mesenchymal transition (EMT) and displaying hallmarks of cancer stem cells exhibit a pro-angiogenic signature, notably by up-regulating the expression of VEGF-A. Indeed, our data demonstrate that VEGF-A is required for EMT-induced angiogenesis in the early events of tumor initiation, a major hallmark of cancer stem cells. However, how the EMT program can induce VEGF-A expression in the absence of hypoxia has remained elusive. By conducting RNA interference studies we could identify JunB as the main upstream regulator of this EMT-induced pro-angiogenic signaling. Indeed, JunB is upregulated during EMT and its siRNA-mediated knockdown decreases VEGF-A production. These data provide important new insights into the molecular mechanisms leading to the secretion of VEGF-A upon EMT reprogramming and may open new avenues for the design of therapeutic strategies.

3.2.2. Introduction

Metastases represent the main cause of lethality in cancer patients (Gupta and Massague 2006). Epithelial-mesenchymal transtition (EMT) is the initial step of the invasion-metastasis cascade (Valastyan and Weinberg 2011). This program - integral in embryonic development - is reactivated during tumor progression (Thiery, Acloque et al. 2009). During this process, epithelial cells, characterized by apico-basal polarity, cell-cell contacts and expression of epithelial markers, such as E-cadherin or ZO-1, loose expression of epithelial markers in favor of mesenchymal markers, such as N-cadherin and vimentin, disassemble their cell-cell and cell-matrix contacts and gain migratory capacity (Thiery and Sleeman 2006, Lamouille, Xu et al. 2014).

Associated secretion of proteases allows mesenchymal cells to remodel the surrounding microenvironment and invade locally (Saxena and Christofori 2013).

EMT and its reverse process (MET) illustrate the intrinsic plasticity of cancer cells. This complex process is accompanied with dedifferentiation, an essential criteria for cancer cells allowing them to initiate tumors *de novo* at the metastatic site. It has been suggested that metastatic cancer cells could present cancer stem cell (CSC) traits (Brabletz, Jung et al. 2005). Confirming this hypothesis, Mani and colleagues demonstrated that normal and neoplastic cells undergoing an EMT express stem cells markers and are able to initiate tumors more efficiently than epithelial cells (Mani, Guo et al. 2008). Our laboratory and others have recently reported that EMT-induced stem cells express pro-angiogenic markers, notably VEGF-A (Beck, Driessens et al. 2011, Lee, Lee et al. 2011, Fantozzi, Gruber et al. 2014). This pro-angiogenic signature allows them to recruit blood vessels and significantly increases tumor initiation, independently of CSCs-specific features, such as asymmetric cell division and self-renewal abilities. However, the molecular mechanisms inducing VEGF-A expression in mesenchymal cells have remained elusive.

Here, we have identified JunB as the main regulator of VEGF-A in mesenchymal cells. Notably, the JunB-mediated induction of VEGF-A expression occurs independent of hypoxia and the activities of HIF1α, a known strong inducer of VEGF-A under hypoxia (Forsythe, Jiang et al. 1996). In fact, though HIF1α is expressed in cells undergoing an EMT, it is not recruited into cell nuclei and its target genes are not upregulated in mesenchymal cells compared with epithelial cells. However, by performing a siRNA-mediated screen for few transcription factors known to induce VEGF-A mRNA expression in other systems, we have observed that JunB downregulation significantly decreases VEGF-A mRNA expression. Furthermore, JunB nuclear expression is increased during an EMT. These findings are validated in several EMT systems both at the mRNA and protein levels. We therefore propose a new role for JunB as a regulator of EMT-induced pro-angiogenic signaling.

3.2.3. Results

3.2.3.1. VEGF-A secreted by mesenchymal cell increases endothelial cell survival

To assess the angiogenic signature in mesenchymal versus epithelial cells, 4 different EMT systems were employed. MTFlECad cells are breast cancer cells isolated from a tumor of a MMTV-Neu mouse carrying floxed alleles of the E-cadherin gene. After Cre-recombinase-mediated recombination and subsequent loss of E-cadherin these cells become stably mesenchymal (MTΔECad) (Lehembre, Yilmaz et al. 2008). Py2T breast cancer cells were isolated from MMTV-PyMT mice (Waldmeier, Meyer-Schaller et al. 2012). These cells become mesenchymal in response to TGF-β treatment. 4T1 cells, though exhibiting an aggressive phenotype, can be used as an additional EMT model as they express epithelial markers (E-cadherin, miR-200) and gain mesenchymal properties when treated with TGF-β (Dykxhoorn, Wu et al. 2009, Wendt, Schiemann et al. 2013). The last cell line employed in this work is the E9 subclone of NMuMG cells (Maeda, Johnson et al. 2005). These cells express E-cadherin and are, as suggested by their name, derived from a normal murine mammary gland. Like the Py2T or 4T1 cells, NMuMG cell undergo reversible EMT when subjected to TGF-β treatment.

Endothelial cells (HUVECs, human umbilical vein endothelial cells) were first cultured with conditioned medium from either epithelial (MTFlECad) or mesenchymal (MTΔECad) cells. HUVECs did not proliferate and had rather difficulties to survive in these growth factors-depleted media (Figure 1A). However, the number of HUVECs was found to decrease strongly when cultured in MTFlEcad (epithelial) conditioned medium compared with HUVECs cultured in MTΔECad (mesenchymal) conditioned suggesting that mesenchymal cells might secrete factors important for endothlial cell survival (Figure 1A). This hypothesis was further confirmed when we assessed the Akt phosphorylation of HUVECs cultured in epithelial or mesenchymal cell conditioned media. Indeed, Akt and its phosphorylation status are well-known survival markers (Brunet, Bonni et al. 1999, Fujio and Walsh 1999). HUVECs cultured in mesenchymal cell-conditioned medium

showed increased AKT phosphorylation compared with cells cultured in epithelial cell-conditioned medium (Figure 1B).

We then aimed to identify the factors secreted by the mesenchymal cells that increased HUVEC survival. RNA-sequencing data performed on MTFlECad and MTΔECad revealed an increased expression of several growth factors and cytokines known to induce angiogenesis (data not shown). Amongst them, Vascular Endothelial Growth Factor-A (VEGF-A) caught our attention. Indeed, this prototypic pro-angiogenic factor induces endothelial cell survival through activaction of the PI3K/AKT signaling pathways and has been shown to prevent serum-starvation-induced apoptosis in HUVECs (Gerber, Dixit et al. 1998, Gerber, McMurtrey et al. 1998). VEGF-A mRNA and protein levels were increased in MTΔECad and Py2T LT cells, and to a lesser extent in NMuMG LT cells, suggesting a more crucial role of VEGF-A in cancer-related EMT (Figure 1C and 1D). To further test whether mesenchymal cell-derived VEGF-A was responsible of endothelial cell survival, VEGF-A was either stably overexpressed in epithelial cells (MTFlECad) or stably down-regulated in mesenchymal cells (MTΔECad). Conditioned medium prepared from these different cell lines was then used to culture endothelial cells and their survival was assessed by cell counting. Confirming our hypothesis, overexpression of VEGF-A in epithelial cells led to increased endothelial cell survival. Further, shRNA-mediated knockdown of VEGF-A expression in mesenchymal cells led to decreased endothelial cell survival (Figure 1E).

Altogether, these data suggest that mesenchymal cell-secreted VEGF-A leads to increased endothelial cell survival.

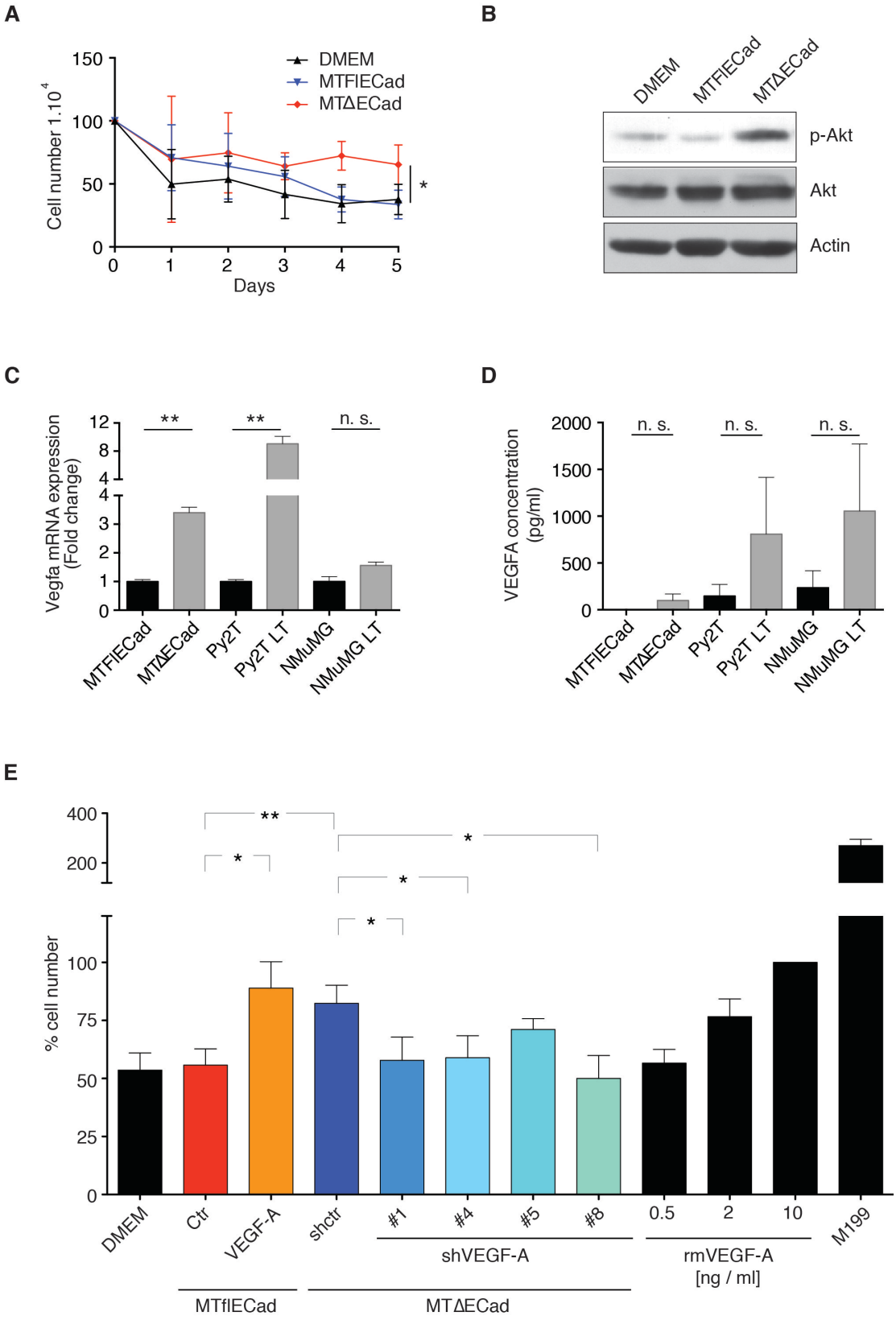

Figure 1: Mesenchymal cells increase endothelial cell survival through VEGF-A secretion.
(A) HUVECs were cultured in DMEM, epithelial (MTFlECad) or mesenchymal (MTΔECad) tumor cell conditioned medium and the number of viable cells was quantified at different time points using Neubauer chamber and Trypan blue exclusion. Mean values of 3 different experiments are plotted with the SD. Statistical significances were calculated by unpaired Student's t-test. * = $p < 0.05$.

(B) Survival of HUVECs cultured in DMEM, epithelial (MTFlECad) or mesenchymal (MTΔECad) tumor cell conditioned medium was assessed by immunoblotting against p-Akt. Total Akt and actin were used as loading controls.
(C-D) Quantification of VEGF-A mRNA level by RT-qPCR **(C)** and protein concentration by ELISA **(D)** on several epithelial (MTFlECad, Py2T and NMuMG) and mesenchymal (MTΔECad, Py2T LT and NMuMG LT) cell lines. Mean values of 3 different experiments are plotted with the SD. Statistical significances were calculated by unpaired Student's t-test. n. s., non significant; ** = $p < 0.01$.
(E) HUVEC cells were cultured in conditioned media of VEGF-A overexpressing (VEGF-A) or control retrovirus-infected MTFlECad cells, or in conditioned media of MTΔECad cells expressing different VEGF-A-targeting (shVA) or control shRNAs. After 5 days of culture viable cell number was quantified using Neubauer chamber and Trypan blue exclusion. M-199 supplemented culture medium (as described in Methods) together with DMEM containing diverse recombinant mouse VEGF-A (rmVEGF-A) concentrations were used as positive controls, while DMEM was used as a negative control. Cell numbers are represented as % of HUVECs treated with 10 ng/ml recombinant VEGF-A. Mean values of 4 different experiments are plotted with the SEM. Statistical significances were calculated by paired Student's t-test. * = $p < 0.05$; ** = $p < 0.01$. This graph corresponds to Supplemental Figure S8 in (Fantozzi, Gruber et al. 2014).

3.2.3.2. VEGF-A expression is not induced by an hypoxic signature

We next asked how EMT reprogramming could lead to VEGF-A secretion. Hypoxia and its master transcription regulator, HIF1α, are well-known inducers of VEGF-A expression (Forsythe, Jiang et al. 1996). While so far unproven, the common hypothesis in the field suggests that mesenchymal cells can express HIF1α in normoxic conditions (Goel and Mercurio 2013). Indeed, recent reports describe normoxic expression of HIF1α (Cao, Eble et al. 2013). Further, in the context of TGF-β-induced EMT, other laboratories have demonstrated the ability of TGF-β to induce HIF1α stability and DNA binding. McMahon and colleagues recently described the TGF-β1-mediated inhibition of PHD2 and subsequent HIF1α stability (McMahon, Charbonneau et al. 2006). HIF2α possesses a high homology with HIF1α and can also bind to the HRE motif in the *VEGF-A* gene promoter therefore inducing *VEGF-A* transcription (Carroll and Ashcroft 2006, Holmquist-Mengelbier, Fredlund et al. 2006, Keith, Johnson et al. 2012). HIF2α has recently been described as a regulator of angiogenesis in mesenchymal glioblastoma (Mathew, Skuli et al. 2014). Hence, we considered HIF2α as a second potential regulator of *VEGF-A* transcription in mesenchymal cells.

However, we found that TGF-β-induced EMT did not affect HIF1α and HIF2α expression in either 4T1 or in Py2T cells (Figure 2A). As transcription factor activity does not only depend on their expression but also rely on their recruitment to the nucleus we additionally analyzed their subcellular localization. Neither HIF1α nor

HIF2α were recruited to the nucleus during EMT. Furthermore, expression of known target genes of HIF1α and HIF2α, such as Slc2a1 (Glut1) (Figure 2D) or Ca9 (Figure 2E) remained either unchanged or decreased during EMT, thus definitively ruling out HIF1α and HIF2α activation during an EMT (Keith, Johnson et al. 2012).

NFκB is another transcription factor regulated during hypoxia (Koong, Chen et al. 1994). While absent on the human *VEGF-A* promoter, consensus sites for NFκB are located 90 and 185 bp upstream of the transcription initiation site in mouse *VEGF-A* promoter (Shima, Kuroki et al. 1996). Immunofluorescence staining for the p65 subunit of NFκB did not reveal any increase in protein expression or nuclear recruitment during EMT (Figure 2F). This observation suggests that NFκB is also not responsible for EMT-induced VEGF-A expression.

We then measured VEGF-A mRNA expression in cells undergoing an EMT in either normoxic or hypoxic condition. We observed that EMT and hypoxia have additive effects on VEGF-A expression (Figure 2G). Again, these results suggest that two distinct signaling pathways regulate VEGF-A expression in EMT and hypoxia.

Taken together, these data indicate that HIF1α, HIF2α and NFκB are not induced during EMT and rule out the implication of hypoxia-related proteins in EMT-mediated VEGF-A expression.

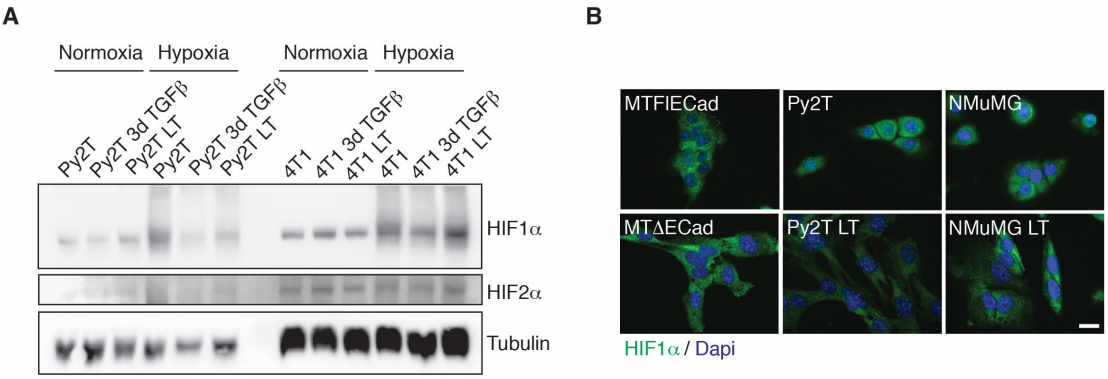

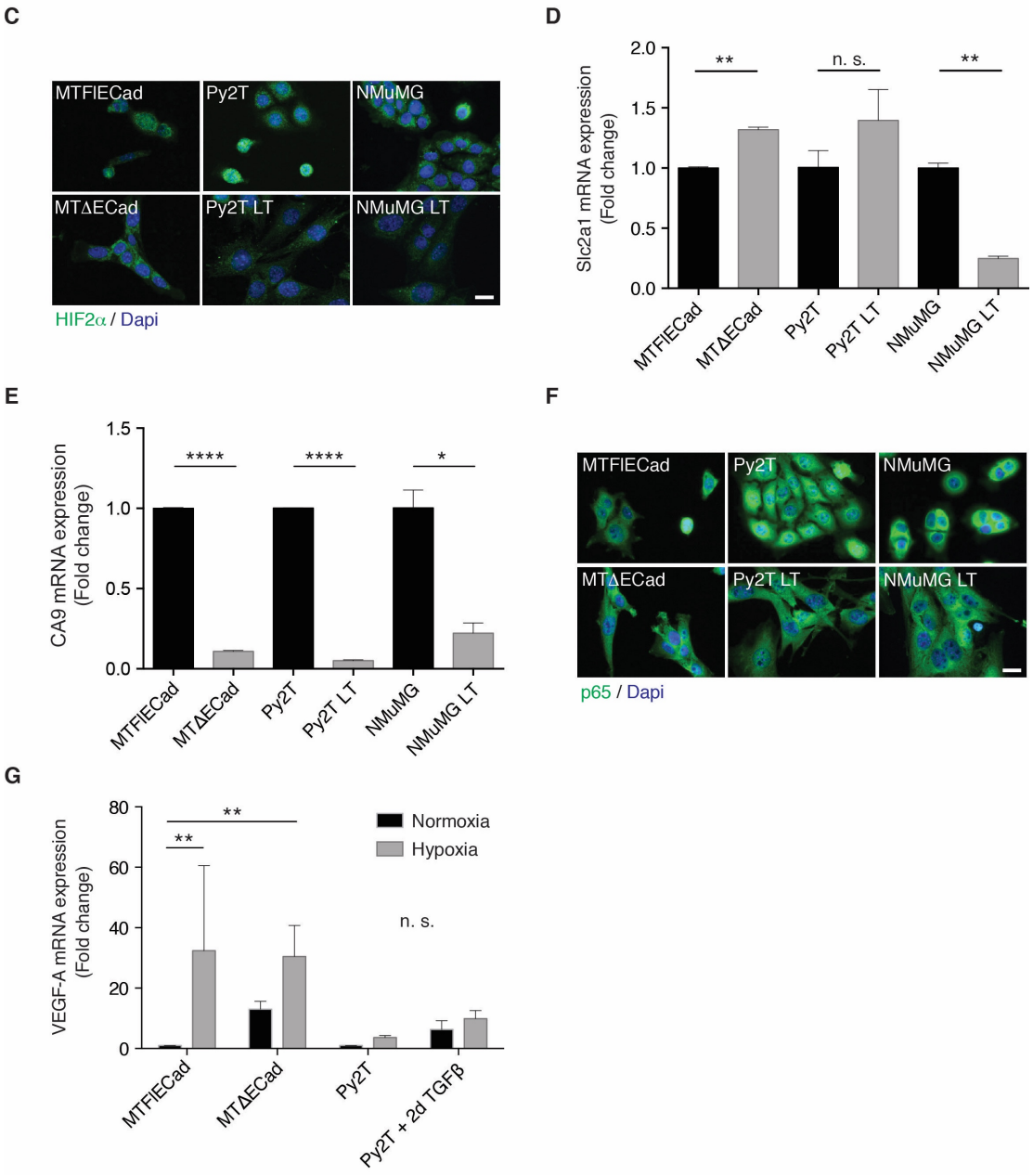

Figure 2: The EMT reprogramming does not induce a hypoxic signature.
(A) HIF1α and HIF2 α protein expression were assessed by immunoblotting in Py2T and 4T1 cell lines after 3 days or LT TGF-β treatment in comparison with untreated cells. Cells cultured under hypoxic conditions served as positive control and tubulin was used as loading control.
(B-C) HIF1α (B) and HIF2α (C) protein concentration and subcellular localization were assessed by immunofluorescence. DAPI was used to visualize cell nuclei. Scale bars, 20 µm.
(D-E) Slc2a1 (D) and CA9 (E) mRNA expression were quantified by quantitative RT-qPCR in several epithelial (MTFlECad, Py2T and NMuMG) and mesenchymal (MTΔECad, Py2T LT and NMuMG LT) cell lines. Mean values of 3 different experiments are plotted with the SD. Statistical significances were calculated by unpaired Student's t-test. n. s., non significant; ** = $p < 0.01$.
(F) p65/Rela protein concentration and subcellular localization were assessed by immunofluorescence. DAPI was used to visualize cell nuclei. Scale bars, 20 µm.
(G) Quantification of VEGF-A mRNA level by RT-qPCR on epithelial (MTFlECad, Py2T) and mesenchymal (MTΔECad, Py2T treated for 2 days with TGF-β) cell lines subjected to normoxic or hypoxic culture conditions. Mean values of 5 different experiments are plotted with the SD. Statistical significances were calculated by 2-ways ANOVA-test. n. s., non significant; * = $p < 0.05$; ** = $p < 0.01$.

3.2.3.3. A siRNA-screen identified JunB as the main regulator of VEGF-A in mesenchymal cells

In order to identify the regulators of VEGF-A expression in mesenchymal cells we performed a low throughput siRNA-screen targeting six transcription factors possessing a binding site on the *VEGF-A* gene promoter and already known as VEGF-A regulators in other systems, namely HIF1α, HIF2α (Epas1), Rela (NFκB p65 subunit), Sp1, Stat3 and JunB (Jung, Isaacs et al. 2003, Schafer, Cramer et al. 2003, Schmidt, Textor et al. 2007). While siRNA-mediated knockdown of HIF1α and Rela decreased VEGF-A mRNA expression in MTΔECad cells, knockdown of JunB induced the strongest repression of VEGF-A expression (Figure 3A). This observation was also confirmed in Py2T LT cells where only JunB downregulation was found to significantly decrease VEGF-A mRNA levels (Figure 3B). In order to rule out the possibility of off target effects, we performed JunB knockdown using four different siRNAs. Three of these JunB targeting siRNA significantly repressed VEGF-A mRNA expression in mesenchymal cells (Figure 3C). VEGF-A protein levels were also measured using an ELISA. In three of the mesenchymal cell lines siRNA-mediated knockdown of JunB slightly decreased VEGF-A protein expression (Figure 3D). Unlike HIF1α, HIF2α and NFκB, JunB protein was expressed in the cell nuclei, and its expression was increased in mesenchymal cells, suggesting its increased transcriptional activity (Figure 3E). Using immunoblotting, both JunB protein levels and phosphorylation were shown to be increased in mesenchymal cancer cells (Figure 3F). When injected in the mammary fat pad of immunodeficient female mice (RG), MTΔECad cells retained a strong nuclear expression, suggesting the importance of JunB in tumorigenesis (Figure 3G). We finally assessed the ability of JunB to directly bind to the Activated Protein-1 (AP-1) binding site and mediate *VEGF-A* transcription in Py2T LT cells. For this, we used *VEGF-A*-promoter luciferase reporter constructs presenting either a wild type *VEGF-A* promoter or a *VEGF-A* promoter with mutated AP-1 and/or HRE (Hypoxia Response Element) binding sites (Schmidt, Textor et al. 2007). As expected, *VEGF-A* promoter activity was increased when Py2T LT cells were cultured under hypoxic condition and this transcriptional activity was repressed in cells expressed a mutated HRE binding site. However, we could not demonstrate the direct binding of JunB on the *VEGF-A* promoter. Indeed, *VEGF-A* promoter

activity was not repressed when the AP1 binding site was mutated. Similar data were obtained in MTΔECad and NMuMG LT cells (data not shown).

Together, our data indicate that JunB regulates VEGF-A expression in mesenchymal cells, but its direct binding on the *VEGF-A* promoter remains to be shown.

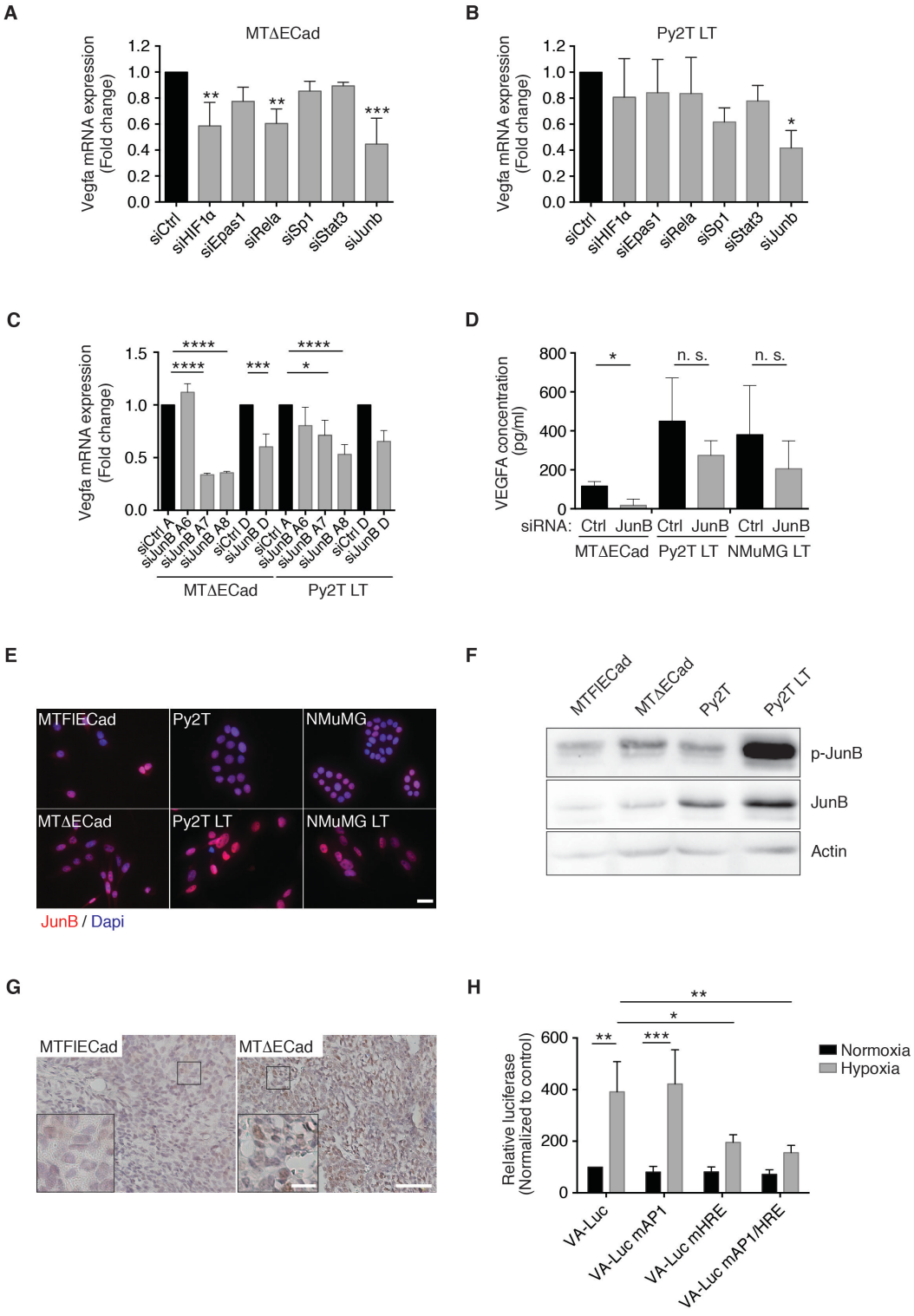

Figure 3: JunB induces VEGF-A expression in mesenchymal cells.
(A-B) VEGF-A mRNA expression was assessed by RT-qPCR after siRNA-mediated knockdown of HIF1a, Epas1, Rela, Sp1, Stat3 and JunB in MTΔECad **(A)** and Py2T LT **(B)** cells. Mean values of 3 different experiments are plotted with the SD. Statistical significances were calculated by 1-way ANOVA-test. *, p = 0.05; ** = p < 0.01; *** = p < 0.001.
(C) VEGF-A mRNA expression was assessed by RT-qPCR after siRNA-mediated knockdown of JunB in MTΔECad and Py2T LT cells. A, Ambion; D, Dharmacon, A6, A7 and A8, Ambion siRNA s68566, s68567 and s68568, respectively. Mean values of 3 different experiments are plotted with the SD. Statistical significances were calculated by 1-way ANOVA-test. *, p = 0.05; *** = p < 0.001; **** = p < 0.0001.
(D) Intracellular VEGF-A protein level was measured using in ELISA following JunB siRNA-mediated knockdown in MTΔECad, Py2T LT and NMuMG LT cells. Mean values of 3 different experiments are plotted with the SD. Statistical significances were calculated by unpaired Student's t-test. n. s., non significant; *, p = 0.05.
(E) JunB protein concentration and localization were assessed by immunofluorescence in MTFlECad, MTΔECad, Py2T, Py2T LT, NMuMG and NMuMG LT cells. DAPI was used to visualize cell nuclei. Due to lower JunB expression in MTFlECad and MTΔECad different settings were used for this EMT system. JunB expression in these cells should therefore not be compared with the other EMT systems analyzed here. Scale bars, 30 μm.
(F) JunB protein expression and phosphorylation were measured by Western blot in MTFlECad, MTΔECad, Py2T and Py2T LT cells. Actin was used as loading control.
(G) MTFlECad and MTΔECad cells were injected in the fat pad of immunodeficient mice and JunB protein expression (brown) was assessed by immunohistochemistry. Scale bar, 50 μm and 10 μm for the high magnification inserts.
(H) *VEGF-A* transcription in Py2T LT cells was measured using a wild type *VEGF-A* promoter luciferase reporter or *VEGF-A* promoter luciferase reporter constructs with a mutated form of the AP-1 and/or HRE binding sites. VA-Luc, *VEGF-A*-Luciferase; m, mutated. Mean values of 3 different experiments are plotted with the SD. Statistical significances were calculated by 2-ways ANOVA-test. * = p < 0.05; ** = p < 0.01; *** = p < 0.001.

3.2.3.4. Other members of the AP-1 complex can modulate VEGF-A

JunB belongs to the AP-1 family of transcription factors. These proteins always act as homo- or heterodimers (Eferl and Wagner 2003). Therefore, in order to next identify JunB partners in mesenchymal cells we assessed the ability of the other AP-1 family members to induce VEGF-A mRNA expression. For this, we downregulated their expression by siRNA-mediated knockdown either alone or in combination with JunB-targeting siRNA. In MTΔECad cells only Jun knockdown was able to reduce VEGF-A mRNA level in a similar manner to the JunB knockdown (Figure 4A). In Py2T cells, both Jun and JunD siRNAs were able to decrease VEGF-A expression (Figure 4B). Moreover, Jun and JunD inhibition in combination with JunB targeting siRNA had an additive effect on VEGF-A mRNA expression, suggesting that Jun and JunB might dimerize in mesenchymal cells.

Together, these results identify Jun as an alternative regulator of VEGF-A expression in mesenchymal cells and suggest the implication of a Jun/JunB heterodimer in this process.

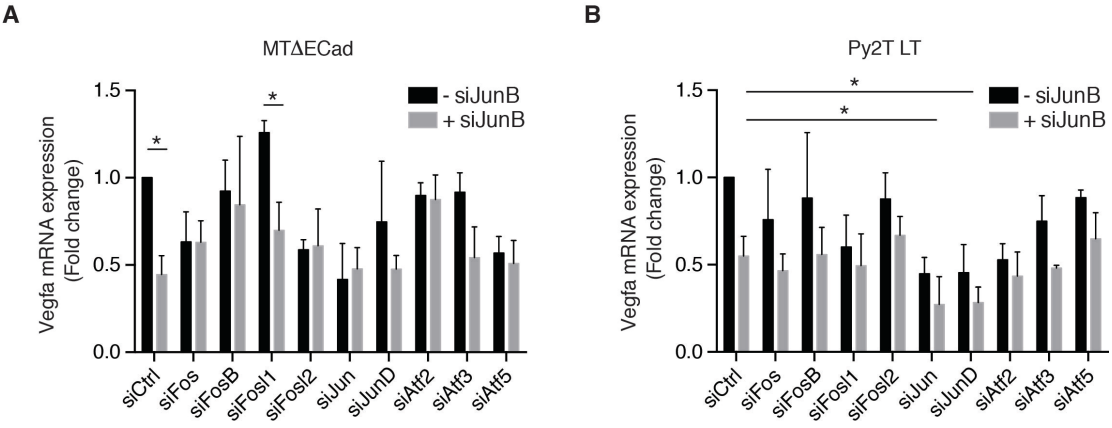

Figure 4: Jun knockdown decreases VEGF-A expression.
(A-B) VEGF-A mRNA expression in MTΔECad (A) and Py2T LT (B) cells was quantified by RT-qPCR after siRNA-mediated knockdown of the different members of the AP-1 family either alone or in combination with JunB. Mean values of 3 different experiments are plotted with the SD. Statistical significances were calculated by 2-ways ANOVA-test. * = $p < 0.05$.

3.2.3.5. Different branches of the MAPK signaling induce VEGF-A expression

Transcriptional, translational but also post-translational regulation of the AP-1 family members relies on Mitogen-Activated Protein Kinases (MAPK) signaling pathways. Depending on the cellular system and the AP-1 members analyzed, p38, Jnk or Erk signaling can be implicated (Karin 1995, Eferl and Wagner 2003). In order to gain insight into the upstream regulation of JunB-mediated VEGF-A expression, we studied the effect of MAPK signaling inhibition on VEGF-A mRNA expression. p38, Erk and Jnk signaling all play an important role in EMT and are know to be activated in our cellular systems (Waldmeier, Meyer-Schaller et al. 2012, Lamouille, Xu et al. 2014). MTΔECad and Py2T LT cells were treated with various concentrations of SB203580, PD98059 and SP600125 in order to pharmacologically inhibit p38, Erk and Jnk signaling pathways, respectively (Cuenda, Rouse et al. 1995).

SB203580 demonstrated a strong inhibition of MAPKAPK2 phosphorylation - a known substrate of p38 MAPK - with doses as low as 1 µM in both cell lines (Figure 5A) (Xu, Chen et al. 2006). PD98059 inhibited Erk phosphorylation at 10 µM (Figure 5B). As highlighted by MTT assay, pharmacological inhibition of the Jnk signaling pathway using SP600125 induced cell death in MTΔECad and Py2T LT cells (Figure 5C). Thus, we decided to inhibit Jnk by using siRNA-mediated knockdown. We achieved an efficient knockdown with no visible toxic effect (Figure

5D). We then quantified VEGF-A mRNA expression in response to inhibition of the different MAPK signaling pathways. While Erk and Jnk inhibition decreased VEGF-A expression in MTΔECad cells, in Py2T LT cells, VEGF-A levels were reduced following p38 inhibition (Figure 5E-F). In order to avoid compensatory mechanisms, we also performed combined inhibition of the signaling pathways. The additive effects observed when we inhibited several pathways together suggests redundancy of these pathways in VEGF-A regulation and possible compensation or cooperation mechanisms occurring when inhibiting each one of them individually (Figure 5E-F).

Altogether our data suggest that VEGF-A expression is mediated by Erk and Jnk signaling pathways in MTΔECad cells, while p38 seems to play a more important role in a TGF-β-induced EMT model.

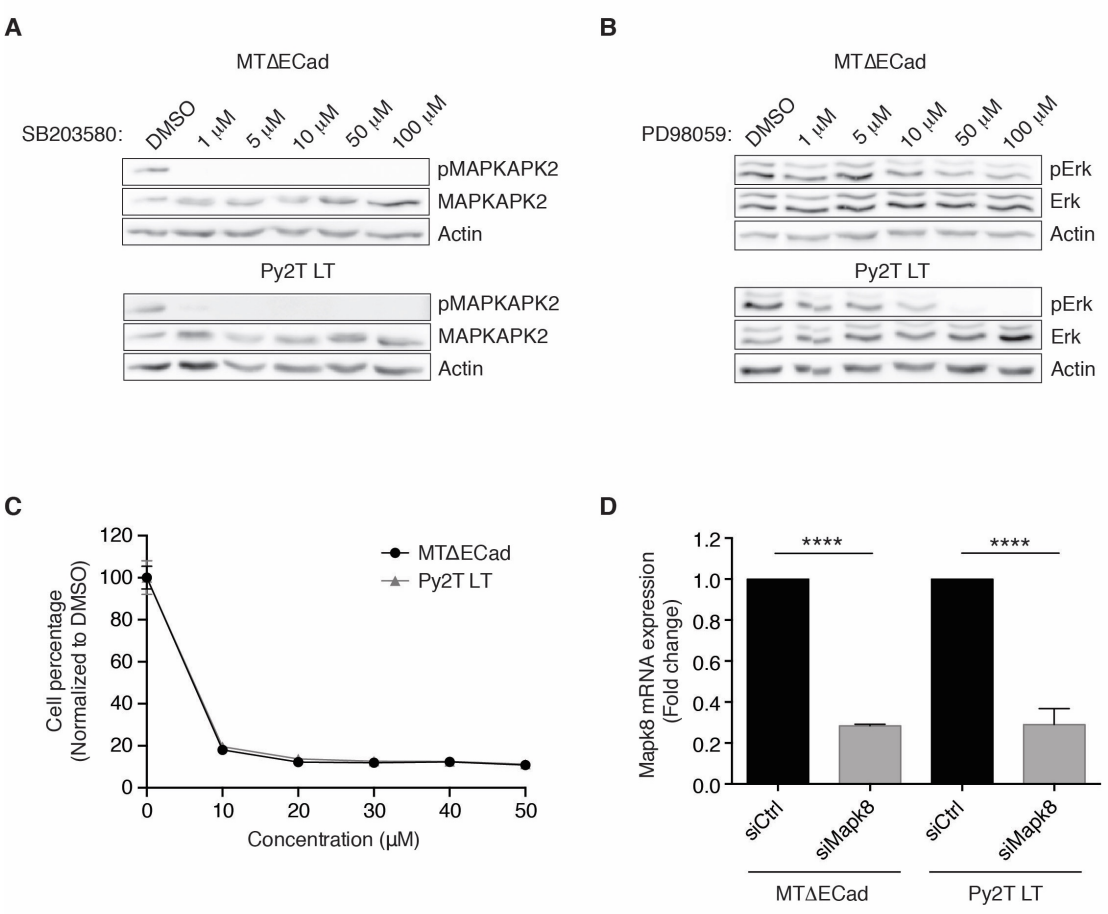

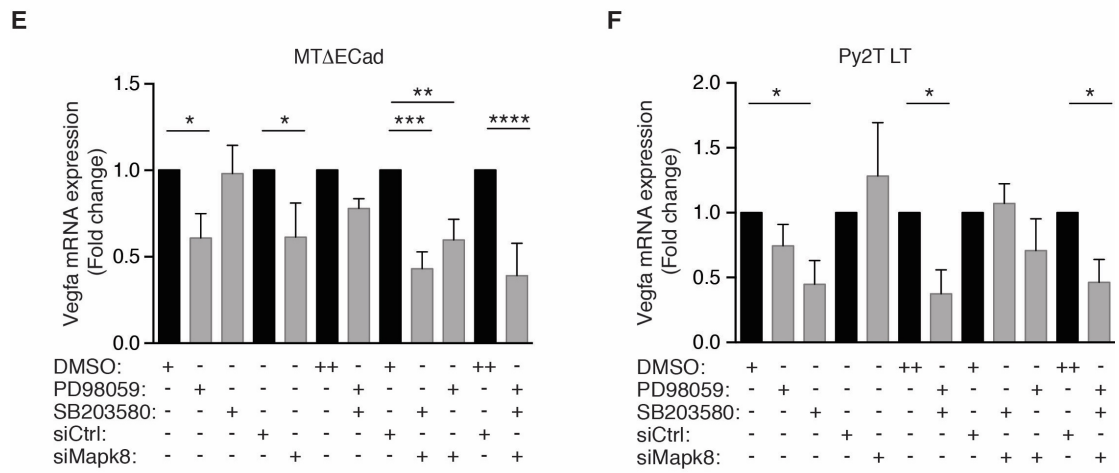

Figure 5: MAPK signaling pathways act in concert to regulate VEGF-A expression.
(A) SB203580 efficacy in MTΔECad and Py2T LT cells was assessed using Western blot against phospho-MAPKAPK2, a direct downstream target of p38. Total MAPKAPK2 and Actin served as loading controls.
(B) Western blot against phospho-Erk was performed to evaluate PD98059 efficacy in MTΔECad and Py2T LT cells. Total Erk and Actin served as loading controls.
(C) SP600125 toxicity on MTΔECad and Py2T LT cells was determined using MTT assay. Mean values of 3 different experiments are plotted with the SD. Values were normalized to DMSO control.
(D) Mapk8 knockdown efficiency in MTΔECad and Py2T LT cells was quantified by RT-qPCR. Mean values of 3 different experiments are plotted with the SD. Statistical significances were calculated by unpaired Student's t-test. ****, p = 0.0001.
(E-F) VEGF-A mRNA expression after inhibition of the different branches of the MAPK signaling in MTΔECad (E) and Py2T LT (F) cells was assessed by RT-qPCR. -, inhibitor or siRNA was not added; +, inhibitor or siRNA was added; ++, double volume of DMSO was added. PD98059 and SB203580 were used at a concentration of 10 μM. Mean values of 3 different experiments are plotted with the SD. Statistical significances were calculated by 1-way ANOVA-test. * = $p < 0.05$; ** = $p < 0.01$; *** = $p < 0.001$; ****, p = 0.0001.

3.2.3.6. JunB expression protects cells against apoptosis

JunB seems to play a more complex role in cancer cells than primarily anticipated. Indeed, while it did not affect survival of NMuMG LT cells it decreased mesenchymal cancer cell survival (Figure 6A). Cleaved-caspase3 staining revealed increased apoptosis in cells presenting an efficient knockdown of JunB (Figure 6B).

All together these findings indicate an important role of Junb in protecting cancer cells against apoptosis during an EMT.

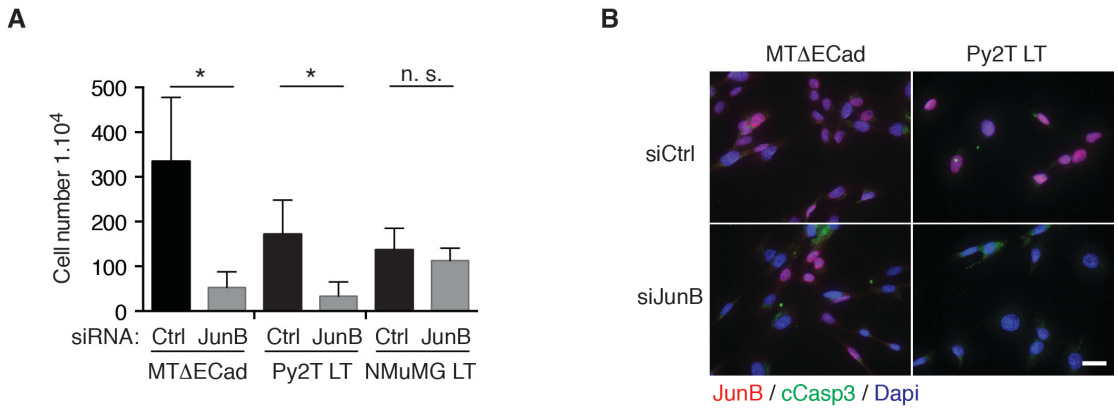

Figure 6: JunB downregulation leads to cell apoptosis
(A) Cell number was determined 4 days after transfection with either a non-targeting siRNA (siCtrl) or a siRNA against JunB. Mean values of 3 different experiments are plotted with the SD. Statistical significances were calculated by unpaired Student's t-test. n. s., non significant; *, $p < 0.05$.
(B) One day after siRNA transfection, cells were stained for JunB and cleaved caspase 3 to assess the effect of JunB inhibition on apoptosis. Due to lower JunB expression in MTΔECad cells different settings were used for this cell line. JunB expression in these cells should therefore not be compared with JunB expression in Py2T LT cells. DAPI was used to visualize cell nuclei. Scale bar, 30 µm.

3.2.4. Methods

Chemicals

Unless otherwise mentioned, all chemical compounds were purchased from Sigma-Aldrich.

Cell culture

MTFlECad, MTΔECad, Py2T, 4T1 and NMuMG/E9 cells were cultured in Dulbecco's modified Eagle's medium (DMEM, D5671, Sigma-Aldrich) supplemented with 10% FBS (F7524, Sigma-Aldrich), 2 mM L-glutamine (G7513, Sigma-Aldrich), 100U penicillin and 0.1 mg/ml streptomycin (P4333, Sigma-Aldrich). In order to induce EMT, cells were treated with 2 ng/ml TGF-β1 (240-B, R&D systems). HUVEC cells were cultured in M-199 medium (M4530, Sigma-Aldrich) supplemented with 40 µg/ml bovine pituitary gland extract (13028-014, Thermofischer Scientific), 80 U/ml Heparin (H3393, Sigma-Aldrich), 20% FCS, 2 mM glutamine, 100U penicillin and 0.1 mg/ml streptomycin. Recombinant mouse VEGF-A was purchased from R&D (493-MV-005). All the cells were cultured at 37°C with 5% CO2 in humid incubator except for hypoxia experiments where cells were grown in 1% O_2.

Cell growth quantification

$1x10^4$ cells were plated in triplicates in 24-well plates and quantified at different time points by using Neubauer chamber and Trypan blue exclusion.

MTT assay

Five hundred cells were plated in triplicates in a 96-well plate and allowed to attach overnight. On the following day the indicated concentrations of SP600125 (tlrl-sp60, InvivoGen) were added to the cells. Three days later, an MTT assay was performed as follows: medium was replaced by fresh complete medium containing 0.5 mg/ml MTT (CellTiter 96® Non-Radioactive Cell Proliferation Assay, G4000, Promega). Cells were incubated for 1h at 37°C. MTT-containing medium was then replaced by 100 µl of a solution of 95% isopropanol/5% formic acid. 100 µl of 10% SDS were added to each well. After 5 minutes incubation at 37°C, solution was mixed by pipetting and transferred in a new 96-well plate. Absorbance was measured at 570 nm. A second reading at 620 nm was used for normalization.

Viral infections

shRNA-mediated knockdown was performed using the following lentiviral constructs: Mission Non-Targeting shRNA control vector: SHC002; shVEGF-A #1: TRCN0000066818, #4: TRCN0000304451, #5: TRCN0000310985, #8: TRCN0000316047 (Sigma-Aldrich). VEGF-A overexpression was achieved using the retroviral pAMFG-mVEGF-A_IRES_CD8 expression vector kindly provided by Dr. Andrea Banfi (University of Basel). Plat-E or HEK293T cells were transfected using Fugene HD transfection reagent (E2311, Promega) together with the packaging vector pR8.92 and the envelope encoding plasmids pVSV for the HEK293T cells. On the next day virus containing supernatant was filtered and added to the target cells following addition of 8 µg/ml polybrene. Cells were centrifuged for 90 min and medium was replaced after 3 hours of incubation at 37°C.

Immunoblotting

For phospho-protein studies, cells were treated with 2 mmol/L sodium orthovanadate 20 min prior to cell lysis. After 2 PBS washes, cells were lyzed directly on the plate in HNIG buffer (50 mmol/L HEPES, pH 7.5, 150 mmol/L NaCl, 10% glycerol, 1%

Triton X-100, 1.5 mmol/L MgCl, 1 mmol/L EDTA, 10 mmol/L sodium PP_i, 2 mmol/L sodium orthovanadate, 100 mmol/L NaF, 1 mmol/L phenylmethylsulfonylfluoride) containing protease inhibitor cocktail (P2714, Sigma-Aldrich) for 30 min. Lysates were cleared by centrifugation and protein concentration was determined by Bradford assay (500-0006, Biorad). Equal amounts of protein were diluted in loading buffer (10% glycerol, 2% SDS, 65 mM Tris, 0.01 mg/ml Bromphenolblue, 1% betamercaptoethanol) resolved by SDS-PAGE and blotted on polyvinylidene difluoride (PVDF) membranes (IPVH00010, Millipore) by wet transfer. Membranes were then blocked with 5% milk in Tris-buffered saline with 0.05% Tween 20 for 1h and incubated overnight at 4°C with the primary antibodies listed in Table 1 (diluted in 5% bovine serum albumin, Sigma-Aldrich). HRP conjugated antibodies (Jackson Immunoresearch Laboratories) were diluted in 5% milk in Tris-buffered saline with 0.05% Tween 20 (1:5000) and incubated for 1h at room temperature. Signal was detected using Immobilon Western Chemiluminescent HRP Substrate (WBKLS0500, Millipore) and a Fusion FX imaging system (Vilber Lourmat).

Table 1: List of antibodies used for immunobloting

Protein	Catalog #	Manufacturer	Specie	Dilution
JunB	sc-8051	Santa Cruz	Mouse	1:1000
phospho-JunB Thr102/104	8053	Cell Signaling	Rabbit	1:1000
Erk	M7927	Sigma	Rabbit	1:5000
phopsho-Erk	M8159	Sigma	Mouse	1:5000
MAPKAPK2	3042P	Cell Signaling	Rabbit	1:1000
phospho-MAPKAPK2	3007P	Cell Signaling	Rabbit	1:1000
HIF1α	NB 100-449	Novus Biologicals	Rabbit	1:2000
HIF2α	NB 100-122	Novus Biologicals	Rabbit	1:2000
α -tubulin	T-9026	Sigma-Aldrich	Mouse	1:5000
Actin	sc-1616	Santa Cruz	Goat	1:1000

RNA interference

Gene down-regulation was achieved using the different siRNAs presented in Table 2 (20 nM) and the following protocol: $3.5x10^4$ cells were plated in a 6-well plate. Reverse transfection was immediately performed using 4 µl (MTΔECad) or 8 µl (Py2T LT cells) Lipofectamine RNAiMax (1668-019, Invitrogen) diluted in OptiMEM (11058, Gibco). Two days later, transfection was repeated and cells were analyzed after 2 further days in culture.

Table 2: List of siRNAs used

Gene	Gene ID	Catalog #	Manufacturer
Junb	16477	s68566 s68567 s68568	Silencer Select Ambion
Hif1a	15251	s67531	
Epas1	13819	s65526	
Sp1	20683	s74195	
Stat3	20848	s74452	
Rela	19697	s72857	
Jun	16476	s68564	
Jund	16478	s201553	
Fos	14281	s66198/s66199 1:1 mix	
Fosb	14282	s201359	
Fosl1	14283	s66205	
Fosl2	14284	s66208	
Atf2	11909	s62683/s62685 1:1 mix	
Atf3	11910	s62686	
Atf5	107503	s98868	
Mapk8	26419	s77120	
Non-targeting	-	4390847	
JunB	16477	L-041158-00-0005	ON-Target Plus siRNA Dharmacon
Non-targeting	-	D-001810-10-20	

Drug treatment

$3.5x10^4$ cells were plated in 6-well plates and allowed to attach overnight. On the next day, cells were treated with the indicated concentrations of SB203580 (tlrl-sb20, InvivoGen), PD98059 (tlrl-pd98, InvivoGen). Cells were harvested to assess drug efficiency and response of downstream targets after 1h or 72h of treatment, respectively.

Enzyme-linked immunesorbent assay

$5x10^4$ cells were plated in 6 cm dishes in duplicates. Three days later medium was replaced and conditioned overnight. On the measurement day, conditioned medium was harvested and cleared by centrifugation. Cells were washed twice with cold PBS and lysed following the protocol described for immunoblotting. VEGF-A concentration was quantified in cell culture supernatants and lysates using the Quantikine ELISA kit (MMV00, R&D) following the manufacturer's protocol. Optical density of each sample was determined in duplicate by using the microplate reader Spectra MAX 340 (Bucher Biotec AG) set to 450 nm wavelength. In parallel, cells from the second dish were trypsinized and counted in order to normalize the VEGF-A concentration to cell number for each cell line.

Luciferase assay

$1x10^4$ MTΔECad or Py2T cells and $1.5x10^4$ MTFlECad, Py2T LT, NMuMG/E9 or NMuMG/E9 LT cells were plated in triplicates in a 24-well plate. To increase transfection efficiency cells were reverse transfected using 500 ng Vegfa-luciferase WT or mutated constructs (kindly provided by Dr Marina Schorpp-Kistner, DKFZ Heidelberg), 10 ng Renilla encoding plasmids and 0.75 µl Lipofectamine 3000 (L3000015, Thermofischer Scientific). After 3 days, cells were lysed directly in the plate using 1x passive lysis buffer (E194, Promega) and lysates were analyzed using the Dual-Luciferase Reporter Assay System (E1960, Promega) and a Berthold Luminometer LB960. Measured luciferase values were normalized to internal Renilla control.

Orthotopic transplantation

Two hundred MTFlECad or MTΔECad cells were injected in the ninth mammary fat pad of 7-10 weeks old BALB/c Rag2−/−;common γ receptor−/− female mice (kindly provided by Antonius Rolink, University of Basel).

Immunostainings

For immunohistochemistry staining, tumors were fixed at 4°C in 4% phosphate-buffered paraformaldehyde (PFA) overnight. Following ethanol/xylene dehydration, tumors were embedded in paraffin. Five μm thick sections were stained as follows: after deparaffinization, antigen retrieval was performed using "Retriever 2100" (EMS) with 10 mM citrate buffer pH 6.0. Sections were then quenched in 3% H2O2 for 15 min and blocked for 1h in 5% goat serum at room temperature. JunB antibody (sc-8051, Santa Cruz, 1:50 in blocking solution) was incubated overnight at 4°C. Biotinylated secondary antibody (1:200) was incubated for 1h at room temperature. AEC substrate was then added for 5 min (ABC kit, PK6100, Vector Laboratories). Sections were finally counterstained and mounted using CytoSeal XYL (8312-16E, Thermo Scientific). Images were acquired using Axioskop2 plus microscope equipped with an AxioCam MRc camera (Zeiss).

Immunofluorescence staining of cultured cells

Cells were grown on microscopy glass slides (80841, Ibidi) and fixed with 4% PFA at room temperature for 15 min. Following 5 min permeabilization with 0.5% NP40, blocking step was performed using 3% BSA in PBS-Triton (0.01%) during 30 min. Primary antibody diluted in 3% BSA in PBS-Triton (see dilutions in Table 3) were incubated for 1.5 h at room temperature. Finally, Alexa-Fluor-coupled antibodies (Invitrogen) were diluted 1:300 in 3% BSA in PBS-Triton and incubated for 1h at room temperature. 6-diamidino-2-phenylindol (Dapi; D9542, Sigma-Aldrich; 1:5000 for 7 min) was used to visualize nuclei and mounting was performed using Dako fluorescence mounting medium (S3023, Dako). Images were taken with Leica DMI 4000 microscope (Leica Microsystems) and data was analyzed using ImageJ software.

Table 3: Antibodies used for immunohistochemistry/immunofluorescence staining

Protein	Catalog #	Manufacturer	Specie	Dilution
JunB	sc-8051	Santa Cruz	Mouse	1:75
Cleaved Caspase 3	9664	Cell Signaling	Rabbit	1:50
p65 (NFKB)	sc-372X	Santa Cruz	Rabbit	1:300
HIF1α	NB 100-449	Novus Biologicals	Rabbit	1:100
HIF2α	NB 100-122	Novus Biologicals	Rabbit	1:100

RNA extraction, reverse transcription and qPCR

Total RNA was isolated using TriReagent (T9424, Sigma-Aldrich) and reverse transcribed using Moloney Murine Leukemia Virus Reverse Transcriptase (ImProm-II Reverse Transcriptase, M314C 28692233, Promega). Transcripts listed in Table 4 were then quantified by Real Time quantitative PCR (Step One Plus, Applied Biosystems) using SYBR-green PCR MasterMix (4909155, Invitrogen). Ribosomal protein L19 primers were used for normalization. Fold induction was calculated using the comparative Ct method (ΔΔCt).

Table 4: Primers used (5' -> 3')

Gene	Forward	Reverse
Vegfa	actggaccctggctttactg	tctgctctccttctgtcgtg
Junb	accacggagggagagaaaag	agttggcagctgtgcgtaa
Hif1a	gcactagacaaagttcacctgaga	cgctatccacatcaaagcaa
Epas1	ccccagggaacactacacc	caagggattctccaaggatg
Sp1	gctatagcaaacaccccaggt	tccacctgctgtctcatcat
Stat3	caagggattctccaaggatg	gttcctggcaccttggatt
Rela	cccagaccgcagtatccat	gctccaggtctcgcttctt
Jun	ccagaagatggtgtggtgttt	ctgaccctctcccccttgc
Jund	gagtgagattctgtttcaaaacgtc	tgggtgcagtcacgtttactt
Fos	cgggtttcaacgccgacta	ttggcactagagacggacaga
Fosb	gttcgcagagagcggaac	gccttttcctcttcaagctg
Fosl1	cccagtacagtccccctca	tcctcctctgggctgatct
Fosl2	acgccgagtcctactccag	caggcatatctacccggaac

Atf2	tttggtccagcacgtaatga	atcttgttggcgttggagtc
Atf3	gctggagtcagttaccgtcaa	cgcctccttttcctctcat
Atf5	ctcccaattgttggtgcag	ccaggagtgacatggctgt
Mapk8	aactgttccccgatgtgct	tctcttgcctgactggcttt
Rpl19	ctcgttgccggaaaaaca	tcatccaggtcaccttctca

Statistical analysis

Statistical analysis and graphs were generated using the GraphPad Prism software (GraphPad Software Inc, San Diego, CA). n. s., non significant; *, $p \leq 0.05$; **, $p \leq 0.01$; ***, $p \leq 0.001$; ****, $p \leq 0.0001$.

3.2.5. Discussion

Angiogenesis and EMT play a central role in tumor progression. We recently demonstrated that EMT reprogramming induces the secretion of pro-angiogenic factors, such as VEGF-A (Fantozzi, Gruber et al. 2014). Furthermore, we associated this pro-angiogenic signature with tumor initiation. Our study revealed that mesenchymal cell-derived VEGF-A actively induced angiogenesis *in vivo*, hence increasing the tumorigenic potential of these cells. However, the molecular mechanisms regulating secretion of VEGF-A during EMT remained elusive.

Here, we show that mesenchymal cell-derived VEGF-A is sufficient to induce endothelial cell survival, through Akt signaling activation. EMT is proposed to induce a "hypoxic" signature (Goel and Mercurio 2013). Indeed, TGF-β is known to stabilize HIF1α in normoxic conditions (McMahon, Charbonneau et al. 2006). However, even though HIF1α knockdown decreased VEGF-A mRNA expression in MTΔECad cells, our data did not support activation of such a hypoxic signature in our EMT systems. Indeed, HIF1α was not recruited to the nucleus during EMT. Interestingly, Villa and colleagues recently described a new mechanism of action for HIF1α (Villa, Chiu et al. 2014). They demonstrated that HIF1α activates the Notch pathway though a non-transcriptional mechanism. The possibility for HIF1α to regulate VEGF-A expression through a non-transcriptional and non-canonical mechanism cannot be excluded in our models. However, we also did not observe increased HIF1α protein expression in mesenchymal versus epithelial cells. In a similar manner, HIF2α and NFκB - two

other hypoxia-related factors that can bind the *VEGF-A* promoter - were shown by other laboratories to be essential for EMT and breast cancer metastases (Huber, Azoitei et al. 2004, Helczynska, Larsson et al. 2008). However, these signaling pathways were not found activated in our systems.

Instead, by performing a small siRNA screen we have identified JunB as the main regulator of VEGF-A expression in mesenchymal cells. Moreover, we show its increased expression and phosphorylation in mesenchymal cells. Until recent years JunB has been considered a tumor suppressor gene with low if any transcriptional activity on AP-1-responsive genes. Compared to Jun, JunB is thought to present reduced DNA-binding activity and lack phosphorylation sites. It has been long thought to dimerize with Jun in order to decrease Jun transcriptional activity and therefore repress its pro-tumorigenic potential (Deng and Karin 1993). However, its role in tumor progression is currently being reevaluated. Indeed, recent publications implicated JunB in EMT, angiogenesis and tumor metastases (Schmidt, Textor et al. 2007, Gurzov, Bakiri et al. 2008, Gervasi, Bianchi-Smiraglia et al. 2012, Kanno, Kamba et al. 2012). Therefore, JunB seems to play a more complex role in cancer progression and cell biology than primarily anticipated and it is now proposed as a new target in cancer therapy (Gurzov, Bakiri et al. 2008).

JunB can form homo- or heterodimers with other members of the AP-1 family. Our data reveals that Jun inhibition also leads to decreased VEGF-A mRNA expression and that combining Jun and JunB inhibition enhance *VEGF-A* gene repression. This implies that Jun might dimerize with JunB in order to induce VEGF-A expression. Co-immunoprecipitation experiment should be performed to test this hypothesis.

We finally have observed that siRNA-mediated inhibition of JunB led to apoptosis in cancer cells. EMT has been described as the "ultimate survival mechanism for cancer cells" (Tiwari, Gheldof et al. 2012). It would not be surprising, if JunB plays a central role in this process. Interestingly, JunB is already known to protect pancreatic β-cells against apoptosis by activating the Unfolded Protein Response element Xpb1, a gene also implicated in EMT and in VEGF-A expression (Gurzov, Ortis et al. 2008, Ghosh, Lipson et al. 2010, Cunha, Gurzov et al. 2014, Martin, Loibl et al. 2015). Junb phosphorylation by JNK has been implicated in tissue

regeneration in Zebrafish (Ishida, Nakajima et al. 2010). In this case, and as suggested by our data, JunB phosphorylation is required for cell survival and proliferation.

In conclusion, we demonstrate that i) EMT-induced VEGF-A expression is not due to the activation of hypoxic pathways and that ii) JunB is responsible for VEGF-A expression in mesenchymal cells (Figure 7).

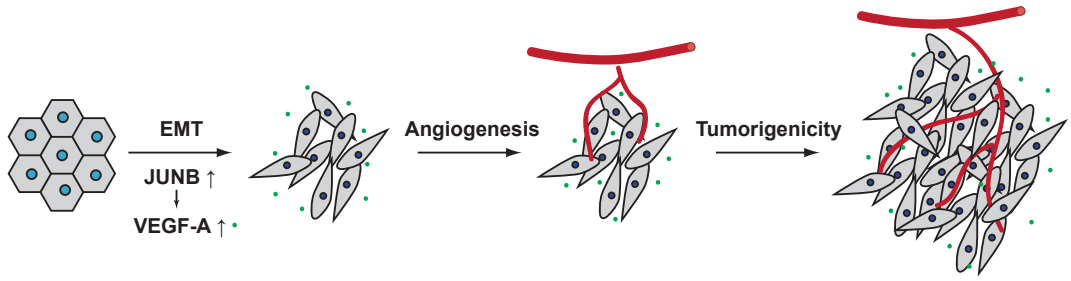

Figure 7: JunB mediates VEGF-A expression during EMT
We have recently shown that EMT program is associated with a pro-angiogenic signature, notably through the expression of VEGF-A. VEGF-A induces angiogenesis *in vivo* and increases the tumorigenic potential of mesenchymal cells. Here, we have identified JunB as a main regulator of VEGF-A expression in mesenchymal cells.

Some additional experiments remain to be performed to better characterize the implication of JunB in EMT-induced VEGF-A expression. For example, we have not been able to prove the direct binding of JunB to the *VEGF-A* promoter. JunB might bind to an alternative binding site (enhancer e.g.) or might not directly induce *VEGF-A* gene transcription. Therefore, we are currently optimizing a chromatin immunoprecipitation (ChIP) for JunB in mesenchymal cells. This experiment will allow us to assess the direct binding of JunB on the *VEGF-A* promoter. Furthermore, by overlapping the ChIP-sequencing data with RNA-sequencing data from an EMT time course we will be able to decipher the global role of JunB in EMT progression.

It will also be interesting to assess whether JunB inhibition *in vivo* represses VEGF-A expression and would result in delayed tumor onset. I have already generated doxycyclin-inducible shJunB cell lines for this purpose. However, this experiment may be hampered by the pro-apoptotic effect of JunB inhibition. Finally, despite its expression in human breast carcinomas, the role of JunB in human breast cancer progression and metastasis still has to be determined (Kharman-Biz, Gao et al. 2013).

4. General discussion and outlook

Over forty years have passed since the concept of anti-angiogenic therapy has been suggested for the first time. During these decades the work of several generations of scientists transformed this idea into clinical reality. However, anti-angiogenic therapy, proposed as the ultimate treatment that would "resist to resistance", offered only limited benefits to the patients, due to the development of therapy resistance (Kerbel 1997).

During my Ph.D., I have studied different aspects of angiogenesis, from the molecular mechanisms inducing VEGF-A secretion to those leading to the development of resistance against anti-angiogenic therapy. The work presented here, together with other projects to which I contributed, has demonstrated the importance of angiogenesis not only during tumor growth but also during tumor initiation and metastasis. In order to profit by anti-angiogenic therapy, one should continue deciphering the molecular basis of the angiogenic process.

Development of multikinase inhibitors, such as nintedanib, hold great promise in overcoming resistance to anti-angiogenic therapy. However, despite their potent and stable inhibition of tumor vascularization, tumors are still able to escape therapy. Our observations that tumor cells can adapt their metabolism to survive into nutrient-deprived environment has led us to propose anti-angiogenic/anti-glycolytic treatment combination. Even though MCT4 KO has evoked a striking decrease in tumor volume in combination with anti-angiogenic therapy, tumor progression is still not completely halted. However, one should not forget that metabolic symbiosis does not only occur between tumors cells and that the tumor microenvironment can also be incriminated. Therefore, pharmaceutical approaches using MCT4 inhibitors that will target all different tumor compartments should give better results.

Here, I have restricted my analysis to the primary tumor. However, in many breast cancer patients anti-angiogenic therapy is used as a neo-adjuvant therapy, i.e. patients receive it after removal of the primary tumor in order to control metastatic outgrowth. Interestingly, only few data support the use of anti-angiogenic therapy in such settings and most data suggest that anti-angiogenic therapy might increase metastatic spread. Therefore, it will be interesting to study the response of the

(pre)metastatic lesions to anti-angiogenics. Would they also become glycolytic? Would they also grow despite a lack of blood vessels?

Our observation that EMT-induced cancer stem cells induce angiogenesis raises questions regarding the stem cell niche (Fantozzi, Gruber et al. 2014). It is well established that CSCs reside in close vicinity of the blood vessels, but for still unknown reasons. Are stem cells only able to survive in the close vicinity of the blood vessels or are they simply localized next to the blood vessels because they foster their recruitment?

My data suggest the implication of JunB in EMT-induced angiogenesis. While originally proposed to be a tumor-suppressor gene, more and more data support a critical role of JunB in tumor progression. Its involvement in EMT and in tumor angiogenesis makes it a prime target to combat cancer. Interestingly, we have observed that JunB inhibition selectively kills tumor cells without harming normal mammary gland cells. However, one question still remains: how does JunB induce VEGF-A expression? Luciferase reporter assays have failed to prove the direct binding of JunB on the AP1 promoter. Does it bind to another site, lying for example within an enhancer? Does JunB indirectly induce VEGF-A expression?

My Ph.D. work underlies the importance of tumor heterogeneity and interactions occurring between the different cell types within a tumor. Indeed, VEGF-A secretion could not support tumor initiation, if endothelial cells would not respond to this growth factor by sprouting. Furthermore, EMT would probably be meaningless, if blood vessels are not present to carry tumor cells to their final destination. Besides these heterotypic interactions, our project about anti-angiogenic resistance reveals the importance of symbiosis between different tumor cell types. In such a situation, exchange of metabolites between tumor cells running on different metabolic needs allows them to survive and proliferate.

The specific interactions established between tumors cells and their microenvironment reveal a high specificity between individual patients that may in addition evolve during tumor progression. These observations underline the increasing need for personalized therapies. Several additional generations of researchers will probably be required in order to fully understand the complexity of tumor angiogenesis and to be able to find the perfect combination therapy that definitively cures cancer.

5. Bibliography

Abramsson, A., P. Lindblom and C. Betsholtz (2003). "Endothelial and nonendothelial sources of PDGF-B regulate pericyte recruitment and influence vascular pattern formation in tumors." J Clin Invest **112**(8): 1142-1151.

Al-Hajj, M., M. S. Wicha, A. Benito-Hernandez, S. J. Morrison and M. F. Clarke (2003). "Prospective identification of tumorigenic breast cancer cells." Proc Natl Acad Sci U S A **100**(7): 3983-3988.

Albrecht, I., L. Kopfstein, K. Strittmatter, T. Schomber, A. Falkevall, C. E. Hagberg, P. Lorentz, M. Jeltsch, K. Alitalo, U. Eriksson, G. Christofori and K. Pietras (2010). "Suppressive effects of vascular endothelial growth factor-B on tumor growth in a mouse model of pancreatic neuroendocrine tumorigenesis." PLoS One **5**(11): e14109.

Algire, G. H. and H. W. Chalkley (1945). "Vascular Reactions of Normal and Malignant Tissues Invivo .1. Vascular Reactions of Mice to Wounds and to Normal and Neoplastic Transplants." Journal of the National Cancer Institute **6**(1): 73-85.

Arcondeguy, T., E. Lacazette, S. Millevoi, H. Prats and C. Touriol (2013). "VEGF-A mRNA processing, stability and translation: a paradigm for intricate regulation of gene expression at the post-transcriptional level." Nucleic Acids Res **41**(17): 7997-8010.

Armulik, A., A. Abramsson and C. Betsholtz (2005). "Endothelial/pericyte interactions." Circ Res **97**(6): 512-523.

Awasthi, N., S. Hinz, R. A. Brekken, M. A. Schwarz and R. E. Schwarz (2014). "Nintedanib, a triple angiokinase inhibitor, enhances cytotoxic therapy response in pancreatic cancer." Cancer Lett.

Awasthi, N., S. Hinz, R. A. Brekken, M. A. Schwarz and R. E. Schwarz (2015). "Nintedanib, a triple angiokinase inhibitor, enhances cytotoxic therapy response in pancreatic cancer." Cancer Lett **358**(1): 59-66.

Bachelder, R. E., A. Crago, J. Chung, M. A. Wendt, L. M. Shaw, G. Robinson and A. M. Mercurio (2001). "Vascular endothelial growth factor is an autocrine survival factor for neuropilin-expressing breast carcinoma cells." Cancer Res **61**(15): 5736-5740.

Bais, C., X. Wu, J. Yao, S. Yang, Y. Crawford, K. McCutcheon, C. Tan, G. Kolumam, J. M. Vernes, J. Eastham-Anderson, P. Haughney, M. Kowanetz, T. Hagenbeek, I. Kasman, H. B. Reslan, J. Ross, N. Van Bruggen, R. A. Carano, Y. J. Meng, J. A. Hongo, J. P. Stephan, M. Shibuya and N. Ferrara (2010). "PlGF blockade does not inhibit angiogenesis during primary tumor growth." Cell **141**(1): 166-177.

Batchelor, T. T., A. G. Sorensen, E. di Tomaso, W. T. Zhang, D. G. Duda, K. S. Cohen, K. R. Kozak, D. P. Cahill, P. J. Chen, M. Zhu, M. Ancukiewicz, M. M. Mrugala, S. Plotkin, J. Drappatz, D. N. Louis, P. Ivy, D. T. Scadden, T. Benner, J. S. Loeffler, P. Y. Wen and R. K. Jain (2007). "AZD2171, a pan-VEGF receptor tyrosine kinase inhibitor, normalizes tumor vasculature and alleviates edema in glioblastoma patients." Cancer Cell **11**(1): 83-95.

Bates, R. C., J. D. Goldsmith, R. E. Bachelder, C. Brown, M. Shibuya, P. Oettgen and A. M. Mercurio (2003). "Flt-1-dependent survival characterizes the epithelial-mesenchymal transition of colonic organoids." Curr Biol **13**(19): 1721-1727.

Beck, B., G. Driessens, S. Goossens, K. K. Youssef, A. Kuchnio, A. Caauwe, P. A. Sotiropoulou, S. Loges, G. Lapouge, A. Candi, G. Mascre, B. Drogat, S. Dekoninck, J. J. Haigh, P. Carmeliet and C. Blanpain (2011). "A vascular niche and a VEGF-Nrp1 loop regulate the initiation and stemness of skin tumours." Nature **478**(7369): 399-403.

Beenken, A. and M. Mohammadi (2009). "The FGF family: biology, pathophysiology and therapy." Nat Rev Drug Discov **8**(3): 235-253.

Bergers, G., R. Brekken, G. McMahon, T. H. Vu, T. Itoh, K. Tamaki, K. Tanzawa, P. Thorpe, S. Itohara, Z. Werb and D. Hanahan (2000). "Matrix metalloproteinase-9 triggers the angiogenic switch during carcinogenesis." Nat Cell Biol **2**(10): 737-744.

Bergers, G. and D. Hanahan (2008). "Modes of resistance to anti-angiogenic therapy." Nat Rev Cancer **8**(8): 592-603.

Bergers, G. and S. Song (2005). "The role of pericytes in blood-vessel formation and maintenance." Neuro Oncol **7**(4): 452-464.

Bergers, G., S. Song, N. Meyer-Morse, E. Bergsland and D. Hanahan (2003). "Benefits of targeting both pericytes and endothelial cells in the tumor vasculature with kinase inhibitors." J Clin Invest **111**(9): 1287-1295.

Bill, R. and G. Christofori (2015). "The relevance of EMT in breast cancer metastasis: Correlation or causality?" FEBS Lett **589**(14): 1577-1587.

Bill, R., E. Fagiani, A. Zumsteg, H. Antoniadis, D. Johansson, S. Haefliger, I. Albrecht, F. Hilberg and G. Christofori (2015). "Nintedanib Is a Highly Effective Therapeutic for Neuroendocrine Carcinoma of the Pancreas (PNET) in the Rip1Tag2 Transgenic Mouse Model." Clin Cancer Res **21**(21): 4856-4867.

Blancher, C., J. W. Moore, K. L. Talks, S. Houlbrook and A. L. Harris (2000). "Relationship of hypoxia-inducible factor (HIF)-1alpha and HIF-2alpha expression to vascular endothelial growth factor induction and hypoxia survival in human breast cancer cell lines." Cancer Res **60**(24): 7106-7113.

Blum, Y., H. G. Belting, E. Ellertsdottir, L. Herwig, F. Luders and M. Affolter (2008). "Complex cell rearrangements during intersegmental vessel sprouting and vessel fusion in the zebrafish embryo." Dev Biol **316**(2): 312-322.

Bonapace, L., M. M. Coissieux, J. Wyckoff, K. D. Mertz, Z. Varga, T. Junt and M. Bentires-Alj (2014). "Cessation of CCL2 inhibition accelerates breast cancer metastasis by promoting angiogenesis." Nature **515**(7525): 130-133.

Bonnet, D. and J. E. Dick (1997). "Human acute myeloid leukemia is organized as a hierarchy that originates from a primitive hematopoietic cell." Nat Med **3**(7): 730-737.

Borovski, T., E. M. F. De Sousa, L. Vermeulen and J. P. Medema (2011). "Cancer stem cell niche: the place to be." Cancer Res **71**(3): 634-639.

Brabletz, T., A. Jung, S. Spaderna, F. Hlubek and T. Kirchner (2005). "Opinion: migrating cancer stem cells - an integrated concept of malignant tumour progression." Nat Rev Cancer **5**(9): 744-749.

Braun, J., K. Strittmatter, T. Nubel, D. Komljenovic, M. Sator-Schmitt, T. Bauerle, P. Angel and M. Schorpp-Kistner (2014). "Loss of stromal JUNB does not affect tumor growth and angiogenesis." Int J Cancer **134**(6): 1511-1516.

Brown, D. M. and E. Ruoslahti (2004). "Metadherin, a cell surface protein in breast tumors that mediates lung metastasis." Cancer Cell **5**(4): 365-374.

Brunet, A., A. Bonni, M. J. Zigmond, M. Z. Lin, P. Juo, L. S. Hu, M. J. Anderson, K. C. Arden, J. Blenis and M. E. Greenberg (1999). "Akt promotes cell survival by phosphorylating and inhibiting a Forkhead transcription factor." Cell **96**(6): 857-868.

Bry, M., R. Kivela, T. Holopainen, A. Anisimov, T. Tammela, J. Soronen, J. Silvola, A. Saraste, M. Jeltsch, P. Korpisalo, P. Carmeliet, K. B. Lemstrom, M. Shibuya, S. Yla-Herttuala, L. Alhonen, E. Mervaala, L. C. Andersson, J. Knuuti and K. Alitalo (2010). "Vascular endothelial growth factor-B acts as a coronary growth factor in transgenic rats without inducing angiogenesis, vascular leak, or inflammation." Circulation **122**(17): 1725-1733.

Butler, J. M., H. Kobayashi and S. Rafii (2010). "Instructive role of the vascular niche in promoting tumour growth and tissue repair by angiocrine factors." Nat Rev Cancer **10**(2): 138-146.

Cao, Y., J. M. Eble, E. Moon, H. Yuan, D. H. Weitzel, C. D. Landon, C. Y. Nien, G. Hanna, J. N. Rich, J. M. Provenzale and M. W. Dewhirst (2013). "Tumor cells upregulate normoxic HIF-1alpha in response to doxorubicin." Cancer Res **73**(20): 6230-6242.

Carmeliet, P. (2005). "Angiogenesis in life, disease and medicine." Nature **438**(7070): 932-936.

Carmeliet, P., V. Ferreira, G. Breier, S. Pollefeyt, L. Kieckens, M. Gertsenstein, M. Fahrig, A. Vandenhoeck, K. Harpal, C. Eberhardt, C. Declercq, J. Pawling, L. Moons, D. Collen, W. Risau and A. Nagy (1996). "Abnormal blood vessel development and lethality in embryos lacking a single VEGF allele." Nature **380**(6573): 435-439.

Carmeliet, P. and R. K. Jain (2011). "Molecular mechanisms and clinical

applications of angiogenesis." Nature **473**(7347): 298-307.

Carmeliet, P. and R. K. Jain (2011). "Principles and mechanisms of vessel normalization for cancer and other angiogenic diseases." Nat Rev Drug Discov **10**(6): 417-427.

Carmeliet, P., L. Moons, A. Luttun, V. Vincenti, V. Compernolle, M. De Mol, Y. Wu, F. Bono, L. Devy, H. Beck, D. Scholz, T. Acker, T. DiPalma, M. Dewerchin, A. Noel, I. Stalmans, A. Barra, S. Blacher, T. VandenDriessche, A. Ponten, U. Eriksson, K. H. Plate, J. M. Foidart, W. Schaper, D. S. Charnock-Jones, D. J. Hicklin, J. M. Herbert, D. Collen and M. G. Persico (2001). "Synergism between vascular endothelial growth factor and placental growth factor contributes to angiogenesis and plasma extravasation in pathological conditions." Nat Med **7**(5): 575-583.

Carmeliet, P. and M. Tessier-Lavigne (2005). "Common mechanisms of nerve and blood vessel wiring." Nature **436**(7048): 193-200.

Carroll, V. A. and M. Ashcroft (2006). "Role of hypoxia-inducible factor (HIF)-1alpha versus HIF-2alpha in the regulation of HIF target genes in response to hypoxia, insulin-like growth factor-I, or loss of von Hippel-Lindau function: implications for targeting the HIF pathway." Cancer Res **66**(12): 6264-6270.

Casanovas, O., D. J. Hicklin, G. Bergers and D. Hanahan (2005). "Drug resistance by evasion of antiangiogenic targeting of VEGF signaling in late-stage pancreatic islet tumors." Cancer Cell **8**(4): 299-309.

Casazza, A., D. Laoui, M. Wenes, S. Rizzolio, N. Bassani, M. Mambretti, S. Deschoemaeker, J. A. Van Ginderachter, L. Tamagnone and M. Mazzone (2013). "Impeding macrophage entry into hypoxic tumor areas by Sema3A/Nrp1 signaling blockade inhibits angiogenesis and restores antitumor immunity." Cancer Cell **24**(6): 695-709.

Cavallaro, U., B. Schaffhauser and G. Christofori (2002). "Cadherins and the tumour progression: is it all in a switch?" Cancer Lett **176**(2): 123-128.

Chambers, A. F., A. C. Groom and I. C. MacDonald (2002). "Dissemination and growth of cancer cells in metastatic sites." Nat Rev Cancer **2**(8): 563-572.

Chng, Z., A. Teo, R. A. Pedersen and L. Vallier (2010). "SIP1 mediates cell-fate decisions between neuroectoderm and mesendoderm in human pluripotent stem cells." Cell Stem Cell **6**(1): 59-70.

Christofori, G. (2006). "New signals from the invasive front." Nature **441**(7092): 444-450.

Chung, A. S., X. Wu, G. Zhuang, H. Ngu, I. Kasman, J. Zhang, J. M. Vernes, Z. Jiang, Y. G. Meng, F. V. Peale, W. Ouyang and N. Ferrara (2013). "An interleukin-17-mediated paracrine network promotes tumor resistance to anti-angiogenic therapy." Nat Med **19**(9): 1114-1123.

Claffey, K. P., S. C. Shih, A. Mullen, S. Dziennis, J. L. Cusick, K. R. Abrams, S. W. Lee and M. Detmar (1998). "Identification of a human VPF/VEGF 3' untranslated region mediating hypoxia-induced mRNA stability." Mol Biol Cell **9**(2): 469-481.

Clem, B., S. Telang, A. Clem, A. Yalcin, J. Meier, A. Simmons, M. A. Rasku, S. Arumugam, W. L. Dean, J. Eaton, A. Lane, J. O. Trent and J. Chesney (2008). "Small-molecule inhibition of 6-phosphofructo-2-kinase activity suppresses glycolytic flux and tumor growth." Mol Cancer Ther **7**(1): 110-120.

Coffelt, S. B., C. E. Lewis, L. Naldini, J. M. Brown, N. Ferrara and M. De Palma (2010). "Elusive identities and overlapping phenotypes of proangiogenic myeloid cells in tumors." Am J Pathol **176**(4): 1564-1576.

Compagni, A., P. Wilgenbus, M. A. Impagnatiello, M. Cotten and G. Christofori (2000). "Fibroblast growth factors are required for efficient tumor angiogenesis." Cancer Res **60**(24): 7163-7169.

Cooke, V. G., V. S. LeBleu, D. Keskin, Z. Khan, J. T. O'Connell, Y. Teng, M. B. Duncan, L. Xie, G. Maeda, S. Vong, H. Sugimoto, R. M. Rocha, A. Damascena, R. R. Brentani and R. Kalluri (2012). "Pericyte depletion results in hypoxia-associated epithelial-to-mesenchymal transition and metastasis mediated by met signaling pathway." Cancer Cell **21**(1): 66-81.

Crawford, Y. and N. Ferrara (2009). "VEGF inhibition: insights from preclinical and clinical studies." Cell Tissue Res **335**(1): 261-269.

Cuenda, A., J. Rouse, Y. N. Doza, R. Meier, P. Cohen, T. F. Gallagher, P. R. Young and J. C. Lee (1995). "SB 203580 is a specific inhibitor of a MAP kinase homologue which is stimulated by cellular stresses and interleukin-1." FEBS Lett **364**(2): 229-233.

Cunha, D. A., E. N. Gurzov, N. Naamane, F. Ortis, A. K. Cardozo, M. Bugliani, P. Marchetti, D. L. Eizirik and M. Cnop (2014). "JunB protects beta-cells from lipotoxicity via the XBP1-AKT pathway." Cell Death Differ **21**(8): 1313-1324.

Curtarello, M., E. Zulato, G. Nardo, S. Valtorta, G. Guzzo, E. Rossi, G. Esposito, A. Msaki, A. Pasto, A. Rasola, L. Persano, F. Ciccarese, R. Bertorelle, S. Todde, M. Plebani, H. Schroer, S. Walenta, W. Mueller-Klieser, A. Amadori, R. M. Moresco and S. Indraccolo (2014). "VEGF-Targeted Therapy Stably Modulates the Glycolytic Phenotype of Tumor Cells." Cancer Res.

Curtarello, M., E. Zulato, G. Nardo, S. Valtorta, G. Guzzo, E. Rossi, G. Esposito, A. Msaki, A. Pasto, A. Rasola, L. Persano, F. Ciccarese, R. Bertorelle, S. Todde, M. Plebani, H. Schroer, S. Walenta, W. Mueller-Klieser, A. Amadori, R. M. Moresco and S. Indraccolo (2015). "VEGF-targeted therapy stably modulates the glycolytic phenotype of tumor cells." Cancer Res **75**(1): 120-133.

Davies, M. A. and Y. Samuels (2010). "Analysis of the genome to personalize therapy for melanoma." Oncogene **29**(41): 5545-5555.

de Kruijf, E. M., J. G. van Nes, C. J. van de Velde, H. Putter, V. T. Smit, G. J. Liefers, P. J. Kuppen, R. A. Tollenaar and W. E. Mesker (2011). "Tumor-stroma ratio in the primary tumor is a prognostic factor in early breast cancer patients, especially in triple-negative carcinoma patients." Breast Cancer Res Treat **125**(3): 687-696.

Dean, M., T. Fojo and S. Bates (2005). "Tumour stem cells and drug resistance." Nat Rev Cancer **5**(4): 275-284.

Dejana, E., F. Orsenigo, C. Molendini, P. Baluk and D. M. McDonald (2009). "Organization and signaling of endothelial cell-to-cell junctions in various regions of the blood and lymphatic vascular trees." Cell Tissue Res **335**(1): 17-25.

Deng, T. and M. Karin (1993). "JunB differs from c-Jun in its DNA-binding and dimerization domains, and represses c-Jun by formation of inactive heterodimers." Genes Dev **7**(3): 479-490.

Doyen, J., C. Trastour, F. Ettore, I. Peyrottes, N. Toussant, J. Gal, K. Ilc, D. Roux, S. K. Parks, J. M. Ferrero and J. Pouyssegur (2014). "Expression of the hypoxia-inducible monocarboxylate transporter MCT4 is increased in triple negative breast cancer and correlates independently with clinical outcome." Biochem Biophys Res Commun **451**(1): 54-61.

Dykxhoorn, D. M., Y. Wu, H. Xie, F. Yu, A. Lal, F. Petrocca, D. Martinvalet, E. Song, B. Lim and J. Lieberman (2009). "miR-200 enhances mouse breast cancer cell colonization to form distant metastases." PLoS One **4**(9): e7181.

Ebos, J. M. and R. S. Kerbel (2011). "Antiangiogenic therapy: impact on invasion, disease progression, and metastasis." Nat Rev Clin Oncol **8**(4): 210-221.

Ebos, J. M., C. R. Lee, J. G. Christensen, A. J. Mutsaers and R. S. Kerbel (2007). "Multiple circulating proangiogenic factors induced by sunitinib malate are tumor-independent and correlate with antitumor efficacy." Proc Natl Acad Sci U S A **104**(43): 17069-17074.

Ebos, J. M., C. R. Lee, W. Cruz-Munoz, G. A. Bjarnason, J. G. Christensen and R. S. Kerbel (2009). "Accelerated metastasis after short-term treatment with a potent inhibitor of tumor angiogenesis." Cancer Cell **15**(3): 232-239.

Eferl, R. and E. F. Wagner (2003). "AP-1: a double-edged sword in tumorigenesis." Nat Rev Cancer **3**(11): 859-868.

Egeblad, M., E. S. Nakasone and Z. Werb (2010). "Tumors as organs: complex tissues that interface with the entire organism." Dev Cell **18**(6): 884-901.

Ellis, L. M. and D. J. Hicklin (2008). "VEGF-targeted therapy: mechanisms of anti-tumour activity." Nat Rev Cancer **8**(8): 579-591.

Escudier, B., T. Eisen, W. M. Stadler, C. Szczylik, S. Oudard, M. Staehler, S. Negrier, C. Chevreau, A. A. Desai, F. Rolland, T. Demkow, T. E. Hutson, M. Gore, S. Anderson, G. Hofilena, M. Shan, C. Pena, C. Lathia and R. M. Bukowski (2009). "Sorafenib for

treatment of renal cell carcinoma: Final efficacy and safety results of the phase III treatment approaches in renal cancer global evaluation trial." J Clin Oncol **27**(20): 3312-3318.

Escudier, B., A. Pluzanska, P. Koralewski, A. Ravaud, S. Bracarda, C. Szczylik, C. Chevreau, M. Filipek, B. Melichar, E. Bajetta, V. Gorbunova, J. O. Bay, I. Bodrogi, A. Jagiello-Gruszfeld, N. Moore and A. T. investigators (2007). "Bevacizumab plus interferon alfa-2a for treatment of metastatic renal cell carcinoma: a randomised, double-blind phase III trial." Lancet **370**(9605): 2103-2111.

Escudier, B., J. Roigas, S. Gillessen, U. Harmenberg, S. Srinivas, S. F. Mulder, G. Fountzilas, C. Peschel, P. Flodgren, E. C. Maneval, I. Chen and N. J. Vogelzang (2009). "Phase II study of sunitinib administered in a continuous once-daily dosing regimen in patients with cytokine-refractory metastatic renal cell carcinoma." J Clin Oncol **27**(25): 4068-4075.

Fan, F., J. S. Wey, M. F. McCarty, A. Belcheva, W. Liu, T. W. Bauer, R. J. Somcio, Y. Wu, A. Hooper, D. J. Hicklin and L. M. Ellis (2005). "Expression and function of vascular endothelial growth factor receptor-1 on human colorectal cancer cells." Oncogene **24**(16): 2647-2653.

Fantozzi, A., D. C. Gruber, L. Pisarsky, C. Heck, A. Kunita, M. Yilmaz, N. Meyer-Schaller, K. Cornille, U. Hopfer, M. Bentires-Alj and G. Christofori (2014). "VEGF-mediated angiogenesis links EMT-induced cancer stemness to tumor initiation." Cancer Res **74**(5): 1566-1575.

Ferrara, N. (2010). "Role of myeloid cells in vascular endothelial growth factor-independent tumor angiogenesis." Curr Opin Hematol **17**(3): 219-224.

Ferrara, N., K. Carver-Moore, H. Chen, M. Dowd, L. Lu, K. S. O'Shea, L. Powell-Braxton, K. J. Hillan and M. W. Moore (1996). "Heterozygous embryonic lethality induced by targeted inactivation of the VEGF gene." Nature **380**(6573): 439-442.

Ferrara, N., K. J. Hillan, H. P. Gerber and W. Novotny (2004). "Discovery and development of bevacizumab, an anti-VEGF antibody for treating cancer." Nat Rev Drug Discov **3**(5): 391-400.

Ferrara, N. and R. S. Kerbel (2005). "Angiogenesis as a therapeutic target." Nature **438**(7070): 967-974.

Folkman, J. (1971). "Tumor angiogenesis: therapeutic implications." N Engl J Med **285**(21): 1182-1186.

Fong, G. H., J. Rossant, M. Gertsenstein and M. L. Breitman (1995). "Role of the Flt-1 receptor tyrosine kinase in regulating the assembly of vascular endothelium." Nature **376**(6535): 66-70.

Forsythe, J. A., B. H. Jiang, N. V. Iyer, F. Agani, S. W. Leung, R. D. Koos and G. L. Semenza (1996). "Activation of vascular endothelial growth factor gene transcription by hypoxia-inducible factor 1." Mol Cell Biol **16**(9): 4604-4613.

Fujio, Y. and K. Walsh (1999). "Akt mediates cytoprotection of endothelial cells by vascular endothelial growth factor in an anchorage-dependent manner." J Biol Chem **274**(23): 16349-16354.

Gajewski, T. F., H. Schreiber and Y. X. Fu (2013). "Innate and adaptive immune cells in the tumor microenvironment." Nat Immunol **14**(10): 1014-1022.

Gerber, H. P., V. Dixit and N. Ferrara (1998). "Vascular endothelial growth factor induces expression of the antiapoptotic proteins Bcl-2 and A1 in vascular endothelial cells." J Biol Chem **273**(21): 13313-13316.

Gerber, H. P., A. McMurtrey, J. Kowalski, M. Yan, B. A. Keyt, V. Dixit and N. Ferrara (1998). "Vascular endothelial growth factor regulates endothelial cell survival through the phosphatidylinositol 3'-kinase/Akt signal transduction pathway. Requirement for Flk-1/KDR activation." J Biol Chem **273**(46): 30336-30343.

Gerhardt, H., M. Golding, M. Fruttiger, C. Ruhrberg, A. Lundkvist, A. Abramsson, M. Jeltsch, C. Mitchell, K. Alitalo, D. Shima and C. Betsholtz (2003). "VEGF guides angiogenic sprouting utilizing endothelial tip cell filopodia." J Cell Biol **161**(6): 1163-1177.

Gervasi, M., A. Bianchi-Smiraglia, M. Cummings, Q. Zheng, D. Wang, S. Liu and A. V. Bakin (2012). "JunB contributes to Id2 repression and the epithelial-mesenchymal transition in response to transforming growth factor-beta." J Cell Biol **196**(5): 589-603.

Geudens, I. and H. Gerhardt (2011). "Coordinating cell behaviour during blood vessel formation." Development **138**(21): 4569-4583.

Ghajar, C. M., H. Peinado, H. Mori, I. R. Matei, K. J. Evason, H. Brazier, D. Almeida, A. Koller, K. A. Hajjar, D. Y. Stainier, E. I. Chen, D. Lyden and M. J. Bissell (2013). "The perivascular niche regulates breast tumour dormancy." Nat Cell Biol **15**(7): 807-817.

Ghosh, R., K. L. Lipson, K. E. Sargent, A. M. Mercurio, J. S. Hunt, D. Ron and F. Urano (2010). "Transcriptional regulation of VEGF-A by the unfolded protein response pathway." PLoS One **5**(3): e9575.

Goel, H. L. and A. M. Mercurio (2013). "VEGF targets the tumour cell." Nat Rev Cancer **13**(12): 871-882.

Grivennikov, S. I., F. R. Greten and M. Karin (2010). "Immunity, inflammation, and cancer." Cell **140**(6): 883-899.

Gupta, G. P. and J. Massague (2006). "Cancer metastasis: building a framework." Cell **127**(4): 679-695.

Gurzov, E. N., L. Bakiri, J. M. Alfaro, E. F. Wagner and M. Izquierdo (2008). "Targeting c-Jun and JunB proteins as potential anticancer cell therapy." Oncogene **27**(5): 641-652.

Gurzov, E. N., F. Ortis, L. Bakiri, E. F. Wagner and D. L. Eizirik (2008). "JunB Inhibits ER Stress and Apoptosis in Pancreatic Beta Cells." PLoS One **3**(8): e3030.

Hahn, W. C. and R. A. Weinberg (2002). "Rules for making human tumor cells." N Engl J Med **347**(20): 1593-1603.

Hanahan, D. (1985). "Heritable formation of pancreatic beta-cell tumours in transgenic mice expressing recombinant insulin/simian virus 40 oncogenes." Nature **315**(6015): 115-122.

Hanahan, D. and R. A. Weinberg (2000). "The hallmarks of cancer." Cell **100**(1): 57-70.

Hanahan, D. and R. A. Weinberg (2011). "Hallmarks of cancer: the next generation." Cell **144**(5): 646-674.

Harris, A. L. (2002). "Hypoxia--a key regulatory factor in tumour growth." Nat Rev Cancer **2**(1): 38-47.

Hay, E. D. (1995). "An overview of epithelio-mesenchymal transformation." Acta Anat (Basel) **154**(1): 8-20.

Helczynska, K., A. M. Larsson, L. Holmquist Mengelbier, E. Bridges, E. Fredlund, S. Borgquist, G. Landberg, S. Pahlman and K. Jirstrom (2008). "Hypoxia-inducible factor-2alpha correlates to distant recurrence and poor outcome in invasive breast cancer." Cancer Res **68**(22): 9212-9220.

Hellstrom, M., M. Kalen, P. Lindahl, A. Abramsson and C. Betsholtz (1999). "Role of PDGF-B and PDGFR-beta in recruitment of vascular smooth muscle cells and pericytes during embryonic blood vessel formation in the mouse." Development **126**(14): 3047-3055.

Hendrix, M. J., E. A. Seftor, A. R. Hess and R. E. Seftor (2003). "Vasculogenic mimicry and tumour-cell plasticity: lessons from melanoma." Nat Rev Cancer **3**(6): 411-421.

Herbert, S. P. and D. Y. Stainier (2011). "Molecular control of endothelial cell behaviour during blood vessel morphogenesis." Nat Rev Mol Cell Biol **12**(9): 551-564.

Hicklin, D. J. and L. M. Ellis (2005). "Role of the vascular endothelial growth factor pathway in tumor growth and angiogenesis." J Clin Oncol **23**(5): 1011-1027.

Hilberg, F., G. J. Roth, M. Krssak, S. Kautschitsch, W. Sommergruber, U. Tontsch-Grunt, P. Garin-Chesa, G. Bader, A. Zoephel, J. Quant, A. Heckel and W. J. Rettig (2008). "BIBF 1120: triple angiokinase inhibitor with sustained receptor blockade and good antitumor efficacy." Cancer Res **68**(12): 4774-4782.

Ho, J., M. B. de Moura, Y. Lin, G. Vincent, S. Thorne, L. M. Duncan, L. Hui-Min, J. M. Kirkwood, D. Becker, B. Van Houten and S. J. Moschos (2012). "Importance of glycolysis and oxidative phosphorylation in advanced melanoma." Mol Cancer **11**: 76.

Holmquist-Mengelbier, L., E. Fredlund, T. Lofstedt, R. Noguera, S. Navarro, H. Nilsson, A. Pietras, J. Vallon-Christersson, A. Borg, K. Gradin, L. Poellinger and S. Pahlman (2006). "Recruitment of HIF-1alpha and HIF-2alpha to common target genes is differentially regulated in neuroblastoma: HIF-2alpha promotes an aggressive phenotype." Cancer Cell **10**(5): 413-423.

Hoshino, A., B. Costa-Silva, T. L. Shen, G. Rodrigues, A. Hashimoto, M. Tesic Mark, H. Molina, S. Kohsaka, A. Di Giannatale, S. Ceder, S. Singh, C. Williams, N. Soplop, K. Uryu, L. Pharmer, T. King, L. Bojmar, A. E. Davies, Y. Ararso, T. Zhang, H. Zhang, J. Hernandez, J. M. Weiss, V. D. Dumont-Cole, K. Kramer, L. H. Wexler, A. Narendran, G. K. Schwartz, J. H. Healey, P. Sandstrom, K. J. Labori, E. H. Kure, P. M. Grandgenett, M. A. Hollingsworth, M. de Sousa, S. Kaur, M. Jain, K. Mallya, S. K. Batra, W. R. Jarnagin, M. S. Brady, O. Fodstad, V. Muller, K. Pantel, A. J. Minn, M. J. Bissell, B. A. Garcia, Y. Kang, V. K. Rajasekhar, C. M. Ghajar, I. Matei, H. Peinado, J. Bromberg and D. Lyden (2015). "Tumour exosome integrins determine organotropic metastasis." Nature **527**(7578): 329-335.

Huang, R. Y., P. Guilford and J. P. Thiery (2012). "Early events in cell adhesion and polarity during epithelial-mesenchymal transition." J Cell Sci **125**(Pt 19): 4417-4422.

Huber, M. A., N. Azoitei, B. Baumann, S. Grunert, A. Sommer, H. Pehamberger, N. Kraut, H. Beug and T. Wirth (2004). "NF-kappaB is essential for epithelial-mesenchymal transition and metastasis in a model of breast cancer progression." J Clin Invest **114**(4): 569-581.

Huez, I., L. Creancier, S. Audigier, M. C. Gensac, A. C. Prats and H. Prats (1998). "Two independent internal ribosome entry sites are involved in translation initiation of vascular endothelial growth factor mRNA." Mol Cell Biol **18**(11): 6178-6190.

Hurwitz, H., L. Fehrenbacher, W. Novotny, T. Cartwright, J. Hainsworth, W. Heim, J. Berlin, A. Baron, S. Griffing, E. Holmgren, N. Ferrara, G. Fyfe, B. Rogers, R. Ross and F. Kabbinavar (2004). "Bevacizumab plus irinotecan, fluorouracil, and leucovorin for metastatic colorectal cancer." N Engl J Med **350**(23): 2335-2342.

Ishibashi, H., K. Nakagawa, M. Onimaru, E. J. Castellanous, Y. Kaneda, Y. Nakashima, K. Shirasuna and K. Sueishi (2000). "Sp1 decoy transfected to carcinoma cells suppresses the expression of vascular endothelial growth factor, transforming growth factor beta1, and tissue factor and also cell growth and invasion activities." Cancer Res **60**(22): 6531-6536.

Ishida, T., T. Nakajima, A. Kudo and A. Kawakami (2010). "Phosphorylation of Junb family proteins by the Jun N-terminal kinase supports tissue regeneration in zebrafish." Dev Biol **340**(2): 468-479.

Jain, R. K. (2003). "Molecular regulation of vessel maturation." Nat Med **9**(6): 685-693.

Jain, R. K. and P. Carmeliet (2012). "SnapShot: Tumor angiogenesis." Cell **149**(6): 1408-1408 e1401.

Jakobsson, L., C. A. Franco, K. Bentley, R. T. Collins, B. Ponsioen, I. M. Aspalter, I. Rosewell, M. Busse, G. Thurston, A. Medvinsky, S. Schulte-Merker and H. Gerhardt (2010). "Endothelial cells dynamically compete for the tip cell position during angiogenic sprouting." Nat Cell Biol **12**(10): 943-953.

Jiang, B. H. and L. Z. Liu (2009). "PI3K/PTEN signaling in angiogenesis and tumorigenesis." Adv Cancer Res **102**: 19-65.

Jung, Y. J., J. S. Isaacs, S. Lee, J. Trepel and L. Neckers (2003). "IL-1beta-mediated up-regulation of HIF-1alpha via an NFkappaB/COX-2 pathway identifies HIF-1 as a critical link between inflammation and oncogenesis." FASEB J **17**(14): 2115-2117.

Kalluri, R. and M. Zeisberg (2006). "Fibroblasts in cancer." Nat Rev Cancer **6**(5): 392-401.

Kanno, T., T. Kamba, T. Yamasaki, N. Shibasaki, R. Saito, N. Terada, Y. Toda, Y. Mikami, T. Inoue, A. Kanematsu, H. Nishiyama, O. Ogawa and E. Nakamura (2012). "JunB promotes cell invasion and angiogenesis in VHL-defective renal cell carcinoma." Oncogene **31**(25): 3098-3110.

Karin, M. (1995). "The regulation of AP-1 activity by mitogen-activated protein kinases." J Biol Chem **270**(28): 16483-16486.

Keith, B., R. S. Johnson and M. C. Simon (2012). "HIF1alpha and HIF2alpha: sibling rivalry in hypoxic tumour growth and progression." Nat Rev Cancer **12**(1): 9-22.

Kerbel, R. S. (1997). "A cancer therapy resistant to resistance." Nature **390**(6658): 335-336.

Kerbel, R. S. (2009). "Issues regarding improving the impact of antiangiogenic drugs for the treatment of breast cancer." Breast **18 Suppl 3**: S41-47.

Kessenbrock, K., V. Plaks and Z. Werb (2010). "Matrix metalloproteinases: regulators of the tumor microenvironment." Cell **141**(1): 52-67.

Keunen, O., M. Johansson, A. Oudin, M. Sanzey, S. A. Rahim, F. Fack, F. Thorsen, T. Taxt, M. Bartos, R. Jirik, H. Miletic, J. Wang, D. Stieber, L. Stuhr, I. Moen, C. B. Rygh, R. Bjerkvig and S. P. Niclou (2011). "Anti-VEGF treatment reduces blood supply and increases tumor cell invasion in glioblastoma." Proc Natl Acad Sci U S A **108**(9): 3749-3754.

Kharman-Biz, A., H. Gao, R. Ghiasvand, C. Zhao, K. Zendehdel and K. Dahlman-Wright (2013). "Expression of activator protein-1 (AP-1) family members in breast cancer." BMC Cancer **13**: 441.

Kiba, A., H. Sagara, T. Hara and M. Shibuya (2003). "VEGFR-2-specific ligand VEGF-E induces non-edematous hyper-vascularization in mice." Biochem Biophys Res Commun **301**(2): 371-377.

Kim, R., M. Emi and K. Tanabe (2007). "Cancer immunoediting from immune surveillance to immune escape." Immunology **121**(1): 1-14.

Kinzler, K. W. and B. Vogelstein (1997). "Cancer-susceptibility genes. Gatekeepers and caretakers." Nature **386**(6627): 761, 763.

Kitamura, T., B. Z. Qian and J. W. Pollard (2015). "Immune cell promotion of metastasis." Nat Rev Immunol **15**(2): 73-86.

Koong, A. C., E. Y. Chen and A. J. Giaccia (1994). "Hypoxia causes the activation of nuclear factor kappa B through the phosphorylation of I kappa B alpha on tyrosine residues." Cancer Res **54**(6): 1425-1430.

Kopfstein, L., T. Veikkola, V. G. Djonov, V. Baeriswyl, T. Schomber, K. Strittmatter, S. A. Stacker, M. G. Achen, K. Alitalo and G. Christofori (2007). "Distinct roles of vascular endothelial growth factor-D in lymphangiogenesis and metastasis." Am J Pathol **170**(4): 1348-1361.

Krueger, J., D. Liu, K. Scholz, A. Zimmer, Y. Shi, C. Klein, A. Siekmann, S. Schulte-Merker, M. Cudmore, A. Ahmed and F. le Noble (2011). "Flt1 acts as a negative regulator of tip cell formation and branching morphogenesis in the zebrafish embryo." Development **138**(10): 2111-2120.

Kuchnio, A., S. Moens, U. Bruning, K. Kuchnio, B. Cruys, B. Thienpont, M. Broux, A. A. Ungureanu, R. Leite de Oliveira, F. Bruyere, H. Cuervo, A. Manderveld, A. Carton, J. R. Hernandez-Fernaud, S. Zanivan, C. Bartic, J. M. Foidart, A. Noel, S. Vinckier, D. Lambrechts, M. Dewerchin, M. Mazzone and P. Carmeliet (2015). "The Cancer Cell Oxygen Sensor PHD2 Promotes Metastasis via Activation of Cancer-Associated Fibroblasts." Cell Rep **12**(6): 992-1005.

Kumar, K., S. Wigfield, H. E. Gee, C. M. Devlin, D. Singleton, J. L. Li, F. Buffa, M. Huffman, A. L. Sinn, J. Silver, H. Turley, R. Leek, A. L. Harris and M. Ivan (2013). "Dichloroacetate reverses the hypoxic adaptation to bevacizumab and enhances its antitumor effects in mouse xenografts." J Mol Med (Berl) **91**(6): 749-758.

Kutluk Cenik, B., K. T. Ostapoff, D. E. Gerber and R. A. Brekken (2013). "BIBF 1120 (nintedanib), a triple angiokinase inhibitor, induces hypoxia but not EMT and blocks progression of preclinical models of lung and pancreatic cancer." Mol Cancer Ther **12**(6): 992-1001.

Ladomery, M. R., S. J. Harper and D. O. Bates (2007). "Alternative splicing in angiogenesis: the vascular endothelial growth factor paradigm." Cancer Lett **249**(2): 133-142.

Lamouille, S., J. Xu and R. Derynck (2014). "Molecular mechanisms of epithelial-mesenchymal transition." Nat Rev Mol Cell Biol **15**(3): 178-196.

LeBleu, V. S., J. T. O'Connell, K. N. Gonzalez Herrera, H. Wikman, K. Pantel, M. C. Haigis, F. M. de Carvalho, A. Damascena, L. T. Domingos Chinen, R. M. Rocha, J. M. Asara and R. Kalluri (2014). "PGC-1alpha mediates mitochondrial biogenesis and oxidative phosphorylation in cancer cells to promote metastasis." Nat Cell Biol **16**(10): 992-1003, 1001-1015.

Lee, J., J. Lee, H. Yu, K. Choi and C. Choi (2011). "Differential dependency of human cancer cells on vascular endothelial growth factor-mediated autocrine growth and survival." Cancer Lett **309**(2): 145-150.

Lee, M. K., C. Pardoux, M. C. Hall, P. S. Lee, D. Warburton, J. Qing, S. M. Smith and R. Derynck (2007). "TGF-beta activates Erk MAP kinase signalling through direct

phosphorylation of ShcA." EMBO J **26**(17): 3957-3967.

Lee, S., T. T. Chen, C. L. Barber, M. C. Jordan, J. Murdock, S. Desai, N. Ferrara, A. Nagy, K. P. Roos and M. L. Iruela-Arispe (2007). "Autocrine VEGF signaling is required for vascular homeostasis." Cell **130**(4): 691-703.

Lehembre, F., M. Yilmaz, A. Wicki, T. Schomber, K. Strittmatter, D. Ziegler, A. Kren, P. Went, P. W. Derksen, A. Berns, J. Jonkers and G. Christofori (2008). "NCAM-induced focal adhesion assembly: a functional switch upon loss of E-cadherin." EMBO J **27**(19): 2603-2615.

Leung, D. W., G. Cachianes, W. J. Kuang, D. V. Goeddel and N. Ferrara (1989). "Vascular endothelial growth factor is a secreted angiogenic mitogen." Science **246**(4935): 1306-1309.

Levental, K. R., H. Yu, L. Kass, J. N. Lakins, M. Egeblad, J. T. Erler, S. F. Fong, K. Csiszar, A. Giaccia, W. Weninger, M. Yamauchi, D. L. Gasser and V. M. Weaver (2009). "Matrix crosslinking forces tumor progression by enhancing integrin signaling." Cell **139**(5): 891-906.

Llovet, J. M., S. Ricci, V. Mazzaferro, P. Hilgard, E. Gane, J. F. Blanc, A. C. de Oliveira, A. Santoro, J. L. Raoul, A. Forner, M. Schwartz, C. Porta, S. Zeuzem, L. Bolondi, T. F. Greten, P. R. Galle, J. F. Seitz, I. Borbath, D. Haussinger, T. Giannaris, M. Shan, M. Moscovici, D. Voliotis, J. Bruix and S. I. S. Group (2008). "Sorafenib in advanced hepatocellular carcinoma." N Engl J Med **359**(4): 378-390.

Lu, K. V., J. P. Chang, C. A. Parachoniak, M. M. Pandika, M. K. Aghi, D. Meyronet, N. Isachenko, S. D. Fouse, J. J. Phillips, D. A. Cheresh, M. Park and G. Bergers (2012). "VEGF inhibits tumor cell invasion and mesenchymal transition through a MET/VEGFR2 complex." Cancer Cell **22**(1): 21-35.

Lu, P., V. M. Weaver and Z. Werb (2012). "The extracellular matrix: a dynamic niche in cancer progression." J Cell Biol **196**(4): 395-406.

Lyttle, D. J., K. M. Fraser, S. B. Fleming, A. A. Mercer and A. J. Robinson (1994). "Homologs of vascular endothelial growth factor are encoded by the poxvirus orf virus." J Virol **68**(1): 84-92.

Maeda, M., K. R. Johnson and M. J. Wheelock (2005). "Cadherin switching: essential for behavioral but not morphological changes during an epithelium-to-mesenchyme transition." J Cell Sci **118**(Pt 5): 873-887.

Mak, P., I. Leav, B. Pursell, D. Bae, X. Yang, C. A. Taglienti, L. M. Gouvin, V. M. Sharma and A. M. Mercurio (2010). "ERbeta impedes prostate cancer EMT by destabilizing HIF-1alpha and inhibiting VEGF-mediated snail nuclear localization: implications for Gleason grading." Cancer Cell **17**(4): 319-332.

Makanya, A. N., R. Hlushchuk and V. G. Djonov (2009). "Intussusceptive angiogenesis and its role in vascular morphogenesis, patterning, and remodeling." Angiogenesis **12**(2): 113-123.

Mandriota, S. J., L. Jussila, M. Jeltsch, A. Compagni, D. Baetens, R. Prevo, S. Banerji, J. Huarte, R. Montesano, D. G. Jackson, L. Orci, K. Alitalo, G. Christofori and M. S. Pepper (2001). "Vascular endothelial growth factor-C-mediated lymphangiogenesis promotes tumour metastasis." EMBO J **20**(4): 672-682.

Mani, S. A., W. Guo, M. J. Liao, E. N. Eaton, A. Ayyanan, A. Y. Zhou, M. Brooks, F. Reinhard, C. C. Zhang, M. Shipitsin, L. L. Campbell, K. Polyak, C. Brisken, J. Yang and R. A. Weinberg (2008). "The epithelial-mesenchymal transition generates cells with properties of stem cells." Cell **133**(4): 704-715.

Marchiq, I. and J. Pouyssegur (2015). "Hypoxia, cancer metabolism and the therapeutic benefit of targeting lactate/H symporters." J Mol Med (Berl).

Martin, M., S. Loibl, G. von Minckwitz, S. Morales, N. Martinez, A. Guerrero, A. Anton, B. Aktas, W. Schoenegg, M. Munoz, J. A. Garcia-Saenz, M. Gil, M. Ramos, M. Margeli, E. Carrasco, C. Liedtke, G. Wachsmann, K. Mehta and J. R. De la Haba-Rodriguez (2015). "Phase III trial evaluating the addition of bevacizumab to endocrine therapy as first-line treatment for advanced breast cancer: the letrozole/fulvestrant and avastin (LEA) study." J Clin Oncol **33**(9): 1045-1052.

Mathew, L. K., N. Skuli, V. Mucaj, S. S. Lee, P. O. Zinn, P. Sathyan, H. Z. Imtiyaz, Z. Zhang, R. V. Davuluri, S. Rao, S. Venneti, P. Lal, J. D. Lathia, J. N. Rich, B. Keith, A. J.

Minn and M. C. Simon (2014). "miR-218 opposes a critical RTK-HIF pathway in mesenchymal glioblastoma." Proc Natl Acad Sci U S A **111**(1): 291-296.

McCormack, P. L. (2015). "Nintedanib: first global approval." Drugs **75**(1): 129-139.

McMahon, S., M. Charbonneau, S. Grandmont, D. E. Richard and C. M. Dubois (2006). "Transforming growth factor beta1 induces hypoxia-inducible factor-1 stabilization through selective inhibition of PHD2 expression." J Biol Chem **281**(34): 24171-24181.

McNiven, M. A. (2013). "Breaking away: matrix remodeling from the leading edge." Trends Cell Biol **23**(1): 16-21.

Michelakis, E. D., G. Sutendra, P. Dromparis, L. Webster, A. Haromy, E. Niven, C. Maguire, T. L. Gammer, J. R. Mackey, D. Fulton, B. Abdulkarim, M. S. McMurtry and K. C. Petruk (2010). "Metabolic modulation of glioblastoma with dichloroacetate." Sci Transl Med **2**(31): 31ra34.

Miller, K., M. Wang, J. Gralow, M. Dickler, M. Cobleigh, E. A. Perez, T. Shenkier, D. Cella and N. E. Davidson (2007). "Paclitaxel plus bevacizumab versus paclitaxel alone for metastatic breast cancer." N Engl J Med **357**(26): 2666-2676.

Misteli, H., T. Wolff, P. Fuglistaler, R. Gianni-Barrera, L. Gurke, M. Heberer and A. Banfi (2010). "High-throughput flow cytometry purification of transduced progenitors expressing defined levels of vascular endothelial growth factor induces controlled angiogenesis in vivo." Stem Cells **28**(3): 611-619.

Mitsuhashi, A., H. Goto, A. Saijo, V. T. Trung, Y. Aono, H. Ogino, T. Kuramoto, S. Tabata, H. Uehara, K. Izumi, M. Yoshida, H. Kobayashi, H. Takahashi, M. Gotoh, S. Kakiuchi, M. Hanibuchi, S. Yano, H. Yokomise, S. Sakiyama and Y. Nishioka (2015). "Fibrocyte-like cells mediate acquired resistance to anti-angiogenic therapy with bevacizumab." Nat Commun **6**: 8792.

Monahan-Earley, R., A. M. Dvorak and W. C. Aird (2013). "Evolutionary origins of the blood vascular system and endothelium." J Thromb Haemost **11 Suppl 1**: 46-66.

Mootha, V. K., C. M. Lindgren, K. F. Eriksson, A. Subramanian, S. Sihag, J. Lehar, P. Puigserver, E. Carlsson, M. Ridderstrale, E. Laurila, N. Houstis, M. J. Daly, N. Patterson, J. P. Mesirov, T. R. Golub, P. Tamayo, B. Spiegelman, E. S. Lander, J. N. Hirschhorn, D. Altshuler and L. C. Groop (2003). "PGC-1alpha-responsive genes involved in oxidative phosphorylation are coordinately downregulated in human diabetes." Nat Genet **34**(3): 267-273.

Morais-Santos, F., S. Granja, V. Miranda-Goncalves, A. H. Moreira, S. Queiros, J. L. Vilaca, F. C. Schmitt, A. Longatto-Filho, J. Paredes, F. Baltazar and C. Pinheiro (2015). "Targeting lactate transport suppresses in vivo breast tumour growth." Oncotarget **6**(22): 19177-19189.

Motzer, R. J., T. E. Hutson, P. Tomczak, M. D. Michaelson, R. M. Bukowski, S. Oudard, S. Negrier, C. Szczylik, R. Pili, G. A. Bjarnason, X. Garcia-del-Muro, J. A. Sosman, E. Solska, G. Wilding, J. A. Thompson, S. T. Kim, I. Chen, X. Huang and R. A. Figlin (2009). "Overall survival and updated results for sunitinib compared with interferon alfa in patients with metastatic renal cell carcinoma." J Clin Oncol **27**(22): 3584-3590.

Motzer, R. J., T. E. Hutson, P. Tomczak, M. D. Michaelson, R. M. Bukowski, O. Rixe, S. Oudard, S. Negrier, C. Szczylik, S. T. Kim, I. Chen, P. W. Bycott, C. M. Baum and R. A. Figlin (2007). "Sunitinib versus interferon alfa in metastatic renal-cell carcinoma." N Engl J Med **356**(2): 115-124.

Nagrath, S., L. V. Sequist, S. Maheswaran, D. W. Bell, D. Irimia, L. Ulkus, M. R. Smith, E. L. Kwak, S. Digumarthy, A. Muzikansky, P. Ryan, U. J. Balis, R. G. Tompkins, D. A. Haber and M. Toner (2007). "Isolation of rare circulating tumour cells in cancer patients by microchip technology." Nature **450**(7173): 1235-1239.

Nguyen, D. X., P. D. Bos and J. Massague (2009). "Metastasis: from dissemination to organ-specific colonization." Nat Rev Cancer **9**(4): 274-284.

Niu, G., K. L. Wright, M. Huang, L. Song, E. Haura, J. Turkson, S. Zhang, T. Wang, D. Sinibaldi, D. Coppola, R. Heller, L. M. Ellis, J. Karras, J. Bromberg, D. Pardoll, R. Jove and H. Yu (2002). "Constitutive Stat3 activity up-regulates VEGF expression and tumor angiogenesis." Oncogene **21**(13): 2000-2008.

Nolan, D. J., M. Ginsberg, E. Israely, B. Palikuqi, M. G. Poulos, D. James, B. S. Ding, W. Schachterle, Y. Liu, Z. Rosenwaks, J. M. Butler, J. Xiang, A. Rafii, K. Shido, S. Y. Rabbany, O. Elemento and S. Rafii (2013). "Molecular signatures of tissue-specific microvascular endothelial cell heterogeneity in organ maintenance and regeneration." Dev Cell **26**(2): 204-219.

Novak, E. M., M. Metzger, R. Chammas, M. da Costa, K. Dantas, C. Manabe, J. Pires, A. C. de Oliveira and S. P. Bydlowski (2003). "Downregulation of TNF-alpha and VEGF expression by Sp1 decoy oligodeoxynucleotides in mouse melanoma tumor." Gene Ther **10**(23): 1992-1997.

Ostrand-Rosenberg, S. and P. Sinha (2009). "Myeloid-derived suppressor cells: linking inflammation and cancer." J Immunol **182**(8): 4499-4506.

Oudin, M. J., O. Jonas, T. Kosciuk, L. C. Broye, B. C. Guido, J. Wyckoff, D. Riquelme, J. M. Lamar, S. B. Asokan, C. Whittaker, D. Ma, R. Langer, M. J. Cima, K. B. Wisinski, R. O. Hynes, D. A. Lauffenburger, P. J. Keely, J. E. Bear and F. B. Gertler (2016). "Tumor cell-driven extracellular matrix remodeling enables haptotaxis during metastatic progression." Cancer Discov.

Padera, T. P., A. H. Kuo, T. Hoshida, S. Liao, J. Lobo, K. R. Kozak, D. Fukumura and R. K. Jain (2008). "Differential response of primary tumor versus lymphatic metastasis to VEGFR-2 and VEGFR-3 kinase inhibitors cediranib and vandetanib." Mol Cancer Ther **7**(8): 2272-2279.

Paez-Ribes, M., E. Allen, J. Hudock, T. Takeda, H. Okuyama, F. Vinals, M. Inoue, G. Bergers, D. Hanahan and O. Casanovas (2009). "Antiangiogenic therapy elicits malignant progression of tumors to increased local invasion and distant metastasis." Cancer Cell **15**(3): 220-231.

Pages, F., J. Galon, M. C. Dieu-Nosjean, E. Tartour, C. Sautes-Fridman and W. H. Fridman (2010). "Immune infiltration in human tumors: a prognostic factor that should not be ignored." Oncogene **29**(8): 1093-1102.

Pages, G. and J. Pouyssegur (2005). "Transcriptional regulation of the Vascular Endothelial Growth Factor gene--a concert of activating factors." Cardiovasc Res **65**(3): 564-573.

Paget, S. (1989). "The distribution of secondary growths in cancer of the breast. 1889." Cancer Metastasis Rev **8**(2): 98-101.

Pavlides, S., D. Whitaker-Menezes, R. Castello-Cros, N. Flomenberg, A. K. Witkiewicz, P. G. Frank, M. C. Casimiro, C. Wang, P. Fortina, S. Addya, R. G. Pestell, U. E. Martinez-Outschoorn, F. Sotgia and M. P. Lisanti (2009). "The reverse Warburg effect: aerobic glycolysis in cancer associated fibroblasts and the tumor stroma." Cell Cycle **8**(23): 3984-4001.

Peng, J., L. Zhang, L. Drysdale and G. H. Fong (2000). "The transcription factor EPAS-1/hypoxia-inducible factor 2alpha plays an important role in vascular remodeling." Proc Natl Acad Sci U S A **97**(15): 8386-8391.

Pennacchietti, S., P. Michieli, M. Galluzzo, M. Mazzone, S. Giordano and P. M. Comoglio (2003). "Hypoxia promotes invasive growth by transcriptional activation of the met protooncogene." Cancer Cell **3**(4): 347-361.

Porporato, P. E., S. Dhup, R. K. Dadhich, T. Copetti and P. Sonveaux (2011). "Anticancer targets in the glycolytic metabolism of tumors: a comprehensive review." Front Pharmacol **2**: 49.

Psaila, B. and D. Lyden (2009). "The metastatic niche: adapting the foreign soil." Nat Rev Cancer **9**(4): 285-293.

Pugh, C. W. and P. J. Ratcliffe (2003). "Regulation of angiogenesis by hypoxia: role of the HIF system." Nat Med **9**(6): 677-684.

Quintela-Fandino, M., A. Urruticoechea, J. Guerra, M. Gil, A. Gonzalez-Martin, R. Marquez, E. Hernandez-Agudo, C. Rodriguez-Martin, M. Gil-Martin, R. Bratos, M. J. Escudero, S. Vlassak, F. Hilberg and R. Colomer (2014). "Phase I clinical trial of nintedanib plus paclitaxel in early HER-2-negative breast cancer (CNIO-BR-01-2010/GEICAM-2010-10 study)." Br J Cancer **111**(6): 1060-1064.

Quintieri, L., M. Selmy and S. Indraccolo (2014). "Metabolic effects of antiangiogenic drugs in tumors: therapeutic implications." Biochem Pharmacol **89**(2): 162-170.

Raymond, E., L. Dahan, J. L. Raoul, Y. J. Bang, I. Borbath, C. Lombard-Bohas, J. Valle, P. Metrakos, D. Smith, A. Vinik, J. S. Chen, D. Horsch, P. Hammel, B. Wiedenmann, E.

Van Cutsem, S. Patyna, D. R. Lu, C. Blanckmeister, R. Chao and P. Ruszniewski (2011). "Sunitinib malate for the treatment of pancreatic neuroendocrine tumors." N Engl J Med **364**(6): 501-513.

Reck, M., R. Kaiser, A. Mellemgaard, J. Y. Douillard, S. Orlov, M. Krzakowski, J. von Pawel, M. Gottfried, I. Bondarenko, M. Liao, C. N. Gann, J. Barrueco, B. Gaschler-Markefski and S. Novello (2014). "Docetaxel plus nintedanib versus docetaxel plus placebo in patients with previously treated non-small-cell lung cancer (LUME-Lung 1): a phase 3, double-blind, randomised controlled trial." Lancet Oncol **15**(2): 143-155.

Rivera, L. B. and G. Bergers (2014). "Angiogenesis. Targeting vascular sprouts." Science **344**(6191): 1449-1450.

Robbins, S. L., V. Kumar and R. S. Cotran (2010). Robbins and Cotran pathologic basis of disease. Philadelphia, PA, Saunders/Elsevier.

Rose, S. (2011). "FDA pulls approval for avastin in breast cancer." Cancer Discov **1**(7): OF1-2.

Roth, G. J., A. Heckel, F. Colbatzky, S. Handschuh, J. Kley, T. Lehmann-Lintz, R. Lotz, U. Tontsch-Grunt, R. Walter and F. Hilberg (2009). "Design, synthesis, and evaluation of indolinones as triple angiokinase inhibitors and the discovery of a highly specific 6-methoxycarbonyl-substituted indolinone (BIBF 1120)." J Med Chem **52**(14): 4466-4480.

Ryan, H. E., J. Lo and R. S. Johnson (1998). "HIF-1 alpha is required for solid tumor formation and embryonic vascularization." EMBO J **17**(11): 3005-3015.

Sager, R., K. Tanaka, C. C. Lau, Y. Ebina and A. Anisowicz (1983). "Resistance of human cells to tumorigenesis induced by cloned transforming genes." Proc Natl Acad Sci U S A **80**(24): 7601-7605.

Sandler, A., R. Gray, M. C. Perry, J. Brahmer, J. H. Schiller, A. Dowlati, R. Lilenbaum and D. H. Johnson (2006). "Paclitaxel-carboplatin alone or with bevacizumab for non-small-cell lung cancer." N Engl J Med **355**(24): 2542-2550.

Saxena, M. and G. Christofori (2013). "Rebuilding cancer metastasis in the mouse." Mol Oncol **7**(2): 283-296.

Schafer, G., T. Cramer, G. Suske, W. Kemmner, B. Wiedenmann and M. Hocker (2003). "Oxidative stress regulates vascular endothelial growth factor-A gene transcription through Sp1- and Sp3-dependent activation of two proximal GC-rich promoter elements." J Biol Chem **278**(10): 8190-8198.

Schmidt, D., B. Textor, O. T. Pein, A. H. Licht, S. Andrecht, M. Sator-Schmitt, N. E. Fusenig, P. Angel and M. Schorpp-Kistner (2007). "Critical role for NF-kappaB-induced JunB in VEGF regulation and tumor angiogenesis." EMBO J **26**(3): 710-719.

Schomber, T., L. Kopfstein, V. Djonov, I. Albrecht, V. Baeriswyl, K. Strittmatter and G. Christofori (2007). "Placental growth factor-1 attenuates vascular endothelial growth factor-A-dependent tumor angiogenesis during beta cell carcinogenesis." Cancer Res **67**(22): 10840-10848.

Schoors, S., K. De Bock, A. R. Cantelmo, M. Georgiadou, B. Ghesquiere, S. Cauwenberghs, A. Kuchnio, B. W. Wong, A. Quaegebeur, J. Goveia, F. Bifari, X. Wang, R. Blanco, B. Tembuyser, I. Cornelissen, A. Bouche, S. Vinckier, S. Diaz-Moralli, H. Gerhardt, S. Telang, M. Cascante, J. Chesney, M. Dewerchin and P. Carmeliet (2014). "Partial and transient reduction of glycolysis by PFKFB3 blockade reduces pathological angiogenesis." Cell Metab **19**(1): 37-48.

Schorpp-Kistner, M., Z. Q. Wang, P. Angel and E. F. Wagner (1999). "JunB is essential for mammalian placentation." EMBO J **18**(4): 934-948.

Semenza, G. L. (2008). "Tumor metabolism: cancer cells give and take lactate." J Clin Invest **118**(12): 3835-3837.

Senger, D. R., S. J. Galli, A. M. Dvorak, C. A. Perruzzi, V. S. Harvey and H. F. Dvorak (1983). "Tumor cells secrete a vascular permeability factor that promotes accumulation of ascites fluid." Science **219**(4587): 983-985.

Sennino, B., T. Ishiguro-Oonuma, Y. Wei, R. M. Naylor, C. W. Williamson, V. Bhagwandin, S. P. Tabruyn, W. K. You, H. A. Chapman, J. G. Christensen, D. T. Aftab and D. M. McDonald (2012). "Suppression of

tumor invasion and metastasis by concurrent inhibition of c-Met and VEGF signaling in pancreatic neuroendocrine tumors." Cancer Discov **2**(3): 270-287.

Sennino, B. and D. M. McDonald (2012). "Controlling escape from angiogenesis inhibitors." Nat Rev Cancer **12**(10): 699-709.

Shalaby, F., J. Rossant, T. P. Yamaguchi, M. Gertsenstein, X. F. Wu, M. L. Breitman and A. C. Schuh (1995). "Failure of blood-island formation and vasculogenesis in Flk-1-deficient mice." Nature **376**(6535): 62-66.

Sherr, C. J. and F. McCormick (2002). "The RB and p53 pathways in cancer." Cancer Cell **2**(2): 103-112.

Shibata, A., T. Nagaya, T. Imai, H. Funahashi, A. Nakao and H. Seo (2002). "Inhibition of NF-kappaB activity decreases the VEGF mRNA expression in MDA-MB-231 breast cancer cells." Breast Cancer Res Treat **73**(3): 237-243.

Shields, J. D., I. C. Kourtis, A. A. Tomei, J. M. Roberts and M. A. Swartz (2010). "Induction of lymphoidlike stroma and immune escape by tumors that express the chemokine CCL21." Science **328**(5979): 749-752.

Shima, D. T., M. Kuroki, U. Deutsch, Y. S. Ng, A. P. Adamis and P. A. D'Amore (1996). "The mouse gene for vascular endothelial growth factor. Genomic structure, definition of the transcriptional unit, and characterization of transcriptional and post-transcriptional regulatory sequences." J Biol Chem **271**(7): 3877-3883.

Shipitsin, M., L. L. Campbell, P. Argani, S. Weremowicz, N. Bloushtain-Qimron, J. Yao, T. Nikolskaya, T. Serebryiskaya, R. Beroukhim, M. Hu, M. K. Halushka, S. Sukumar, L. M. Parker, K. S. Anderson, L. N. Harris, J. E. Garber, A. L. Richardson, S. J. Schnitt, Y. Nikolsky, R. S. Gelman and K. Polyak (2007). "Molecular definition of breast tumor heterogeneity." Cancer Cell **11**(3): 259-273.

Shojaei, F., X. Wu, A. K. Malik, C. Zhong, M. E. Baldwin, S. Schanz, G. Fuh, H. P. Gerber and N. Ferrara (2007). "Tumor refractoriness to anti-VEGF treatment is mediated by CD11b+Gr1+ myeloid cells." Nat Biotechnol **25**(8): 911-920.

Simpson, C. D., K. Anyiwe and A. D. Schimmer (2008). "Anoikis resistance and tumor metastasis." Cancer Lett **272**(2): 177-185.

Singh, A. and J. Settleman (2010). "EMT, cancer stem cells and drug resistance: an emerging axis of evil in the war on cancer." Oncogene **29**(34): 4741-4751.

Singh, M. and N. Ferrara (2012). "Modeling and predicting clinical efficacy for drugs targeting the tumor milieu." Nat Biotechnol **30**(7): 648-657.

Sleeman, J. P., G. Christofori, R. Fodde, J. G. Collard, G. Berx, C. Decraene and C. Ruegg (2012). "Concepts of metastasis in flux: the stromal progression model." Semin Cancer Biol **22**(3): 174-186.

Smyth, G. K., J. Michaud and H. S. Scott (2005). "Use of within-array replicate spots for assessing differential expression in microarray experiments." Bioinformatics **21**(9): 2067-2075.

Soker, S., S. Takashima, H. Q. Miao, G. Neufeld and M. Klagsbrun (1998). "Neuropilin-1 is expressed by endothelial and tumor cells as an isoform-specific receptor for vascular endothelial growth factor." Cell **92**(6): 735-745.

Sonveaux, P., F. Vegran, T. Schroeder, M. C. Wergin, J. Verrax, Z. N. Rabbani, C. J. De Saedeleer, K. M. Kennedy, C. Diepart, B. F. Jordan, M. J. Kelley, B. Gallez, M. L. Wahl, O. Feron and M. W. Dewhirst (2008). "Targeting lactate-fueled respiration selectively kills hypoxic tumor cells in mice." J Clin Invest **118**(12): 3930-3942.

Sorrentino, A., N. Thakur, S. Grimsby, A. Marcusson, V. von Bulow, N. Schuster, S. Zhang, C. H. Heldin and M. Landstrom (2008). "The type I TGF-beta receptor engages TRAF6 to activate TAK1 in a receptor kinase-independent manner." Nat Cell Biol **10**(10): 1199-1207.

Sounni, N. E., J. Cimino, S. Blacher, I. Primac, A. Truong, G. Mazzucchelli, A. Paye, D. Calligaris, D. Debois, P. De Tullio, B. Mari, E. De Pauw and A. Noel (2014). "Blocking lipid synthesis overcomes tumor regrowth and metastasis after antiangiogenic therapy withdrawal." Cell Metab **20**(2): 280-294.

Stein, I., A. Itin, P. Einat, R. Skaliter, Z. Grossman and E. Keshet (1998). "Translation of vascular endothelial growth factor mRNA by internal ribosome entry: implications for translation under hypoxia." Mol Cell Biol **18**(6): 3112-3119.

Sternlicht, M. D., A. Lochter, C. J. Sympson, B. Huey, J. P. Rougier, J. W. Gray, D. Pinkel, M. J. Bissell and Z. Werb (1999). "The stromal proteinase MMP3/stromelysin-1 promotes mammary carcinogenesis." Cell **98**(2): 137-146.

Subramanian, A., P. Tamayo, V. K. Mootha, S. Mukherjee, B. L. Ebert, M. A. Gillette, A. Paulovich, S. L. Pomeroy, T. R. Golub, E. S. Lander and J. P. Mesirov (2005). "Gene set enrichment analysis: a knowledge-based approach for interpreting genome-wide expression profiles." Proc Natl Acad Sci U S A **102**(43): 15545-15550.

Sudhakar, A. (2009). "History of Cancer, Ancient and Modern Treatment Methods." J Cancer Sci Ther **1**(2): 1-4.

Sun, J., D. A. Wang, R. K. Jain, A. Carie, S. Paquette, E. Ennis, M. A. Blaskovich, L. Baldini, D. Coppola, A. D. Hamilton and S. M. Sebti (2005). "Inhibiting angiogenesis and tumorigenesis by a synthetic molecule that blocks binding of both VEGF and PDGF to their receptors." Oncogene **24**(29): 4701-4709.

Tammela, T. and K. Alitalo (2010). "Lymphangiogenesis: Molecular mechanisms and future promise." Cell **140**(4): 460-476.

Tammela, T., G. Zarkada, E. Wallgard, A. Murtomaki, S. Suchting, M. Wirzenius, M. Waltari, M. Hellstrom, T. Schomber, R. Peltonen, C. Freitas, A. Duarte, H. Isoniemi, P. Laakkonen, G. Christofori, S. Yla-Herttuala, M. Shibuya, B. Pytowski, A. Eichmann, C. Betsholtz and K. Alitalo (2008). "Blocking VEGFR-3 suppresses angiogenic sprouting and vascular network formation." Nature **454**(7204): 656-660.

Textor, B., M. Sator-Schmitt, K. H. Richter, P. Angel and M. Schorpp-Kistner (2006). "c-Jun and JunB are essential for hypoglycemia-mediated VEGF induction." Ann N Y Acad Sci **1091**: 310-318.

Thiery, J. P., H. Acloque, R. Y. Huang and M. A. Nieto (2009). "Epithelial-mesenchymal transitions in development and disease." Cell **139**(5): 871-890.

Thiery, J. P. and J. P. Sleeman (2006). "Complex networks orchestrate epithelial-mesenchymal transitions." Nat Rev Mol Cell Biol **7**(2): 131-142.

Thurston, G., C. Suri, K. Smith, J. McClain, T. N. Sato, G. D. Yancopoulos and D. M. McDonald (1999). "Leakage-resistant blood vessels in mice transgenically overexpressing angiopoietin-1." Science **286**(5449): 2511-2514.

Tiwari, N., A. Gheldof, M. Tatari and G. Christofori (2012). "EMT as the ultimate survival mechanism of cancer cells." Semin Cancer Biol **22**(3): 194-207.

Tuveson, D. and D. Hanahan (2011). "Translational medicine: Cancer lessons from mice to humans." Nature **471**(7338): 316-317.

Tvorogov, D., A. Anisimov, W. Zheng, V. M. Leppanen, T. Tammela, S. Laurinavicius, W. Holnthoner, H. Helotera, T. Holopainen, M. Jeltsch, N. Kalkkinen, H. Lankinen, P. M. Ojala and K. Alitalo (2010). "Effective suppression of vascular network formation by combination of antibodies blocking VEGFR ligand binding and receptor dimerization." Cancer Cell **18**(6): 630-640.

Valastyan, S. and R. A. Weinberg (2011). "Tumor metastasis: molecular insights and evolving paradigms." Cell **147**(2): 275-292.

Van de Veire, S., I. Stalmans, F. Heindryckx, H. Oura, A. Tijeras-Raballand, T. Schmidt, S. Loges, I. Albrecht, B. Jonckx, S. Vinckier, C. Van Steenkiste, S. Tugues, C. Rolny, M. De Mol, D. Dettori, P. Hainaud, L. Coenegrachts, J. O. Contreres, T. Van Bergen, H. Cuervo, W. H. Xiao, C. Le Henaff, I. Buysschaert, B. Kharabi Masouleh, A. Geerts, T. Schomber, P. Bonnin, V. Lambert, J. Haustraete, S. Zacchigna, J. M. Rakic, W. Jimenez, A. Noel, M. Giacca, I. Colle, J. M. Foidart, G. Tobelem, M. Morales-Ruiz, J. Vilar, P. Maxwell, S. A. Vinores, G. Carmeliet, M. Dewerchin, L. Claesson-Welsh, E. Dupuy, H. Van Vlierberghe, G. Christofori, M. Mazzone, M. Detmar, D. Collen and P. Carmeliet (2010). "Further pharmacological and genetic evidence for the efficacy of PlGF inhibition in cancer and eye disease." Cell **141**(1): 178-190.

van Roy, F. and G. Berx (2008). "The cell-cell adhesion molecule E-cadherin." Cell Mol Life Sci **65**(23): 3756-3788.

Vander Heiden, M. G., L. C. Cantley and C. B. Thompson (2009). "Understanding the Warburg effect: the metabolic requirements of cell proliferation." Science **324**(5930): 1029-1033.

Vanharanta, S. and J. Massague (2013). "Origins of metastatic traits." Cancer Cell **24**(4): 410-421.

Venning, F. A., L. Wullkopf and J. T. Erler (2015). "Targeting ECM Disrupts Cancer Progression." Front Oncol **5**: 224.

Villa, J. C., D. Chiu, A. H. Brandes, F. E. Escorcia, C. H. Villa, W. F. Maguire, C. J. Hu, E. de Stanchina, M. C. Simon, S. S. Sisodia, D. A. Scheinberg and Y. M. Li (2014). "Nontranscriptional role of Hif-1alpha in activation of gamma-secretase and notch signaling in breast cancer." Cell Rep **8**(4): 1077-1092.

Virchow, R. (1859). Die Cellularpathologie in ihrer Begründung auf physiologische und pathologische Gewebelehre, Berlin : Verlag von August Hirschwald.

Wagenblast, E., M. Soto, S. Gutierrez-Angel, C. A. Hartl, A. L. Gable, A. R. Maceli, N. Erard, A. M. Williams, S. Y. Kim, S. Dickopf, J. C. Harrell, A. D. Smith, C. M. Perou, J. E. Wilkinson, G. J. Hannon and S. R. Knott (2015). "A model of breast cancer heterogeneity reveals vascular mimicry as a driver of metastasis." Nature **520**(7547): 358-362.

Waldmeier, L., N. Meyer-Schaller, M. Diepenbruck and G. Christofori (2012). "Py2T murine breast cancer cells, a versatile model of TGFbeta-induced EMT in vitro and in vivo." PLoS One **7**(11): e48651.

Wang, R., K. Chadalavada, J. Wilshire, U. Kowalik, K. E. Hovinga, A. Geber, B. Fligelman, M. Leversha, C. Brennan and V. Tabar (2010). "Glioblastoma stem-like cells give rise to tumour endothelium." Nature **468**(7325): 829-833.

Wang, Y. and D. Becker (1997). "Antisense targeting of basic fibroblast growth factor and fibroblast growth factor receptor-1 in human melanomas blocks intratumoral angiogenesis and tumor growth." Nat Med **3**(8): 887-893.

Warburg, O. (1956). "On respiratory impairment in cancer cells." Science **124**(3215): 269-270.

Warburg, O. (1956). "On the origin of cancer cells." Science **123**(3191): 309-314.

Wei, D., X. Le, L. Zheng, L. Wang, J. A. Frey, A. C. Gao, Z. Peng, S. Huang, H. Q. Xiong, J. L. Abbruzzese and K. Xie (2003). "Stat3 activation regulates the expression of vascular endothelial growth factor and human pancreatic cancer angiogenesis and metastasis." Oncogene **22**(3): 319-329.

Weinberg, R. A. (2014). The biology of cancer. New York, Garland Science, Taylor & Francis Group.

Wendt, M. K., B. J. Schiemann, J. G. Parvani, Y. H. Lee, Y. Kang and W. P. Schiemann (2013). "TGF-beta stimulates Pyk2 expression as part of an epithelial-mesenchymal transition program required for metastatic outgrowth of breast cancer." Oncogene **32**(16): 2005-2015.

Weng, D., J. H. Penzner, B. Song, S. Koido, S. K. Calderwood and J. Gong (2012). "Metastasis is an early event in mouse mammary carcinomas and is associated with cells bearing stem cell markers." Breast Cancer Res **14**(1): R18.

Wheelock, M. J., Y. Shintani, M. Maeda, Y. Fukumoto and K. R. Johnson (2008). "Cadherin switching." J Cell Sci **121**(Pt 6): 727-735.

Wick, A. N., D. R. Drury and T. N. Morita (1955). "2-Deoxyglucose; a metabolic block for glucose." Proc Soc Exp Biol Med **89**(4): 579-582.

Wu, Z., P. Puigserver, U. Andersson, C. Zhang, G. Adelmant, V. Mootha, A. Troy, S. Cinti, B. Lowell, R. C. Scarpulla and B. M. Spiegelman (1999). "Mechanisms controlling mitochondrial biogenesis and respiration through the thermogenic coactivator PGC-1." Cell **98**(1): 115-124.

Xie, T. X., Z. Xia, N. Zhang, W. Gong and S. Huang (2010). "Constitutive NF-kappaB activity regulates the expression of VEGF and IL-8 and tumor angiogenesis of human glioblastoma." Oncol Rep **23**(3): 725-732.

Xu, L., S. Chen and R. C. Bergan (2006). "MAPKAPK2 and HSP27 are downstream effectors of p38 MAP kinase-mediated matrix metalloproteinase type 2 activation and cell invasion in human prostate cancer." Oncogene **25**(21): 2987-2998.

Yamashita, M., K. Fatyol, C. Jin, X. Wang, Z. Liu and Y. E. Zhang (2008). "TRAF6 mediates Smad-independent activation of JNK and p38 by TGF-beta." Mol Cell **31**(6): 918-924.

Yilmaz, M. and G. Christofori (2009). "EMT, the cytoskeleton, and cancer cell invasion." Cancer Metastasis Rev **28**(1-2): 15-33.

Yilmaz, M. and G. Christofori (2010). "Mechanisms of motility in metastasizing cells." Mol Cancer Res **8**(5): 629-642.

Yuan, T. L. and L. C. Cantley (2008). "PI3K pathway alterations in cancer: variations on a theme." Oncogene **27**(41): 5497-5510.

6. Acknowledgements

First of all, I would like to thank Prof. Gerhard Christofori for giving me the opportunity to join his lab and to conduct my Ph.D. projects in such a great environment. Thank you for the help along the way.

I am also grateful to Profs. Markus Affolter, Curzio Rüegg and Christoph Dehio for taking part in my Ph.D. committee.

Many thanks to all the persons who contributed to this work by performing experiments, sharing reagents or giving me feedback. My thoughts particularly go to Ruben Bill, Ernesta Fagiani, Helena Antoniadis, Jörg Hagmann, Ryan Goosen, Sébastien Dubuis, Sarah Dimeloe, Dr Marina Schorpp-Kistner and the members of Profs. Hall, Wymann and Höllander laboratories.

I would also like to thank people who gave me the chance to collaborate on their projects, therefore offering me a chance to discover different topics and techniques: Adrian Zumsteg, Anna Fantozzi, Dorothea Gruber, Ernesta Fagiani and Blaise Calpe.

Meera: Thank you for the hours of proofreading you did for me.

To the entire Christofori lab: Thank you for your friendship, our scientific discussions, and for giving me a taste of your respective cultures. Thanks for making my Ph.D. so memorable.

I would also like to thank the animal caretakers and people from the infrastructure for making our life simpler.

Lénaïc: Thank you for your patience when five more minutes in the lab used to turn into two more hours…

Last but not least, I would like to thank my parents for their continued support.

7. Curriculum vitae

Name: **Laura Estelle Pisarsky**
Place of birth: Sarrebourg, France
Nationality: French
Date of Birth: 08 April, 1988

Educational and professional training

Doctoral studies in cell biology August 2011-Present
Faculty of Philosophy and Science, University of Basel, Switzerland

Master of science in cellular and molecular physiopathology September 2009 – June 2011
Faculty of Medicine,
University of Strasbourg, France

Bachelor of science in cell biology en physiology September 2006 – June 2009
Faculty of Life Sciences,
Louis Pasteur University, Strasbourg, France and
Université de Montréal, Canada (Exchange program)

Research and teaching experience

Department of Biomedicine **Basel, Switzerland** **From August 2011** Group leader: Prof. Dr. Gerhard Christofori	**Ph.D.** 1. Molecular mechanisms of resistance development to anti-angiogenic cancer therapy. 2. Regulation of the angiogenic signature during epithelial-mesenchymal transition.
University of Basel Fall semester of 2014	**Tutor** "Einführung in die Biologie", 10552-01
Institute for Medical Research and Health (INSERM U682) **Hautepierre, France** **September 2010-June 2011** Group leader: Dr. Gertraud Orend	**M.Sc.** Impact of the Laminin alpha1 chain on tumor angiogenesis
Department of Biomedicine **Basel, Switzerland** **July-August 2010** Group leader: Prof. Dr. Gerhard Christofori	**Summer internship** EphrinB2 implication in epithelial-mesenchymal transition
Institute for Research in Immunology and Cancer **Montreal, Canada** **October 2008–April 2009** Group leader: Dr. Louis Gaboury	**Internship** Galectin-7 gene expression in prostatic adenocarcinoma, basal-cell carcinoma and melanoma

Publication list

Research papers:

Published

E. Fagiani, R. Bill, **L. Pisarsky**, R. Ivanek, C. Ruegg and G. Christofori (2015). "An immature B cell population from peripheral blood serves as surrogate marker for monitoring tumor angiogenesis and anti-angiogenic therapy in mouse models." Angiogenesis **18**(3): 327-345.

A. Fantozzi, D. C. Gruber, **L. Pisarsky**, C. Heck, A. Kunita, M. Yilmaz, N. Meyer-Schaller, K. Cornille, U. Hopfer, M. Bentires-Alj and G. Christofori (2014). "VEGF-Mediated Angiogenesis Links EMT-Induced Cancer Stemness to Tumor Initiation." Cancer Res **74**(5): 1566-1575.

A. Zumsteg, C. Caviezel, **L. Pisarsky**, K. Strittmatter, C. Garcia-Echeverria, F. Hofmann and G. Christofori (2012). "Repression of malignant tumor progression upon pharmacologic IGF1R blockade in a mouse model of insulinoma." Mol Cancer Res **10**(6): 800-809.

Accepted manuscript

L. Pisarsky,* R. Bill,* E. Fagiani, S. Dimeloe, R. Goosen, J. Hagmann, C. Hess and G. Christofori. Targeting metabolic symbiosis to overcome resistance to anti-angiogenic therapy. Cell reports. *Equal contribution

Conferences attended

Oral presentation

11th Swiss Stem Cell Network Annual Meeting
Basel, Switzerland. June 2015.

Gordon Research Seminar on Stem Cells and Cancer
Ventura, USA. February 2015.

20st EuCC Meeting on Clinical and Biological Oncology
Strasbourg, France. May 2013.

Poster presentation

DKFZ-ZMBH Alliance Forum on Tumor Microenvironment, Metabolism and Metastasis
Heidelberg, Germany. September 2015.

Gordon Research Conference on Stem Cells and Cancer
Ventura, USA. February 2015.

Charles Rodolphe Brupbacher Symposium: Breakthroughs in cancer research and therapy
Zurich, Switzerland. Januray 2015.

Targeting the Kinome III
Basel, Switzerland. September 2014.

EMBO/EMBL Symposium: Tumor microenvironment and signaling
Heidelberg, Germany. May 2014.

Gordon Research Seminar and **Gordon Research Conference on Angiogenesis**
Newport, USA. August 2013.